Eur. Phys. J. C (2026) 86:247
https://doi.org/10.1140/epjc/s10052-025-15218-2

THE EUROPEAN PHYSICAL JOURNAL C

Regular Article - Experimental Physics

# Search for Beyond the Standard Model physics with anomaly detection in multilepton final states in $pp$ collisions at $\sqrt{s} = 13$ TeV with the ATLAS detector

**ATLAS Collaboration**[*]

CERN, 1211 Geneva 23, Switzerland

Received: 28 August 2025 / Accepted: 17 December 2025


**Abstract** A model-agnostic search for Beyond the Standard Model physics is presented, targeting final states with at least four light leptons (electrons or muons). The search regions are separated by event topology and unsupervised machine learning is used to identify anomalous events in the full 140 fb$^{-1}$ of proton–proton collision data collected with the ATLAS detector during Run 2. No significant excess above the Standard Model background expectation is observed. Model-agnostic limits are presented in each topology, along with limits on several benchmark models including vector-like leptons, wino-like charginos and neutralinos, or smuons. Limits are set on the flavourful vector-like lepton model for the first time.

## Contents



## 1 Introduction

Throughout the data taking years of 2015–2018, the ATLAS detector at the LHC has collected proton–proton collisions amassing 140 fb$^{-1}$ of data. The Standard Model (SM) of particle physics has been able to describe collider physics phenomena to outstanding precision. Its last missing component, the Higgs boson, was discovered in 2012 by the ATLAS and CMS Collaborations [1,2]. However, the SM remains an incomplete theory, as it does not provide answers to open questions such as the hierarchy of masses of elementary fermions, the origin of neutrino masses, the hierarchy and fine-tuning problems, the observed baryon asymmetry in the universe, and the nature of dark matter and dark energy. Many beyond-the-SM (BSM) theories have been proposed to address these and other shortcomings of the SM; however there are no clear indications of which BSM theory (if any) would provide a more accurate description of nature. Consequently the ATLAS experiment continues a broad BSM search program. The traditional route for searching for BSM physics is to design an analysis targeting a specific model that results in detectable signatures at the LHC. However, without a preferred BSM physics model or scale, model-dependent searches will miss signatures of some possible BSM scenarios. This analysis looks to solve this problem in collision events with multiple leptons, by casting a wide net to simultaneously cover a range of possible final states.

High lepton multiplicities are particularly interesting as they provide a comparatively low-SM-background channel to search for potential BSM physics. ATLAS has previously performed searches with minimal model dependence in the multilepton final states [3,4]. The search presented here is focused on light leptons (electrons, $e$, or muons, $\mu$). Tau leptons are allowed inclusively but not explicitly selected. As a result, leptons refer to light leptons unless otherwise stated. This paper explores the potential for BSM physics discovery in a model-agnostic way in final states with $4\ell$ or $\geq 5\ell$, while demonstrating sensitivity to specific benchmark models.

In high energy physics, anomaly detection (AD) is used as a technique to boost the sensitivity to BSM physics in a model-agnostic way. Both the ATLAS and CMS experiments

[*] e-mail: atlas.publications@cern.ch

Published online: 11 March 2026

have published searches involving AD techniques, ranging from weakly supervised searches [5,6], semi-supervised searches [7,8] and fully unsupervised searches [9,10]. The majority of AD searches are performed in jet-focused final states. In this work, the first ever AD search is performed in multilepton final states. This analysis focuses on the branch of AD named outlier detection, where the type of anomalous events targeted are out-of-distribution data (excesses in tails) as opposed to over-densities such as bumps. Using generative models to explicitly calculate the probability density of events originating from SM processes, the sensitivity to rare excesses (SM or BSM) is boosted in a model-agnostic (denoted model-independent in the remainder) way. Due to the complex, high-dimensional input feature space used, interesting anomaly-enriched regions are constructed from the probability density that could have previously been overlooked.

Two separate searches are performed and referred to as 'model-independent' and 'model-dependent'. Both searches analyse the same pre-selected events but categorise them differently according to the multiplicity and flavour of various objects and the AD score. The model-independent search assumes BSM signals populating one signal region at a time, whereas the model-dependent search is designed to assess the sensitivity to specific BSM models by fitting the AD score in all regions in a simultaneous fit.

In order to assess the sensitivity of this search to BSM physics, a range of benchmark BSM scenarios are simulated. This not only demonstrates the generality of model-independent searches but allows comparison to the sensitivity of dedicated searches. The benchmark models tested target the production of high-mass exotic particles that decay to final states with a high lepton multiplicity. The reporting of model-independent limits allows future reinterpretations, and can be used as a benchmark to assess the viability of new BSM models in multilepton final states.

The benchmark models used for model-dependent interpretation in this paper include the production of vector-like leptons (VLLs) or of supersymmetric particles and are described in the following. Vector-like leptons are hypothetical spin-1/2 particles that are part of one of the simplest viable extensions to the SM at the electroweak scale [11–16]. This analysis considers two simple minimal cases of VLLs as defined in Refs. [17,18], namely an "SU(2) Singlet VLL" and an "SU(2) Doublet VLL" model, with mixings to the SM electron or muon. VLLs are predominantly produced in pairs via the electroweak interaction. In the SU(2) Doublet VLL scenario, the charged VLL decay modes are to an electron or muon, and a $Z$ or SM Higgs boson. In contrast, the neutral VLL decay mode is to an electron or muon and a $W$ boson with 100% branching ratio. In the SU(2) Singlet VLL scenario, only the charged VLL is present and its decay modes are to a neutrino and a $W$ boson, an electron or muon and a $Z$ boson, or an electron or muon and a SM Higgs boson, with branching ratios asymptotically reaching 50%, 25%, and 25%, respectively. The corresponding Feynman diagrams can be found in Ref. [19]. VLL models are also considered with the inclusion of a new complex leptophilic scalar $S_{ji}$ which can decay through fermion mixing to leptons of generation $i$ and $j$, opening new decay modes of the VLLs, $\psi_i$, to this scalar, $\psi_i^- \to S_{ji}^* \ell_j^-$ or $\psi_i^0 \to S_{ji}^* \nu_j$, and their conjugates [20]. Once the VLL decay to the $S_{ji}$ scalar is open, the corresponding branching ratio is nearly 100%. The decay mode $S_{ji}^* \to \ell_j^+ \ell_i^-$ with $i = 1, 2$ and $j = 1, 2, 3$, and its conjugate, are considered, with equal branching ratios to the three $j$ lepton flavours for a given $i$ lepton flavour. This can result in final states with large lepton multiplicities (up to six leptons), and allow for lepton flavour violating decays. Figure 1 shows representative Feynman diagrams for this model, referred to as 'flavourful VLL'. Finally, simplified R-parity violating (RPV) SUSY signals are considered, where the lightest SUSY particle is a bino-like neutralino ($\tilde{\chi}_1^0$), and decays as: $\tilde{\chi}_1^0 \to \ell_k^\pm \ell_{i/j}^\mp \nu_{j/i}$. Every pair production event of wino-like charginos and neutralinos $\tilde{\chi}_1^\pm \tilde{\chi}_1^\mp \to \tilde{\chi}_1^0 W^\pm \tilde{\chi}_1^0 W^\mp$ and $\tilde{\chi}_1^\pm \tilde{\chi}_2^0 \to \tilde{\chi}_1^0 W^\pm \tilde{\chi}_1^0 Z/h$ results in at least four lepton final states. In this paper, only light leptons are considered and thus the $\lambda_{ijk} = \lambda_{12k}$ (with $k = 1, 2$) coupling scenario is used as benchmark model. The corresponding Feynman diagrams can be found in Ref. [21]. A variation on the RPV SUSY model is also considered, where smuons are pair produced and decay to a bino-like neutralino, which in turn decays via the RPV coupling $\lambda'_{i33}$ (with $i = 2, 3$). This allows the bino-like neutralino to decay to a lepton and third-generation quarks. This model can result in final states with high lepton multiplicity and high $b$-jet multiplicity. The corresponding Feynman diagrams can be found in Ref. [22].

## 2 ATLAS detector

The ATLAS detector [23] at the LHC covers nearly the entire solid angle around the collision point.[1] It consists of an inner tracking detector surrounded by a thin superconducting solenoid, electromagnetic and hadronic calorimeters, and a muon spectrometer incorporating three large superconducting air-core toroidal magnets.

[1] ATLAS uses a right-handed coordinate system with its origin at the nominal interaction point (IP) in the centre of the detector and the $z$-axis along the beam pipe. The $x$-axis points from the IP to the centre of the LHC ring, and the $y$-axis points upwards. Polar coordinates $(r, \phi)$ are used in the transverse plane, $\phi$ being the azimuthal angle around the $z$-axis. The pseudorapidity is defined in terms of the polar angle $\theta$ as $\eta = -\ln\tan(\theta/2)$ and is equal to the rapidity $y = \frac{1}{2}\ln\left(\frac{E+p_z}{E-p_z}\right)$ in the relativistic limit. Angular distance is measured in units of $\Delta R \equiv \sqrt{(\Delta y)^2 + (\Delta\phi)^2}$

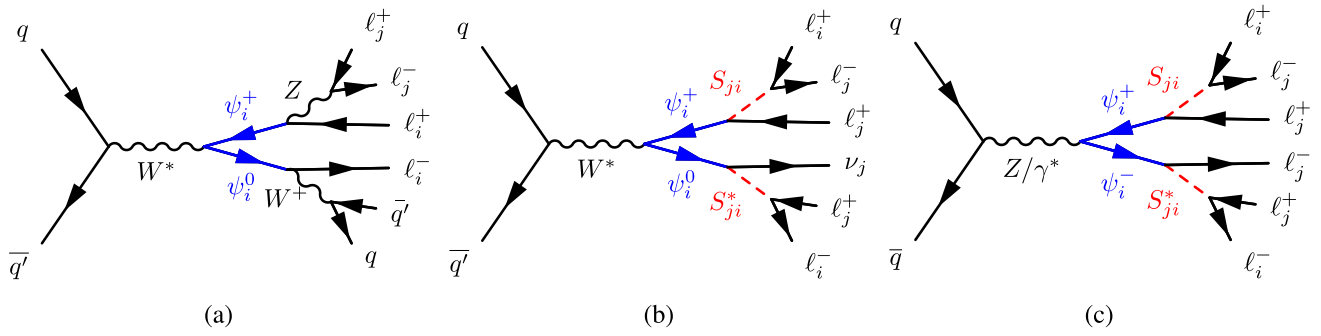


**Fig. 1** Example Feynman diagram for the pair production of VLL, denoted by $\psi_i$, in the flavourful model, with the VLLs produced via a **a**, **b** $W^*$ boson and **c** a $Z$ boson, with the decay of the VLLs into SM leptons and **a** two SM vector bosons, and **b**, **c** two scalars $S_{ji}$. Considering the decays of **a** $W^+ \to q\bar{q}'$ and $Z \to \ell_j^+\ell_j^-$, and **b**, **c** $S_{ji}^{(*)} \to \ell_j^{-(+)}\ell_i^{+(-)}$, these processes result in multilepton final states. The subscripts $i$ and $j$ refer to the lepton generation, with allowed values $i = 1, 2$ and $j = 1, 2, 3$

The inner-detector system (ID) is immersed in a 2 T axial magnetic field and provides charged-particle tracking in the range of $|\eta| < 2.5$. The high-granularity silicon pixel detector covers the vertex region and typically provides four measurements per track, the first hit generally being in the insertable B-layer (IBL) installed before Run 2 [24,25]. It is followed by the SemiConductor Tracker (SCT), which usually provides eight measurements per track. These silicon detectors are complemented by the transition radiation tracker (TRT), which enables radially extended track reconstruction up to $|\eta| = 2.0$. The TRT also provides electron identification information based on the fraction of hits (typically 30 in total) above a higher energy-deposit threshold corresponding to transition radiation.

The calorimeter system covers the pseudorapidity range $|\eta| < 4.9$. Within the region $|\eta| < 3.2$, electromagnetic calorimetry is provided by barrel and endcap high-granularity lead/liquid-argon (LAr) calorimeters, with an additional thin LAr presampler covering $|\eta| < 1.8$ to correct for energy loss in material upstream of the calorimeters. Hadronic calorimetry is provided by the steel/scintillator-tile calorimeter, segmented into three barrel structures within $|\eta| < 1.7$, and two copper/LAr hadronic endcap calorimeters. The solid angle coverage is completed with forward copper/LAr and tungsten/LAr calorimeter modules optimised for electromagnetic and hadronic energy measurements, respectively.

The muon spectrometer (MS) comprises separate trigger and high-precision tracking chambers measuring the deflection of muons in a magnetic field generated by the superconducting air-core toroidal magnets. The field integral of the toroids ranges between 2.0 and 6.0 Tm across most of the detector. Three layers of precision chambers, each consisting of layers of monitored drift tubes, cover the region $|\eta| < 2.7$, complemented by cathode-strip chambers in the forward region, where the background is highest. The muon trigger system covers the range $|\eta| < 2.4$ with resistive-plate chambers in the barrel, and thin-gap chambers in the endcap regions.

The luminosity is measured mainly by the LUCID-2 [26] detector that records Cherenkov light produced in the quartz windows of photomultipliers located close to the beampipe.

Events were selected by the first-level trigger system implemented in custom hardware, followed by selections made by algorithms implemented in software in the high-level trigger [27]. The first-level trigger accepted events from the 40 MHz bunch crossings at a rate close to 100 kHz, which the high-level trigger further reduced to record complete events to disk at about 1.25 kHz.

A software suite [28] is used in data simulation, in the reconstruction and analysis of real and simulated data, in detector operations, and in the trigger and data acquisition systems of the experiment.

## 3 Data and simulated event samples

This analysis uses data from $pp$ collisions at $\sqrt{s} = 13$ TeV collected by the ATLAS experiment from 2015 to 2018. After the application of data-quality requirements [29] to ensure that all parts of the detector are operational during data-taking, the data sample corresponds to an integrated luminosity of 140 fb$^{-1}$. The number of additional $pp$ interactions per bunch crossing (pile-up) in this sample ranges from about 8 to 70, with an average of 34. The trigger requirements are discussed in Sect. 5.

Monte Carlo (MC) simulation samples are produced for the different signal and background processes. Processes contributing to the background with at least one non-prompt lepton or one electron from conversion in the $4\ell$ final state are mainly $t\bar{t}$, $Z$ + jets, $t\bar{t}W$ and $W^{\pm}Z$. The main background contributions with prompt leptons are from the

$t\bar{t}Z/\gamma^*(Z/\gamma^* \to \ell^+\ell^-)$, $ZZ$, and $t\bar{t}H$ processes. In the $\geq 5\ell$ final state, $t\bar{t}Z/\gamma^*(Z/\gamma^* \to \ell^+\ell^-)$ and $ZZ$ processes contribute to the background with at least one non-prompt lepton or electron from photon conversion.

All samples showered with PYTHIA use the A14 set of tuned parameters [30] (referred to as 'tune'), whereas those showered with HERWIG use the H7-UE tune [31]. In all samples simulated with SHERPA [32], the matrix elements (MEs) are calculated with the Comix [33] and OPENLOOPS [34–36] libraries. They are matched with the SHERPA parton shower (PS) [37] using the MEPS@NLO prescription [38–41] with the set of tuned parameters developed by the SHERPA authors. Pile-up is modelled using events from minimum-bias interactions generated with PYTHIA 8.186 [42] with the A3 tune [43], and overlaid onto the simulated hard-scatter events according to the luminosity profile of the recorded data [44]. All samples include leading-logarithm photon emission, either modelled by the PS generator or by PHOTOS [45]. The generated events are processed through either a full simulation of the ATLAS detector geometry and response using GEANT4 [46], or a faster simulation where the full GEANT4 simulation of the calorimeter response is replaced by a detailed parameterisation of the shower shapes (ATLAS Fast Simulation) [47]. Both types of simulated events are processed through the same reconstruction software used for the $pp$ collision data. Corrections are applied to the simulated events so that the particle candidates' selection efficiencies, energy scales and energy resolutions match those determined from data control samples.

Background events from $t\bar{t}Z/\gamma^*$ production were simulated using the MADGRAPH5_AMC@NLO 2.8.1 [48] generator at next-to-leading-order (NLO) in $\alpha_s$ with the NNPDF3.0NLO [49] PDF set. The functional form of the renormalisation and factorisation scales $(\mu_r, \mu_f)$ was set to the default scale $0.5 \times \sum_i \sqrt{m_i^2 + p_{T,i}^2}$, where the sum runs over all the particles generated from the ME calculation. The invariant mass of the lepton pair, $m(\ell\ell)$, in the $t\bar{t}Z/\gamma^*(Z/\gamma^* \to \ell^+\ell^-)$ sample is set to be greater than 1 GeV. Top quarks were decayed at leading-order (LO) using MADSPIN [50,51] to preserve all spin correlations. Showering and hadronisation were performed using PYTHIA 8.244 [52] with the A14 tune, and the NNPDF2.3LO [53] PDF set with $\alpha_s = 0.130$. The decays of bottom and charm hadrons were performed by EVTGEN 1.7.0 [54].

Diboson ($VV$) background processes are simulated with SHERPA 2.2.2 [55] and include $W^\pm Z$, $ZZ$, and $W^+W^-$ processes. The ME is calculated with NLO accuracy in QCD for up to one additional parton and at LO accuracy for up to three additional partons. The NNPDF3.0NNLO set of PDFs is used. The simulation includes off-shell effects and Higgs boson contributions, where appropriate. The invariant mass of any pair of same-flavour opposite-sign (SFOS) leptons is required to be $m(\ell\ell) > 4$ GeV. Samples for the loop-induced processes $gg \to VV$ are simulated using LO-accurate MEs for up to one additional parton emission. The triboson ($VVV$) background processes are also simulated with SHERPA 2.2.2 and using the NNPDF3.0NNLO set of PDFs, with the ME calculated with NLO accuracy in QCD for the inclusive process and LO accuracy for up to two additional partons.

Samples for $t\bar{t}H$, and single top production are simulated using the NLO generator POWHEG BOX v2 [56–62] and interfaced with PYTHIA 8 for the PS and fragmentation. These samples used the NNPDF3.0NLO PDF set. The decays of bottom and charm hadrons are performed by EVTGEN 1.6.0. The production of a top quark in association with a $W$ boson ($tW$) is modelled using the five-flavour scheme. The diagram removal scheme [63] is used to remove interference and overlap with $t\bar{t}$ production. Single-top $s$- and $t$-channel production is modelled using the five- and four-flavour schemes, respectively.

The production of $t\bar{t}$ events is modelled using the POWHEG BOX v2 generator at NLO with the NNPDF3.0NLO PDF set. The events are interfaced to PYTHIA 8.230 to model the PS, hadronisation, and underlying event, using the NNPDF2.3LO set of PDFs. The decays of bottom and charm hadrons are performed by EVTGEN 1.6.0. The $t\bar{t}$ process is modelled with the $h_{damp}$ parameter[2] set to $1.5\,m_t$ [64]. The $t\bar{t}$ sample is normalised to the cross-section prediction at next-to-next-to-leading-order (NNLO) in QCD including the resummation of next-to-next-to-leading logarithmic (NNLL) soft-gluon terms calculated using TOP++2.0 [65–71]. This cross-section is $\sigma(t\bar{t})_{\text{NNLO+NNLL}} = 832 \pm 51\ pb$.

The $Z/\gamma^* \to \ell\ell$ process (with $\ell = e, \mu, \tau$) is simulated with SHERPA 2.2.11 using the NNPDF3.0NNLO PDF set. Processes with up to two coloured partons are modelled at NLO in the strong coupling, while processes with up to five additional partons are modelled at LO accuracy. The $Z$+jets sample is normalised to the theoretical cross-section calculated at NLO accuracy in QCD [72].

The $t\bar{t}W$ background sample is simulated using MADGRAPH5_AMC@NLO 2.6.7 with NLO multileg merging using the FxFx algorithm [73], where the MEs are calculated for up to one additional partons at NLO in QCD, and up to two partons at LO in QCD. The events are interfaced with PYTHIA 8.244. The NNPDF3.0NLO and NNPDF2.3LO PDF sets are used for the ME and PS, respectively. The merging scale parameter is used in the matching of a ME with the PS and is set to 30 GeV. In addition to this $t\bar{t}W$ prediction at NLO in QCD, higher-order corrections related to elec-

[2] The $h_{damp}$ parameter is a resummation damping factor and one of the parameters that controls the matching of POWHEG MEs to the PS, thus effectively regulating the high-$p_T$ radiation against which the hard-process system recoils.

troweak (EW) contributions are also included. First, event-by-event correction factors are applied that provide virtual NLO EW corrections of the order $\alpha^2\alpha_s^2$ derived using the formalism described in Ref. [74] along with LO corrections of order $\alpha^3$. Second, real emission contributions from the sub-leading EW corrections at order $\alpha^3\alpha_s$ [75] are simulated with MadGraph5_aMC@NLO 2.6.7 produced at LO in QCD and included as a separate sample.

A dedicated $t\bar{t}$ sample with rare $t \to Wb\gamma^*(\to \ell^+\ell^-)$ radiative decays, $t\bar{t} \to W^+bW^-\bar{b}\ell^+\ell^-$, is simulated using a ME calculated at LO in QCD and requiring $m(\ell\ell) > 1$ GeV. In this sample the photon can be radiated from the top quark, the $W$ boson, or the $b$-quark. Both the $t\bar{t}Z/\gamma^*(Z/\gamma^* \to \ell^+\ell^-)$ and $t\bar{t} \to W^+bW^-\bar{b}\ell^+\ell^-$ samples are combined and together form the '$t\bar{t}Z/\gamma^*$' sample. The contribution from internal photon conversions ($\gamma^* \to \ell^+\ell^-$) with $m(\ell\ell) < 1$ GeV is modelled by QED multi-photon radiation via the PS in an inclusive $t\bar{t}$ sample. The contribution from muons from internal conversions for $m(\ell\ell) < 1$ GeV is negligible in this analysis. Dedicated $Z$+jets samples are generated with Powheg Box and interfaced with Pythia 8 for the PS and fragmentation. These samples are used to model the data in a control region enriched in material and internal conversion electrons, as explained in Sect. 5.

The production of $t\bar{t}t\bar{t}$ events was modelled using the MadGraph5_aMC@NLO v2.6.2 generator that provides MEs at NLO in QCD with the NNPDF3.1nlo [76] PDF set. The functional form of the renormalisation and factorisation scales are set to $\mu_r = \mu_f = m_T/4$, where $m_T$ is defined as the scalar sum of the transverse masses $\sqrt{m^2 + p_T^2}$ of the particles generated from the ME calculation. The events are interfaced with Pythia 8.230 for the PS and hadronisation, using the NNPDF2.3lo PDF set. The production of $t\bar{t}t\bar{t}$ events is normalised to a cross section of 12 fb computed at NLO in QCD including EW corrections [75].

Other minor background contributions are included in the analysis: $tZq$, $tWZ$, $W$ + jets and $VH$ processes are normalised to their NLO cross-section, whereas $t\bar{t}t$, $t\bar{t}W^+W^-$, $t\bar{t}ZZ$, $t\bar{t}HH$, and $t\bar{t}WH$ are normalised to their LO cross-section.

Signal samples for VLL$_e$ and VLL$_\mu$ from $SU(2)$ singlet (VLL$_e^S$, VLL$_\mu^S$) and doublet (VLL$_e^D$, VLL$_\mu^D$) models, as well as the flavourful VLL$_e$ and VLL$_\mu$ processes, are simulated using MadGraph5_aMC@NLO 2.9.5 at NLO in QCD with the NNPDF3.0nlo PDF set and Pythia 8.245, and processed through the ATLAS Fast Simulation. The NLO cross-section obtained from MadGraph is used for the normalisation of the signals. The RPV SUSY wino-like chargino and neutralino signal processes are simulated using MadGraph5_aMC@NLO 2.2.2 + Pythia 8.230 at LO in QCD with up to two extra partons. Jet–parton matching followed the CKKW-L prescription [77], with a matching scale set to one quarter of the mass of the pair-produced SUSY particles. The RPV SUSY smuon signal samples were generated with MadGraph5_aMC@NLO 2.9.3 with up to two extra jets at LO in QCD and Pythia 8.245. The matching scale is set at 1/4 of the mass of the SUSY particle being produced. Cross-sections for the RPV SUSY signals were calculated to NLO in the strong coupling constant, adding the resummation of soft gluon emission at next-to-leading-logarithm accuracy [78–85].

## 4 Event reconstruction

Events containing light leptons, and with varying multiplicity of jets with and without $b$-hadrons, and missing transverse momentum content are selected. The corresponding object reconstruction is detailed below. Candidate events are required to have at least one $pp$ interaction vertex. Interaction vertices are reconstructed from at least two tracks with transverse momentum $p_T$ larger than 500 MeV that are consistent with originating from the beam collision region in the $x$–$y$ plane. In events with multiple vertices, the primary vertex is defined as the one with the highest scalar sum of the squared transverse momenta of the associated tracks [86].

Candidate events are selected with a different trigger strategy depending on the lepton multiplicity of the event: single-lepton triggers are used to select events in $2\ell$SS and $3\ell$ regions, and dilepton triggers are used in $4\ell$ and $\geq 5\ell$ regions, requiring the electrons or muons to satisfy identification criteria similar to those used in the offline reconstruction and isolation requirements [87,88]. Single-electron triggers require a minimum $p_T$ threshold of 24 (26) GeV in the 2015 (2016, 2017 and 2018) data-taking period(s), while single-muon triggers have a lowest $p_T$ threshold of 20 (26) GeV in 2015 (2016–2018). The dielectron triggers require two electrons with minimum $p_T$ thresholds ranging from 12 GeV in 2015 to 24 GeV in 2017–2018, whereas the dimuon triggers use asymmetric $p_T$ thresholds for leading (subleading) muons: 18 (8) GeV in 2015 and 22 (8) GeV in 2016–2018. Finally, an electron+muon trigger requires events to have an electron candidate with a 17 GeV threshold and a muon candidate with a 14 GeV threshold for all periods. In the offline selection, leptons are required to match, with $\Delta R < 0.15$, the corresponding leptons reconstructed by the trigger and to have a $p_T$ exceeding the trigger $p_T$ threshold by at least 1 GeV.

Electron candidates are reconstructed from energy clusters in the electromagnetic calorimeter matched to a track in the ID [89]. They are required to satisfy $p_T > 10$ GeV and $|\eta| < 2.47$, excluding the transition region between the endcap and barrel calorimeters ($1.37 < |\eta| < 1.52$). The 'Loose' electron identification working point (WP) is used, based on a likelihood discriminant employing calorimeter,

tracking and combined information that provide separation between electrons and jets.

The reconstruction of muon candidates is based on tracking information from the MS and the ID, as well as energy deposits in the calorimeter system [90]. Muons are required to satisfy $p_{\mathrm{T}} > 10$ GeV and $|\eta| < 2.5$. The 'Loose' muon identification WP is used.

Electron (muon) candidates are matched to the primary vertex by requiring that the significance of their transverse impact parameter, $d_0$ (defined as the distance of closest approach of the track to the beamline in the $x$–$y$ plane) satisfies $|d_0|/\sigma_{d_0} < 5\,(3)$, where $\sigma_{d_0}$ is the measured uncertainty in $d_0$, and by requiring that their longitudinal impact parameter, $z_0$ (defined as the distance in $z$ between the primary vertex and the point on the track used to evaluate $d_0$) satisfies $|z_0 \sin\theta| < 0.5$ mm.

Light lepton candidates are also required to be isolated in the tracker and in the calorimeter to further suppress leptons from heavy-flavour (HF) hadron decays, misidentified jets, or photon conversions (collectively referred to as 'non-prompt leptons'). Electrons with an incorrect charge assignment (referred to as 'QMisID') are further suppressed with a boosted decision tree (BDT) discriminant [91] in $4\ell$ events with total lepton electric charge $Q = \pm 2$ and same-sign electric charge dilepton ($2\ell$SS) $\mu e$ events. Electrons are further separated into three classes, 'material conversion', 'internal conversion', and 'non-conversion', following the same procedure as described in Ref. [19]. Electrons are required to pass the 'non-conversion' class in all regions except in the control region enriched in material and internal conversion electrons, as explained in Sect. 5.

For the control regions enriched in non-prompt leptons from the decay of hadrons that contain bottom- or charm-quarks (referred to as 'HF non-prompt leptons') as described in Sect. 5, leptons are required to fail a selection based on a WP of a BDT discriminant (referred to as the non-prompt-lepton BDT [92]). The BDT uses isolation and lifetime information about a track-jet that matches the selected electron or muon to discriminate between prompt and non-prompt leptons.

The constituents for jet reconstruction are identified by combining measurements from both the ID and the calorimeter using a particle flow (PFlow) algorithm [93]. Jet candidates are reconstructed from these PFlow objects using the anti-$k_{\mathrm{T}}$ algorithm [94,95] with a radius parameter of $R = 0.4$. They are calibrated based on jet energy scale (JES) and resolution (JER), as derived from 13 TeV data and simulation [96], such that in simulation they have on average the same energy and momentum as matched particle level jets. Only jet candidates with $p_{\mathrm{T}} > 25$ GeV and within $|\eta| < 2.5$ are selected. To reduce the effect of pileup, each jet with $p_{\mathrm{T}} < 60$ GeV and $|\eta| < 2.4$ is required to have an origin compatible with the primary vertex, as defined by the jet vertex tagger (JVT) [97] criteria. A set of quality criteria is also applied to reject events containing at least one jet arising from non-collision sources or detector noise [98].

Jets containing $b$-hadrons are identified ($b$-tagged) via an algorithm [99] that uses a deep-learning neural network based on the distinctive features of $b$-hadron decays, primarily the impact parameters of tracks and the displaced vertices reconstructed in the ID. Additional input to this network is provided by discriminating variables constructed by a recurrent neural network, which exploits the spatial and kinematic correlations between tracks originating from the same $b$-hadron. A multivariate $b$-tagging discriminant value is calculated for each jet. In this search, a jet is considered $b$-tagged if it passes the WP corresponding to 77% average expected efficiency[3] to tag a $b$-quark jet in all regions except for the fake light-flavour electron control region where the 85% b-tagging efficiency WP is used. The corresponding light-jet[4] rejection factor [5] is about 40 to 192, and the charm-jet ($c$-jet) rejection factor is about 3 to 6. The $b$-tagging distribution obtained by ordering from higher to lower $b$-jet efficiency the resulting five exclusive bins from the four WPs corresponding to 85%, 77%, 70%, or 60% average expected efficiency to tag a $b$-quark jet, is referred to as pseudo-continuous $b$-tagging score. Each jet is assigned a pseudo-continuous $b$-tagging score that defines if a jet passes a given operating point but fails the adjacent tighter one. The sum of the pseudo-continuous $b$-tagging scores of all jets in the event is used as input to the AD discriminant described in Sect. 5. Correction factors derived from dedicated calibration samples enriched in $b$-jets, $c$-tagged jets, or light-tagged jets, are applied to the simulated event samples [100–102].

To uniquely identify objects, a sequential 'overlap removal' procedure is performed. If two electrons are separated by $\Delta R < 0.1$, only the one with the higher $p_{\mathrm{T}}$ is kept. If an electron and a muon overlap within $\Delta R < 0.1$, the muon is removed if it is reconstructed only from an ID track and calorimeter energy deposits consistent with a minimum-ionising particle (i.e. if it is 'calo-tagged'), otherwise the electron is removed. If an electron and a selected jet are found within $\Delta R < 0.2$, the jet is removed. For each electron in the event a $p_{\mathrm{T}}$-dependent variable-size cone of maximum size $\Delta R = 0.4$ is defined. If a selected jet, surviving all previous overlap criteria, is found in this cone, the lepton is rejected. The same procedure is also applied between jets and muons, with the exception that, if a muon and a jet overlap with $\Delta R < 0.2$, the jet is removed, unless the number of tracks in the jet is more than two.

[3] Efficiencies for tagging $b$-jets are determined for jets with $p_{\mathrm{T}} > 20$ GeV and $|\eta| < 2.5$ in simulated $t\bar{t}$ events.

[4] 'Light jet' refers to a jet originating from the hadronisation of a light quark ($u$, $d$, $s$) or a gluon.

[5] The rejection factor is defined as the reciprocal of the efficiency.

The missing transverse momentum $\mathbf{p}_{\mathrm{T}}^{\mathrm{miss}}$ (with magnitude $E_{\mathrm{T}}^{\mathrm{miss}}$) is defined as the negative vector sum of the $p_{\mathrm{T}}$ of all selected and calibrated objects in the event that satisfy the overlap removal procedure, and an additional term to account for the momenta of soft particles that are not associated with any of the selected objects [103]. This soft term is calculated from inner-detector tracks matched to the primary vertex, which makes it more resilient to contamination from pileup interactions.

## 5 Search region definition

Events containing at least four light leptons are selected and further divided into three orthogonal final states:

- $4\ell$ $Q = 0$: four light leptons with a total charge of zero,
- $4\ell$ $Q = \pm 2$: four light leptons with a total charge of $\pm 2$, and
- $\geq 5\ell$: five or more light leptons.

The total number of observed events in $4\ell$ $Q = 0$, $4\ell$ $Q = \pm 2$, and $\geq 5\ell$ are 4097, 77, and 21, respectively.

Two searches are defined: one following a model-independent strategy consisting of 'discovery regions', and the other designed to be sensitive to the benchmark models described in Sect. 1, consisting of 'benchmark regions'. The different event splitting in each of these regions is described below. However the events in the sum of all discovery regions are the same as the events in the sum of all benchmark regions. Regions are defined through a trade-off between various considerations. First, the sensitivity to specific multilepton final states, covering possible combinations of number of leptons, lepton flavour, number of b-jets, number of SFOS lepton pairs, and those consistent with a $Z$ boson decay. Second, the granularity of the region splitting is limited by the available MC background simulated events to ensure a reliable background estimation in all regions. Third, the reduction of the look-elsewhere effect in the model-independent search is achieved with a smaller region multiplicity than in the model-dependent search.

In the $4\ell$ $Q = 0$ channel, discovery regions are defined by the number of SFOS lepton pairs, and by the number of SFOS lepton pairs with an invariant mass within 10 GeV of the nominal $Z$ boson mass, referred to as a $Z$ boson candidate, allowing the separation of on-shell $Z$ boson processes from off-shell and photon backgrounds. The benchmark regions have the same categorisation of events as the discovery regions, with further splitting based on the $b$-tagged jet multiplicity (zero or $\geq 1$ $b$-jets) and the number of electrons and muons that are not part of a $Z$ boson candidate ($N_e > N_\mu$, $N_e = N_\mu$ and $N_\mu > N_e$). The $b$-jet-based classification improves the discrimination against top-quark processes. The main background contributions originate from $ZZ$ and $t\bar{t}Z/\gamma^*$ processes.

In the $4\ell$ $Q = \pm 2$ channel, where the main background processes contain at least one non-prompt lepton, the discovery region is not split. The benchmark regions are split into events with zero or $\geq 1$ $b$-jets, and these categories are further divided into three sub-regions based on $N_e$ and $N_\mu$ as done in the $Q = 0$ channel. The $Z$ boson candidates are defined as in the $4\ell$ $Q = 0$ channel but without requiring the leptons to have opposite charge.

In the $\geq 5\ell$ channel, the discovery regions are defined by the number of $Z$ boson candidates: $5\ell$ 0Z and $5\ell \geq 1$Z. To define the benchmark regions, events are further split by the presence of $b$-jets (0 or $\geq 1$ $b$-jets) and by lepton flavour when there are no $b$-tagged jets, due to the limited number of data events in $b$-tagged regions. The main background processes are $VVV$, $t\bar{t}H$, and events with at least one non-prompt lepton.

Five control regions (CRs) orthogonal to the discovery/benchmark regions and among each other are defined to fit the normalisation of the leading backgrounds. A region enriched in $W^{\pm}Z$ and $t\bar{t}Z$ is defined ('WZ/ttZ') by selecting events with three leptons, from which one SFOS lepton pair is required to be compatible with a $Z$ boson, $|m_{\ell^+\ell^-}^{\mathrm{SFOS}} - m_Z| < 10$ GeV. Events in the WZ/ttZ CR are also required to have at least one jet and zero $b$-jets satisfying the 77% WP. A region enriched in photon conversions ('Conversions') from $Z \to \mu\mu\gamma^{(*)}(\to ee)$ is defined by requiring three leptons (two muons and one electron), from which the electron must fulfil the material conversion or internal conversion candidate requirements. Events in the Conversion CR are also required to have no SFOS lepton pairs compatible with a $Z$ boson, the three lepton invariant mass fulfilling $|m_{3\ell} - m_Z| < 10$ GeV, and zero $b$-jets satisfying the 77% WP. For the two CRs enriched in HF non-prompt leptons, events with two same-sign leptons are selected, requiring the leading lepton to additionally pass the non-prompt-lepton BDT WP, and the same-sign lepton pair to be $\mu e$ with the electron being the sub-leading lepton and passing the QMisID BDT requirement (CR enriched in non-prompt electrons from HF hadron decays, 'HFe') or $\mu\mu$ (CR enriched in non-prompt muons from HF hadron decays, 'HF$\mu$'). Additionally, at least two jets and exactly one $b$-jet satisfying the 77% WP are required. Finally, a CR enriched in non-prompt electrons from LF hadron decays ('LFe') consists of events with $3\ell$, from which two same-flavour muons with an invariant mass consistent with that of a $Z$ boson plus one additional electron are required. In addition, the $E_{\mathrm{T}}^{\mathrm{miss}}$ has to be lower than 20 GeV to reduce the $W^{\pm}Z$ background contamination and zero $b$-jets satisfying the 85% WP are required. The contamination in the control regions from the non-excluded signal benchmark models described in Sect. 1 is negligible.

## 6 Anomaly detection

An event-level AD technique is used based on normalising flows to enhance the sensitivity to BSM physics in a model-independent way. The AD technique is designed to be sensitive to out-of-distribution data (outlier detection), and it is thus sensitive to BSM physics populating low probability regions of phase space. Anomalies are defined with respect to a reference distribution, for which the simulated SM background is used.

To build an anomaly score that is sensitive to rare (kinematically extreme) events, the normalising flows are used to directly evaluate the probability density of the MC background. Normalising flows are an unsupervised machine learning model typically used to model complex distributions, allowing efficient and exact density estimation [104]. To do so, flows employ a series of invertible bijective functions to transform from a closed-form latent distribution to a target distribution, allowing the explicit calculation of the probability density. In this work, a Real-valued Non-Volume Preserving flow (RealNVP) is used with the standard choice of a Normal distribution in the latent space [105]. In order to use the normalising flows in the context of AD, the flow is trained on the background MC prediction only, using the background probability density $p(x)$, where $x$ is the set of input variables, as the target distribution within the search regions. The training is performed on MC samples rather than data due to the available statistics in multilepton final states and additional complexities with biasing when using data to train the normalising flows. Once learned, the evaluated probability is then transformed to give the anomaly score according to:

$$s(x) = \frac{\log p(x) - \log p_{\text{max}}}{\log p_{\text{min}} - \log p_{\text{max}}}, \tag{1}$$

where $p_{\text{min}}$ and $p_{\text{max}}$ are the minimum and maximum probability densities, respectively, evaluated from the MC background dataset. The transformation is chosen such that the log probability is scaled to be within the range [0, 1] with anomalous events at higher score values.

The choice of input variables used to calculate the background density is crucial for defining the space of BSM models that the AD is sensitive to. Physically motivated high-level variables are chosen which can provide sensitivity to a wide range of BSM models while also aiding in the characterisation of any excess that may be found. Table 1 shows the training variables used in each search region. The pairing of leptons with the closest invariant mass to that of the $Z$ boson is denoted by the label $Z$ ("lepton pair closest to $Z$ boson"), and the remaining pair of leptons amongst the four leptons in the event ("lepton pair second-closest to $Z$ boson") is denoted by the label $\ell\ell$. In the $\geq 5\ell$ region, a reduced number of input variables are used due to the relatively small sample size of the simulated events and the training is performed only on events with at least one $Z$ boson candidate. No AD is applied to $\geq 5\ell$ 0Z region, where event counting is used instead due to limited data yields.

The same AD training is used for the model-dependent and independent analyses. Normalising flows are trained in each of the discovery regions. In the $4\ell$ regions the flows are trained in two sub-regions, after splitting events according to the presence or absence of $b$-jets. The anomaly score distributions are then merged into one distribution for the model-independent analysis, while they are used separately for the model-dependent analysis. The `PyTorch` library was used to train the normalising flows used in this work, and the `normflows` package used to define the architecture of the flows [106,107]. The flows are made up of eight affine coupling layers, each containing two hidden layers of fully connected neural networks (FCN), each with 64 nodes. Each FCN uses the `Tanh` activation function, and the parameters of the flows are initialised to zero. The Adam optimiser [108] is used within back-propagation, along with a small weight decay of $10^{-4}$ (an L2 regularisation on the model weights). Trainings are performed with a fixed learning rate of $10^{-4}$ or $10^{-5}$ depending on the available statistics in the region used, and with a fixed batch size of 512. The flows are trained using weighted MC events, with overall weights calculated through the combination of weights and scale factors as described in Section 4. Weights are applied to the calculated loss per-event to produce the correctly weighted probability density. Events with negative weights are rare and removed from the training to improve stability.

Once the final anomaly score distributions are obtained, two different strategies are used to bin the distribution. For the model-independent search, background rejection points of 90%, 99% and 99.9% are used to define overlapping discovery signal bins. Each discovery signal bin is required to have at least 0.1 expected background events and less than 20% MC statistical uncertainty, or otherwise the bin is dropped. Discovery regions where the 90% bin is dropped use a 50% background rejection point, as long as the above criteria on background events and statistical uncertainty are fulfilled; otherwise, no AD is used in the corresponding region. The remaining low-anomaly score distribution is used as a region for measuring background normalisation effects. For the model-dependent search, the most sensitive bin is defined by tightening the selection on the anomaly score until both threshold criteria on the 0.1 background and 20% MC statistical uncertainty are satisfied. From there, successive bins are defined such that the background yield increases in each bin by a factor of four until the entire distribution is binned. This results in distributions with higher granularity at high-anomaly score, and conversely low granularity at low-anomaly score.

**Table 1** A summary of the input variables used for training the normalising flows for AD in the $4\ell$ $Q = 0$, $4\ell$ $Q = \pm 2$, and $\geq 5\ell$ regions. Each variable is scaled to mean zero and unit variance before being used as training data. The "lepton pair closest to $Z$ boson" is given by the SFOS lepton pair with invariant mass closest to 91.2 GeV, with the remaining pair of leptons amongst the four leptons in the event referred to as the "lepton pair second-closest to $Z$ boson"

| Training variable | Description |
|---|---|
| Input to $4\ell$ $Q = 0$, $4\ell$ $Q = \pm 2$, and $\geq 5\ell$ 1Z | |
| $H_{\mathrm{T}}^{\mathrm{lep}}$ | Sum of transverse momenta of leptons |
| $H_{\mathrm{T}}^{\mathrm{jets}}$ | Sum of transverse momenta of jets |
| $E_{\mathrm{T}}^{\mathrm{miss}}$ | Missing transverse energy |
| $N_{\mathrm{jets}}$ | Number of jets |
| $p_{\mathrm{T}}(Z)$ | Transverse momentum of lepton pair closest to $Z$ boson |
| Input to $4\ell$ $Q = 0$ and $4\ell$ $Q = \pm 2$ | |
| $p_{\mathrm{T}}(\ell\ell)$ | Transverse momentum of lepton pair second-closest to $Z$ boson |
| $m(Z)$ | Invariant mass of lepton pair closest to $Z$ boson |
| $m(\ell\ell)$ | Invariant mass of lepton pair second-closest to $Z$ boson |
| $m^{\mathrm{high}}(3\ell)$ | Largest invariant mass of lepton pair closest to $Z$ boson and another lepton |
| $m^{\mathrm{low}}(3\ell)$ | Smallest invariant mass of lepton pair closest to $Z$ boson and another lepton |
| $m(4\ell)$ | Invariant mass of four-lepton system |
| $m_{\mathrm{T}}(4\ell, E_{\mathrm{T}}^{\mathrm{miss}})$ | Transverse mass of four leptons and $E_{\mathrm{T}}^{\mathrm{miss}}$ |
| $m_{\mathrm{T}}(Z, E_{\mathrm{T}}^{\mathrm{miss}})$ | Transverse mass of lepton pair closest to $Z$ boson and $E_{\mathrm{T}}^{\mathrm{miss}}$ |
| $m_{\mathrm{T}}(\ell\ell, E_{\mathrm{T}}^{\mathrm{miss}})$ | Transverse mass of lepton pair second-closest to $Z$ boson and $E_{\mathrm{T}}^{\mathrm{miss}}$ |
| $\sum_{i=1}^{\mathrm{jets}} \mathrm{pcb}_i$ | Sum of pseudo-continuous $b$-tagging score |

In order to quantify which input features the AD technique is most sensitive to, the distortion of the kinematic variables is quantified after applying a series of cuts to the anomaly score. For this purpose, the Energy Distance [109] is calculated between each input variable after separating by low- and high-anomaly score. Figure 2 shows two example input variable distributions and the distortions after applying the specified background rejection cut to the anomaly score. The most impactful input variables are typically $m_{\mathrm{T}}(4\ell, E_{\mathrm{T}}^{\mathrm{miss}})$, $m(\ell\ell)$, $p_{\mathrm{T}}(Z)$, $m(4\ell)$, and $H_{\mathrm{T}}^{\mathrm{lep}}$.

Two distinct fit setups, as defined in Sect. 9, are used to perform the model-independent and model-dependent searches, as illustrated schematically in Fig. 3. Both searches share the same five control regions ('HFe', 'HF$\mu$', 'LFe', 'Conversions','WZ/ttZ'; coloured in light blue in Fig. 3). The model-independent search includes ten additional low-anomaly score discovery regions ('Discovery regions'; coloured in darker blue in Fig. 3 (left)). These correspond to the pre-selected events categorised following the discovery region definitions in Sect. 5, not passing the discovery signal bin anomaly score cuts (denoted as "$<$ 90%" or "$<$ 50%"). The low-anomaly score discovery regions $4\ell$ $Q = 0$ 1Z 2SFOS and $4\ell$ $Q = 0$ 2Z are further split in events with zero or at least one $b$-jet. Each layer in Fig. 3 (left) represents the model-independent fit performed with the five control regions, the ten low-anomaly score discovery regions, and one discovery signal bin at a time. The discovery signal bin (the stack of differently coloured boxes in Fig. 3 (left)) is defined by the discovery region selection and the cut at the optimised background rejection value "$>$ 99.9/99/90/50%". In total there are 16 discovery signal bins corresponding to 16 different fits. Fitting each discovery signal bin allows to probe BSM physics in different multi-lepton final states. The model-dependent search includes the same pre-selected events as the model-independent search but additionally splitting them according to the flavour of the non-$Z$ leptons and the presence of 0 or $\geq 1$ $b$-jets ('Benchmark regions'; coloured in darker blue in Fig. 3 (right)). A single fit per benchmark signal hypothesis is performed with the five control regions and 32 benchmark regions (and thus only one layer is displayed in Fig. 3 (right)), fitting the anomaly score distribution in all regions except in the $\geq 5\ell$ 0Z regions, where the total event yield is used instead.

## 7 Background estimation

All background processes are estimated by using the simulation samples described in Sect. 3. Before the simultaneous fit to data, the event kinematics of the simulated $t\bar{t}$ and $VV$ backgrounds require dedicated corrections derived from data control samples to better describe the data. During the simul-

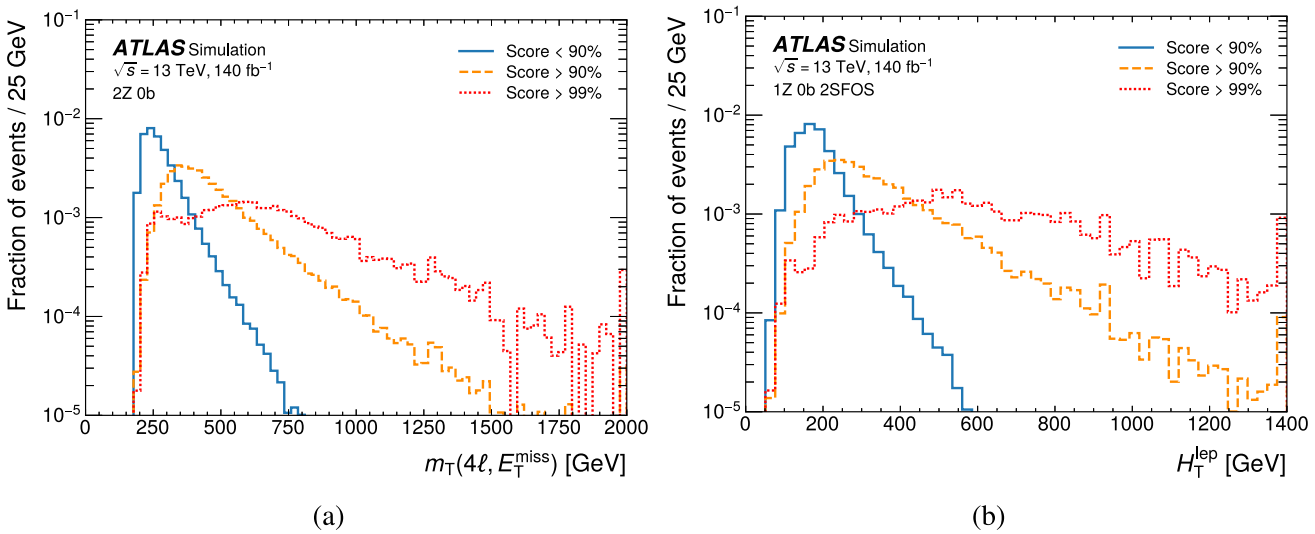


**Fig. 2** Comparison of background shapes for **a** $m_{\mathrm{T}}(4\ell, E_{\mathrm{T}}^{\mathrm{miss}})$ in the 2Z 0b region and **b** $H_{\mathrm{T}}^{\mathrm{lep}}$ in the 1Z 0b 2SFOS region, considering various requirements on the anomaly score corresponding to the specified background rejection cuts. The last bin contains the overflow

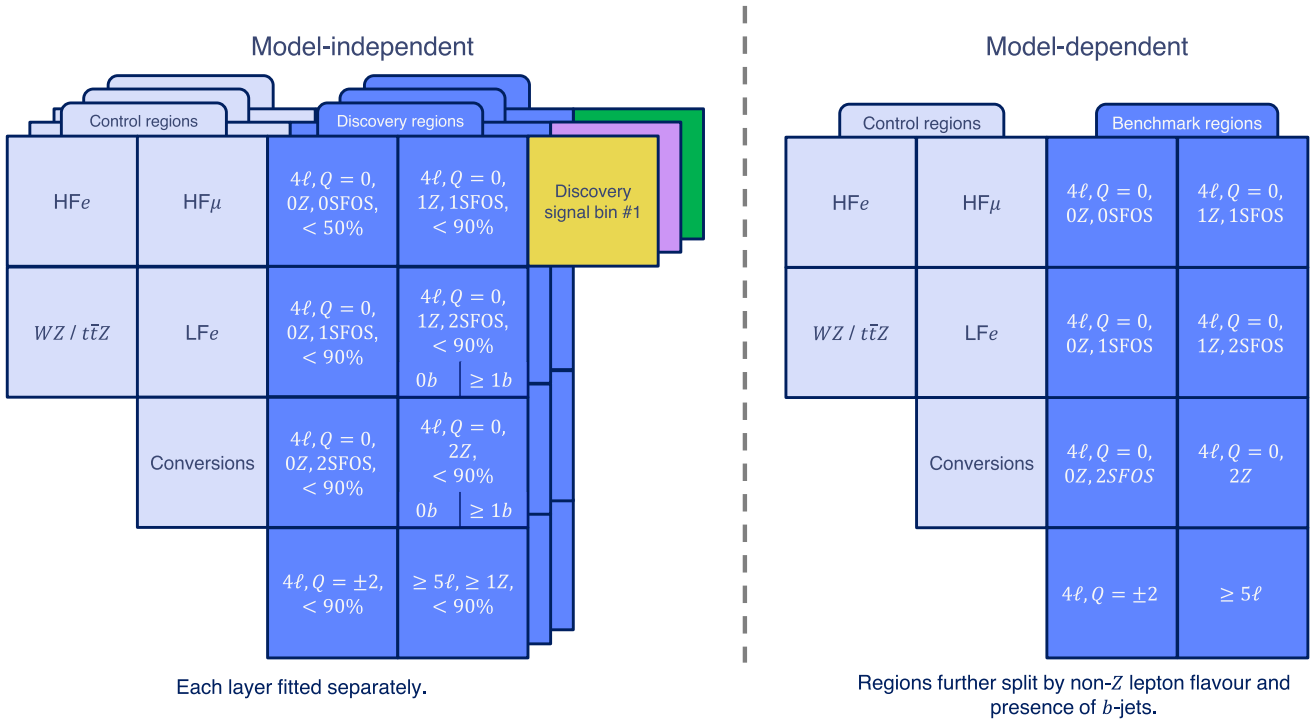


**Fig. 3** Illustrative sketch of the control regions and (left) discovery or (right) benchmark regions in the (left) model-independent or (right) model-dependent search. For the model-independent scenario, the discovery regions correspond to low-anomaly score regions fitted together with a high-anomaly score discovery signal bin at a time. Each layer corresponds to the different fits with the same control regions and low-anomaly score regions, and varying signal bins. The $< 90\%$ ($< 50\%$) label corresponds to the requirement on the anomaly score to be below the 90% (50)% background rejection point. For the model-dependent scenario, all benchmark regions are used simultaneously together with the control regions in a single profile likelihood fit to data, illustrated with one single layer

taneous fit to data discussed in Sect. 9, the yields of $ZZ$ with additional light-flavour jets with zero, one or two on-shell $Z$ boson candidates ($ZZ_{0Z}$ + LF, $ZZ_{1Z}$ + LF, $ZZ_{2Z}$ + LF), $ZZ$ with additional heavy-flavour jets ($ZZ$ + HF), $W^{\pm}Z$ with additional light- and heavy-flavour jets ($W^{\pm}Z$ + LF, $W^{\pm}Z$ + HF), $t\bar{t}Z$, and non-prompt-lepton backgrounds, are adjusted via normalisation factors included in the likelihood fit, as described in Sect. 9.

The main background contributions with prompt leptons in the regions with $\geq 4\ell$ originate from $ZZ$, $t\bar{t}Z/\gamma^*$, and $VVV$ production. Smaller contributions originate from the following rare processes: $t\bar{t}H$, $t\bar{t}t\bar{t}$, $tZq$, $tW$, $tWZ$, $t\bar{t}WW$, and $t\bar{t}t$ production.

A data-driven correction to the $VV$ jet multiplicity spectrum is derived from a $W^{\pm}Z$ region enriched in $W^{\pm}Z$ + LF jets, following the procedure described in Ref. [19]. The WZ/ttZ CR is used in the likelihood fit to improve the prediction of the background contribution from the $W^{\pm}Z$ + LF jets, $W^{\pm}Z$ + HF jets, and $t\bar{t}Z/\gamma^*$ processes. The number of $b$-jets provides good discrimination in the WZ/ttZ CR between the $W^{\pm}Z$ and $t\bar{t}Z/\gamma^*$ processes and is the variable used in this region in the fit. The low-anomaly-score regions, as defined in Sect. 6, are enriched in $ZZ$ background and provide constraints on the $ZZ$ background process, where different normalisation factors are assigned to the contributions from $ZZ$ + LF jets ($ZZ_{0Z}$ + LF, $ZZ_{1Z}$ + LF, $ZZ_{2Z}$ + LF), and $ZZ$ + HF jets. The splitting of the low-anomaly score discovery regions $4\ell$ $Q = 0$ 1Z 2SFOS and $4\ell$ $Q = 0$ 2Z based on the $b$-jet multiplicity allows further discrimination between $ZZ$ + LF jets against $t\bar{t}Z$ and $ZZ$ + HF jets. The modelling of the dominant background processes was validated using events with low-anomaly scores. Figure 4 shows the modelling of some of the input variables to the AD training in regions enriched in $ZZ$ and $t\bar{t}Z/\gamma^*$ processes.

Non-prompt leptons originate from material conversions, LF and HF hadron decays, or the improper reconstruction of other particles, and their relative composition depends on the lepton quality requirements and event categories. These backgrounds are estimated from simulation, with the normalisation determined by the likelihood fit. The main contribution to the non-prompt-lepton background is from $t\bar{t}$ production, with smaller contributions from $V$+jets, single-top-quark, $t\bar{t}W$, and $W^{\pm}Z$ processes. A correction based on theoretical predictions at NNLO QCD and NLO EW [110] is applied to the $t\bar{t}$ process to improve the distributions of the $p_{\mathrm{T}}$ and of the invariant mass of the $t\bar{t}$ system ($m(t\bar{t})$) at parton level. The non-prompt leptons in the simulated samples are labelled according to whether they originate from HF or LF hadron decays, or from a material conversion candidate. The HF category includes leptons from both bottom and charm decays. In the discovery/benchmark regions there are additional contributions from backgrounds with more than one non-prompt lepton (referred to as "multifakes"). The non-prompt lepton composition in multifakes varies depending on the region, and the presence of each non-prompt lepton type is corrected with the corresponding normalisation factor.

Normalisation factors for four non-prompt-lepton background contributions (HF non-prompt electron, HF non-prompt muon, LF non-prompt electron, and electron from internal or material conversion) are estimated from the likelihood fit to data. The measured values of the six prompt-lepton and four non-prompt-lepton background normalisation factors in the fit to data for the background-only hypothesis using the CRs and the low-anomaly score discovery regions are:

$\lambda_{W}^{\pm}Z$ + LF $= 0.98 \pm 0.09$, $\lambda_{W}^{\pm}Z$ + HF $= 1.15 \pm 0.31$, $\lambda_{ZZ_{0Z}+\mathrm{LF}} = 0.87 \pm 0.07$, $\lambda_{ZZ_{1Z}+\mathrm{LF}} = 1.01 \pm 0.04$, $\lambda_{ZZ_{2Z}+\mathrm{LF}} = 1.04 \pm 0.04$, $\lambda_{t\bar{t}Z} = 1.31 \pm 0.11$, $\lambda_{e}^{\mathrm{heavy}} = 0.95 \pm 0.06$, $\lambda_{\mu}^{\mathrm{heavy}} = 0.95 \pm 0.04$, $\lambda_{e}^{\mathrm{light}} = 0.66 \pm 0.09$, and $\lambda_{e}^{\mathrm{conv}} = 1.03 \pm 0.09$.

Kinematic variables were constructed in the fake-enriched CRs in order to validate the modelling of inputs to the AD from fake processes. Figure 5 shows representative variables in the HFe CR, HF$\mu$ CR, LFe CR, and the W$\gamma^*$/$t\bar{t}\gamma^*$ validation region, where good background modelling is seen after the fit to data. The latter validation region is defined as the WZ/ttZ CR with the exception that a $Z$ boson candidate veto is applied. It is used to validate the modelling of the electron conversion background.

Backgrounds with leptons with the charge incorrectly assigned affect primarily the $2\ell SS$ and $4\ell$ $Q = \pm 2$ channels and predominantly arise from $t\bar{t}$ production, where one electron undergoes a hard bremsstrahlung and an asymmetric conversion ($e^{\pm} \to e^{\pm}\gamma^* \to e^{\pm}e^{+}e^{-}$) or a mismeasured track curvature. The muon charge misassignment rate is negligible in the $p_{\mathrm{T}}$ range relevant to this analysis. The electron charge misassignment rate is measured in data using samples of $Z \to e^{+}e^{-}$ events reconstructed as same-charge pairs and as opposite-charge pairs, with the background subtracted via a sideband method [89]. The charge misassignment rate is parameterised as a function of electron $p_{\mathrm{T}}$ and $|\eta|$. It varies from about $10^{-4}$ for low-$p_{\mathrm{T}}$ electrons ($17 \leq p_{\mathrm{T}} \leq 50$ GeV) that satisfy $|\eta| \leq 1.37$, to about $3 \times 10^{-2}$ for high-$p_{\mathrm{T}}$ electrons ($p_{\mathrm{T}} \geq 200$ GeV) in the region $2 \leq |\eta| \leq 2.47$. To estimate the electron QMisID background in each of the corresponding event categories, the measured charge misassignment rate is then applied to data events satisfying the requirements of the $2\ell SS$ and $4\ell$ $Q = \pm 2$ channels, except that the total lepton charge is required to be zero.

## 8 Systematic uncertainties

The search sensitivity is limited by the number of data events rather than by the systematic uncertainties in the background estimate. The uncertainty in the measurement of the

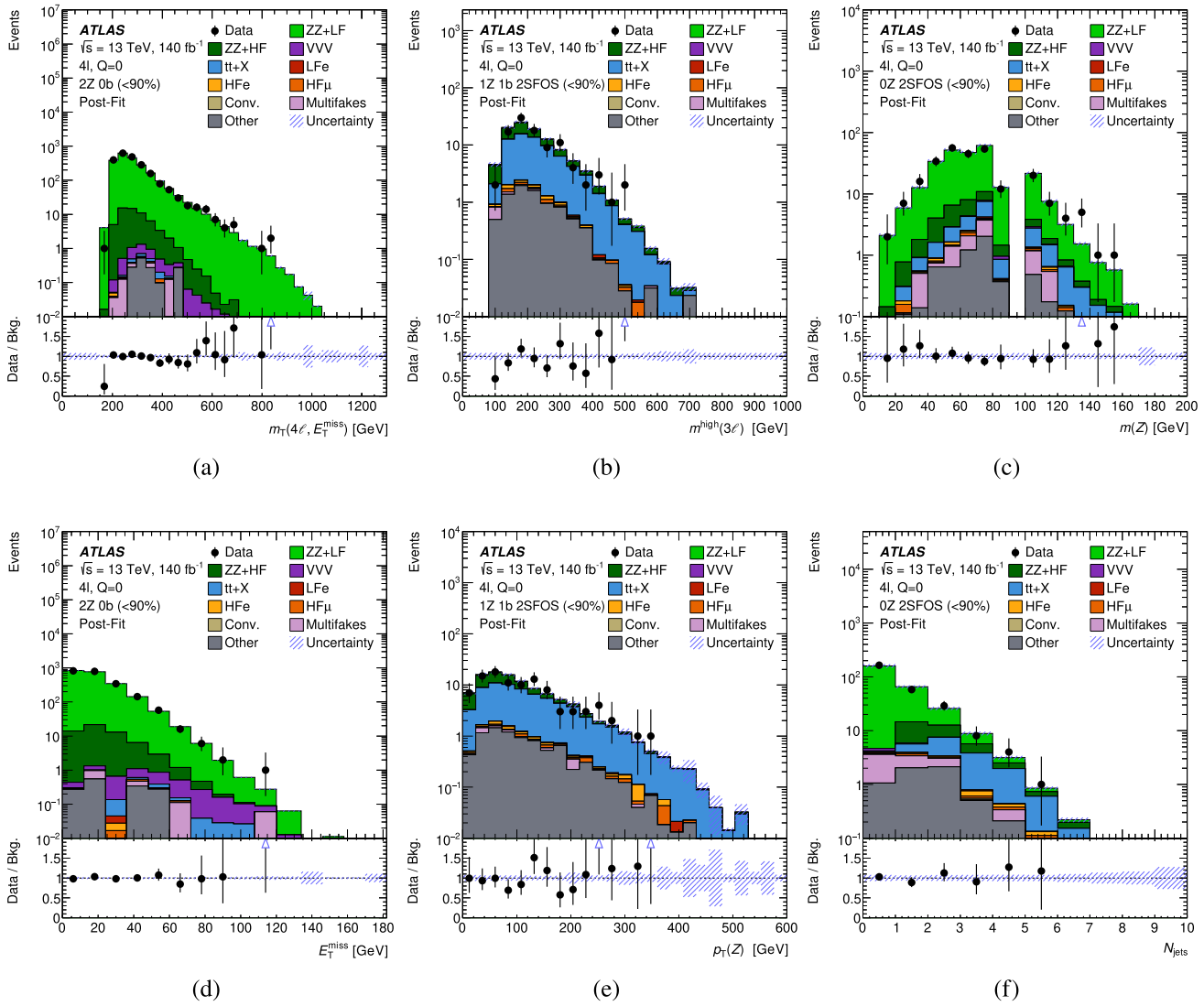


**Fig. 4** Comparison between data and the background prediction for the **a** $m_{\mathrm{T}}(4\ell, E_{\mathrm{T}}^{\mathrm{miss}})$, **b** $m^{\mathrm{high}}(3\ell)$, **c** $m(Z)$, **d** $E_{\mathrm{T}}^{\mathrm{miss}}$, **e** $p_{\mathrm{T}}(Z)$, and **f** $N_{\mathrm{jets}}$ distribution in the **a**, **d** 2Z 0b, **b**, **e** 1Z 1b 2SFOS, and **c**, **f** 0Z 2SFOS region, after requiring the anomaly score to be below the 90% background rejection point. The background contributions after the likelihood fit to data ('post-fit') for the background-only hypothesis are shown as filled histograms. The 'tt+X' background component includes the $t\bar{t}Z$, and $t\bar{t}H$ processes. The 'HF $\ell$' ('LF $\ell$') background component refers to processes containing one non-prompt light lepton from heavy-flavour (light-flavour) hadron decays. The ratio of the data to the background prediction ('Bkg.') is shown in the lower panel. The 'Other' contribution is dominated by the $tWZ$ production. The size of the combined statistical and systematic uncertainty in the background prediction is indicated by the blue hatched band. The upward-pointing blue arrows indicate points for which the data-to-background ('Data/Bkg.') ratio exceeds the vertical range of the figure. The last bin contains the overflow

combined 2015–2018 integrated luminosity is 0.83% [111], obtained using the LUCID-2 detector [26] for the primary measurements, complemented by the ones using the inner detector and calorimeters.

Uncertainties associated with the lepton selection arise from the trigger, reconstruction, identification and isolation efficiencies, and the lepton momentum scale and resolution [89,112,113].

Uncertainties associated with the jet selection arise from the JES, the JVT requirement and the JER [96,97]. The JES and its uncertainties are derived by combining information from test-beam data, collision data and simulation [96]. The JES (JER) have 30 (13) components included in the fit. The uncertainties in the JES, JER and JVT increase at lower jet $p_{\mathrm{T}}$. The efficiency of the flavour-tagging algorithm is measured for each jet flavour using control samples in data and in simulation. From these measurements, correction factors are

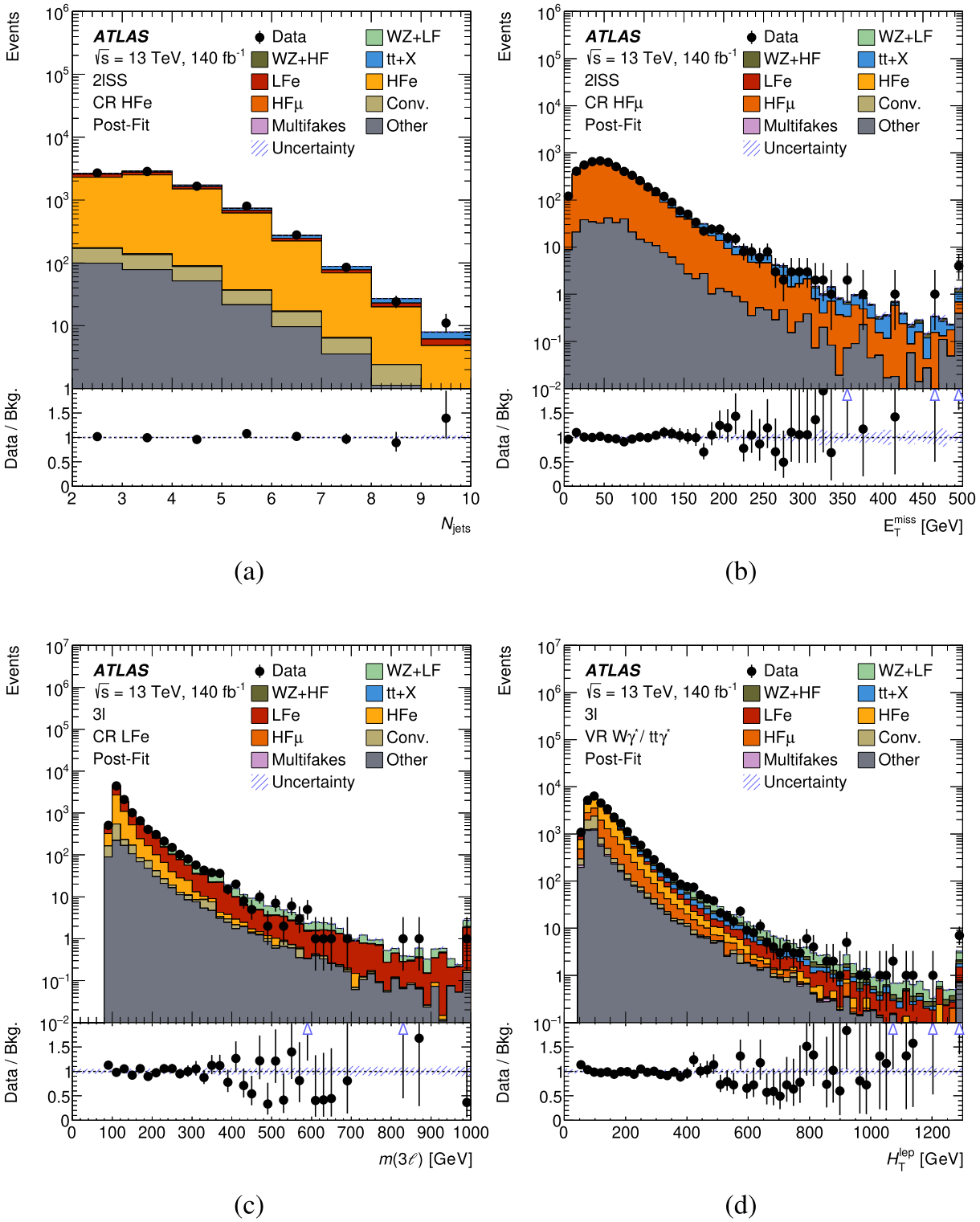


**Fig. 5** Comparison between data and the background prediction for the **a** $N_{\text{jets}}$, **b** $E_{\text{T}}^{\text{miss}}$, **c** $m(3\ell)$, and **d** $H_{\text{T}}^{\text{lep}}$ distribution in the **a** HFe CR, **b** HF$\mu$ CR, **c** LFe CR, and **d** the W$\gamma^*$/$t\bar{t}\gamma^*$ validation region. The background contributions after the likelihood fit to data ('post-fit') for the background-only hypothesis are shown as filled histograms. The ratio of the data to the background prediction ('Bkg.') is shown in the lower panel. The 'tt+X' background component includes the $t\bar{t}W$, $t\bar{t}Z$, and $t\bar{t}H$ processes. The 'Other' contribution in the $2\ell SS$ regions is dominated by the $t\bar{t}$ and $t\bar{t}W$ production, and in the $3\ell$ regions is dominated by the $ZZ$ + LF production. The size of the combined statistical and systematic uncertainty in the background prediction is indicated by the blue hatched band. The upward-pointing blue arrows indicate points for which the data-to-background ('Data/Bkg.') ratio exceeds the vertical range of the figure. The last bin contains the overflow

derived to correct the tagging rates in the simulation [100–102]. Experimental uncertainties in these correction factors are taken as uncorrelated between $b$-jets, $c$-jets, and light-flavour jets. An additional uncertainty is assigned to account for the extrapolation of the $b$-tagging efficiency measurement from the $p_{\mathrm{T}}$ region used to determine the correction factors to regions with higher transverse momentum. Uncertainties on $E_{\mathrm{T}}^{\mathrm{miss}}$ are estimated by propagating the uncertainties on the energy and momentum scale of each of the objects contributing to its calculation, and on the soft term resolution and scale [103].

The modelling uncertainties in the main backgrounds are assessed through comparisons with alternative MC samples. Additional uncertainties are evaluated from renormalisation and factorisation scale variations by a factor of 0.5 and 2, relative to the nominal scales, for the $t\bar{t}$, $Z+$jets, $t\bar{t}W$, $t\bar{t}Z$, and diboson samples. An additional 20% uncertainty is assigned to the $t\bar{t}W$ electroweak contribution [114].

For the $t\bar{t}$ process, four additional uncertainties are considered related to the reweighting method itself, derived by comparing the nominal reweighted SM $t\bar{t}$ sample to a sample obtained through an alternative reweighting, where the renormalisation and the factorisation scales are separately varied by a factor of 0.5 and 2 and the reweighting is applied on the (anti-)top quark $p_{\mathrm{T}}$ or on the $m(t\bar{t})$ distribution independently.

All alternative $t\bar{t}$ MC samples are reweighted to the same higher-order predictions as the nominal POWHEG + PYTHIA 8.230 MC sample. In addition to the comparison to the alternative MC sample POWHEG BOX + HERWIG 7.1.3, the nominal predictions are also compared with those obtained from an alternative sample generated as the nominal sample but setting the $p_{\mathrm{T}}^{\mathrm{hard}}$ parameter in PYTHIA to 1 instead of 0 [115]. This parameter regulates the definition of the vetoed region of the showering to avoid holes or overlaps in the phase space filled by POWHEG and PYTHIA. An uncertainty related to the choice of the $h_{\mathrm{damp}}$ parameter is estimated by comparing the predictions of the nominal sample to those obtained with an alternative sample with the $h_{\mathrm{damp}}$ parameter increased by a factor of 1.5 compared with its nominal value. Variations in the initial-state radiation (ISR) are estimated by varying the factorisation and renormalisation scales independently up and down by a factor of two. Similarly, the uncertainty related to final-state radiation (FSR) is assessed by varying the renormalisation scale for final-state PS emissions up and down by a factor of two. Finally, the uncertainty associated with the A14 tune is derived by varying the A14 tune (Var3c), which affects the renormalisation scale variations in the ISR PS. No theory reweighting is applied to this systematic.

For the $Z+$jets process, the uncertainty related to the upper cut-off of perturbative calculations for PS evolution is known as the re-summation scale. This uncertainty is evaluated at truth level by varying the nominal value of 2 GeV by a factor of 4 up and 1/4 down. Fiducial cuts are applied at truth level to define a phase space close to that used at reconstruction level in the discovery/benchmark regions where $Z+$jets is a dominant background. Additionally, the uncertainty related to the choice of the CKKW merging scale, i.e. the scale for calculating the overlap between jets from the ME and the PS, is derived similarly; the nominal value of 20 GeV is varied down to 15 GeV and up to 30 GeV and differences relative to the nominal distribution are evaluated at truth level.

The statistical uncertainty in the fitted parameters for the $VV$ jet-multiplicity correction is propagated as an uncertainty in the diboson background. Finally, additional normalisation uncertainties are included for all processes whose normalisation is not obtained from the fit. In particular, for the $t\bar{t}t\bar{t}$, $t\bar{t}H$, and $tZ$ processes, cross-section uncertainties of 20% [75], 11% [116], and 5% [117] are assigned, respectively, while for $t\bar{t}t$, $tWZ$, $t\bar{t}WW$, and triboson backgrounds a 50% cross-section uncertainty is assigned as a conservative estimate, since they are small backgrounds and have low impact on the search. Additional modelling uncertainties are considered for $t\bar{t}W$, $t\bar{t}H$, and $t\bar{t}t\bar{t}$ by comparing the nominal MC event generation described in Sect. 3 to alternative samples: SHERPA 2.2.10 ($t\bar{t}W$ and $t\bar{t}t\bar{t}$) and MADGRAPH5_AMC@NLO and PYTHIA 8 ($t\bar{t}H$).

Uncertainties in the modelling of the signal samples are evaluated from independently varying the renormalisation and factorisation scale by a factor of 0.5 and 2, relative to the nominal scales.

A systematic uncertainty of 20% is assigned to the background from electrons with a misidentified charge and accounts for the disagreement observed between the MC simulation for this background and data in the same-sign charge $ee$ inclusive region.

## 9 Results

A maximum-likelihood fit is performed on all bins in the control regions and discovery/benchmark regions considered in this search as shown in Fig. 3 to simultaneously determine the signal and background yields that are most consistent with the data. In the case of the model-independent fit, five cut-based control regions and ten low-anomaly score discovery regions are fitted together with one signal bin at a time (16 discovery signal bins corresponding to 16 different fits). The total event yields are used in all regions, except for the WZ/ttZ CR where the $N_{b-\mathrm{jets}}$ distribution is used. In the case of the model-dependent fit, the same five cut-based control regions are fitted together with 32 benchmark regions. In each benchmark region, the anomaly score distribution is fitted to data with the exception of the $\geq 5\ell$ 0Z benchmark regions, where the total event yield is fitted.

The likelihood function $\mathcal{L}(\mu, \boldsymbol{\lambda}, \boldsymbol{\theta})$ is constructed as a product of Poisson probability terms over all bins considered in the search, and depends on: the signal-strength parameter, $\mu$, a multiplicative factor applied to the predicted yield for the probed signal (model-dependent, as detailed in Sect. 9.2) or a dummy signal (model-independent, as detailed in Sect. 9.1); $\boldsymbol{\lambda}$, the normalisation factors for several backgrounds; $\boldsymbol{\theta}$, a set of nuisance parameters (NPs), encoding systematic uncertainties in the signal and background expectations [118]. Both $\mu$ and $\boldsymbol{\lambda}$ are treated as free parameters in the likelihood fit. The NPs $\boldsymbol{\theta}$ allow variations of the expectations for signal and background according to the systematic uncertainties, subject to Gaussian or Poisson constraints in the likelihood fit. Statistical uncertainties in each bin due to the limited size of the simulated samples are taken into account by dedicated parameters using the Beeston–Barlow 'lite' technique [119].

The test statistic $q_\mu$ is defined as the profile likelihood ratio: $q_\mu = -2\ln(\mathcal{L}(\mu, \hat{\boldsymbol{\lambda}}_\mu, \hat{\boldsymbol{\theta}}_\mu)/\mathcal{L}(\hat{\mu}, \hat{\boldsymbol{\lambda}}_{\hat{\mu}}, \hat{\boldsymbol{\theta}}_{\hat{\mu}}))$, where $\hat{\mu}$, $\hat{\boldsymbol{\lambda}}_{\hat{\mu}}$, and $\hat{\boldsymbol{\theta}}_{\hat{\mu}}$ are the values of the parameters that maximise the likelihood function, and $\hat{\boldsymbol{\lambda}}_\mu$ and $\hat{\boldsymbol{\theta}}_\mu$ are the values of the parameters that maximise the likelihood function for a given value of $\mu$. The test statistic $q_\mu$ is evaluated with the RooFit package [120]. A related statistic is used to determine the probability that the observed data are incompatible with the background-only hypothesis by setting $\mu = 0$ in the profile likelihood ratio ($q_0$). The $p$-value (referred to as $p_0$) representing the probability of the data being compatible with the background-only hypothesis is estimated by integrating the distribution of $q_0$ from background-only pseudo-experiments above the observed value of $q_0$. Upper limits on the signal production cross-section, calculated for either a dummy signal in the model-independent scenario or for each of the signal scenarios considered in the model-dependent scenario, are derived by using $q_\mu$ in the $\mathrm{CL_s}$ method [121,122]. For a given signal scenario, values of the production cross-section (parameterised by $\mu$) yielding $\mathrm{CL_s} < 0.05$ are excluded at $\geq 95\%$ CL, where $\mathrm{CL_s}$ is computed using pseudo-experiments for the model-independent scenario and the flavourful VLL model-dependent search, and the asymptotic approximation [123] for the other model-dependent signal benchmarks.

### 9.1 Model-independent results

Figure 6 shows the data and background prediction for the adjacent anomaly score distributions including all signal bins used. No significant deviations from the SM expectations are observed in any of the signal bins considered, with the largest excess seen in the $Q = \pm 2$ and $0Z$ 2SFOS ($> 99.9\%$) regions corresponding to $2\sigma$ local significance each. The global significance is $0.90\sigma$ and takes into account the look-elsewhere effect. The global significance is estimated through the simulation of a large number of pseudo-experiments according to the background-only expected number of events. Pseudo-experiments are generated using all systematic and statistical uncertainties, by suitably fluctuating each discovery region in a simultaneous and correlated way. Overlaps between discovery regions are further accounted for in the calculation of the look-elsewhere effect.

To calculate an excluded visible cross section, a dummy signal is injected into each signal bin, with a free-floating normalisation parameter (signal strength), denoted $\mu$. The signal bin is then used along with the control regions and low-anomaly score discovery regions in a profile-likelihood fit, and a 95% confidence limit is found. The excluded visible cross section, $\sigma_{vis}$, is then given by:

$$\sigma_{vis} = \mu \frac{N_{sig}}{\mathcal{L}} \tag{2}$$

where $N_{sig}$ is the number of injected dummy signal events and $\mathcal{L}$ is the integrated luminosity.

Figure 7 shows the expected excluded visible cross section, along with the observed excluded cross section for each model-independent signal bin. The expected significances in each of the model-independent fits to some benchmark signal models (single and doublet $\mathrm{VLL}_e$ and $\mathrm{VLL}_\mu$, flavourful $\mathrm{VLL}_e$ and $\mathrm{VLL}_\mu$, wino-like chargino and neutralino, and smuon) can be seen in Fig. 8. The discovery regions with the largest sensitivity to the benchmark models are $4\ell$ $Q = 0$ $0Z$ 2SFOS ($> 99.9\%$) and $\geq 5\ell$ $0Z$ for flavourful $\mathrm{VLL}_e$ and wino-like chargino and neutralino, $4\ell$ $Q = 0$ ($> 99\%$) for $\mathrm{VLL}_\mu^{\mathrm{D}}$, and $\geq 5\ell$ $0Z$ for smuon.

The search is dominated by statistical uncertainties due to the requirement of a large lepton multiplicity: the expected limits obtained with full systematic uncertainties worsen at most 12% relative to the limits including only statistical uncertainties.

### 9.2 Model-dependent results

Comparisons between data and the background prediction for the anomaly score distributions used in a selection of benchmark regions are shown in Fig. 9. Representative benchmark signal models are overlaid in the regions where they are expected to be dominant. No significant deviations from the SM expectations are observed in any of the benchmark regions considered. The smallest p-value for the newly probed flavourful VLL is 0.26 for a $\mathrm{VLL}_\mu$ of mass 800 GeVand a scalar mass of 350 GeV, which corresponds to a local significance of $0.63\ \sigma$.

Limits at 95% CL on the cross-section of relevant benchmark signal models as a function of particle masses are set. Figure 10a–d show the limits on the cross-section for the models: $\mathrm{VLL}_e^{\mathrm{D}}$, $\mathrm{VLL}_\mu^{\mathrm{D}}$, $\mathrm{VLL}_e^{\mathrm{S}}$, and $\mathrm{VLL}_\mu^{\mathrm{S}}$. Limits from

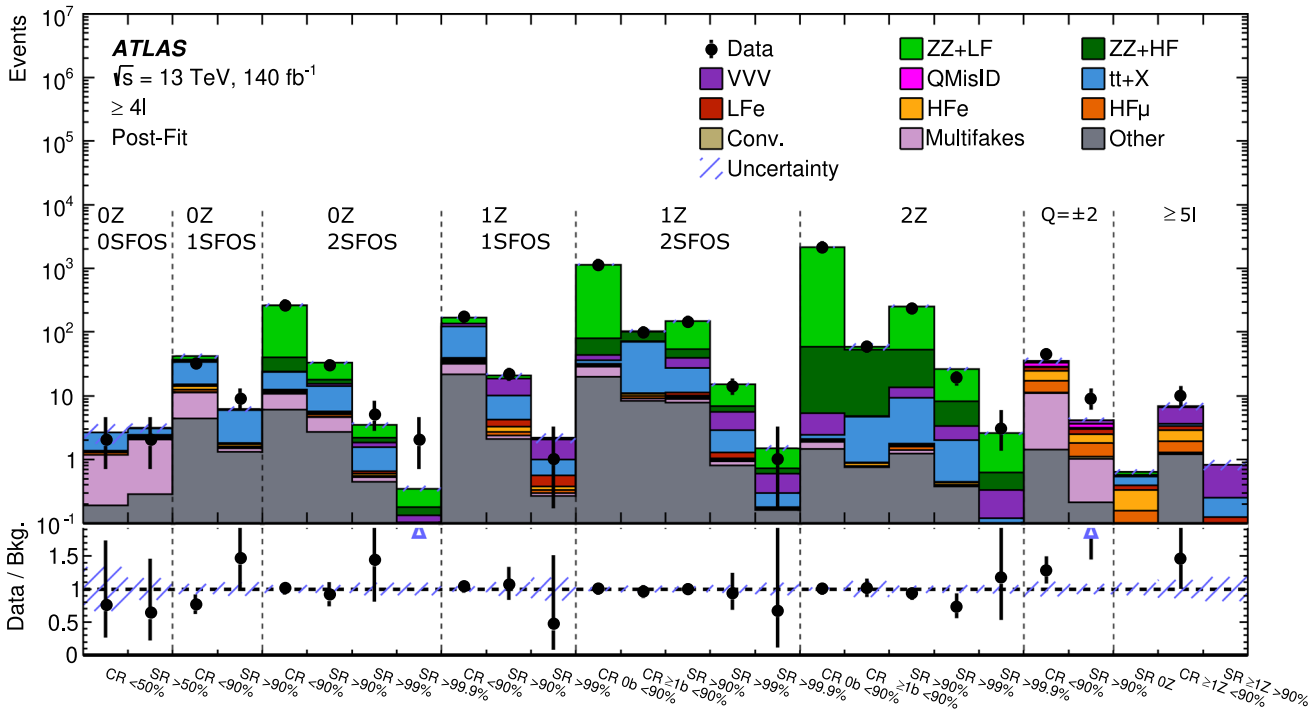


**Fig. 6** Comparison between data and the background prediction for the discovery regions included in the model-independent fit, after a background-only fit to data in the five cut-based control regions and ten low-anomaly score discovery regions ('post-fit'). All signal bins are shown ('SR') together with the low-anomaly score discovery regions ('CR'). The various requirements on the anomaly score corresponding to the specified background rejection cuts (99.9/99/90/50%) are shown for all SRs and CRs, except for the $\geq 5\ell$ 0Z SR, where no AD is applied. The lower panels show the ratio of data to the background estimate ('Bkg'). The 'tt+X' background component includes the $t\bar{t}Z$ ($4\ell$ only) and $t\bar{t}H$ processes. The 'Other' contribution is dominated by the $VH$ process. The size of the combined statistical and systematic uncertainty in the background prediction is indicated by the blue hatched band. The upward-pointing blue arrows indicate points for which the data-to-background ('Data/Bkg.') ratio exceeds the vertical range of the figure

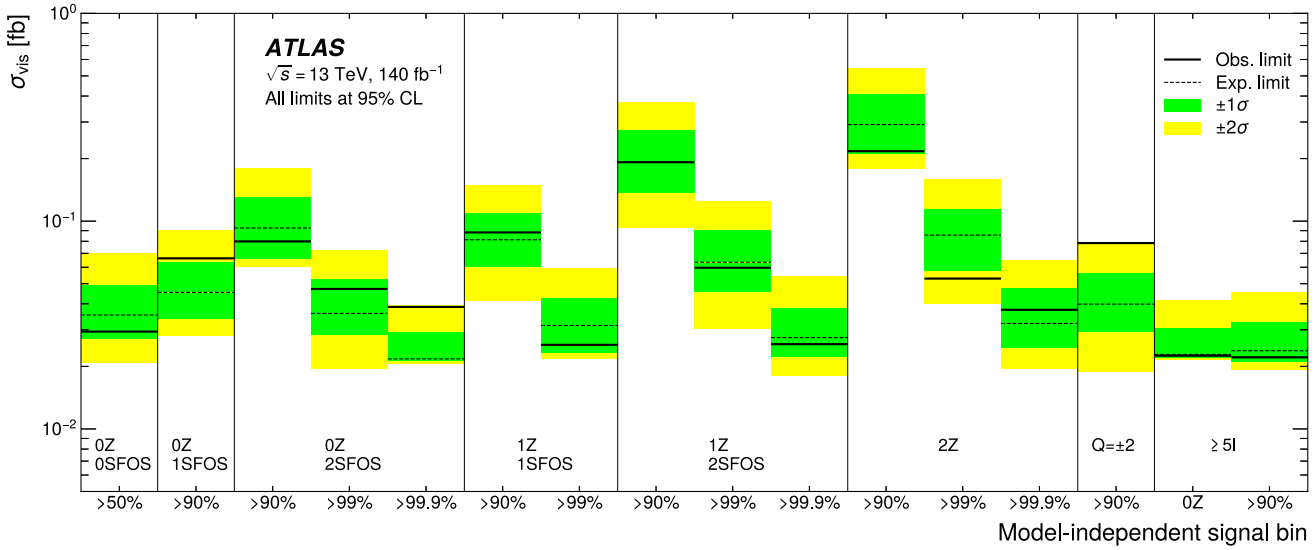


**Fig. 7** Observed and expected excluded visible cross section limits, $\sigma_{\text{vis}}$ for the model-independent regions. The various requirements on the anomaly score corresponding to the specified background rejection cuts (99.9/99/90/50%) are shown for all regions, except for the $\geq 5\ell$ 0Z SR, where no AD is applied

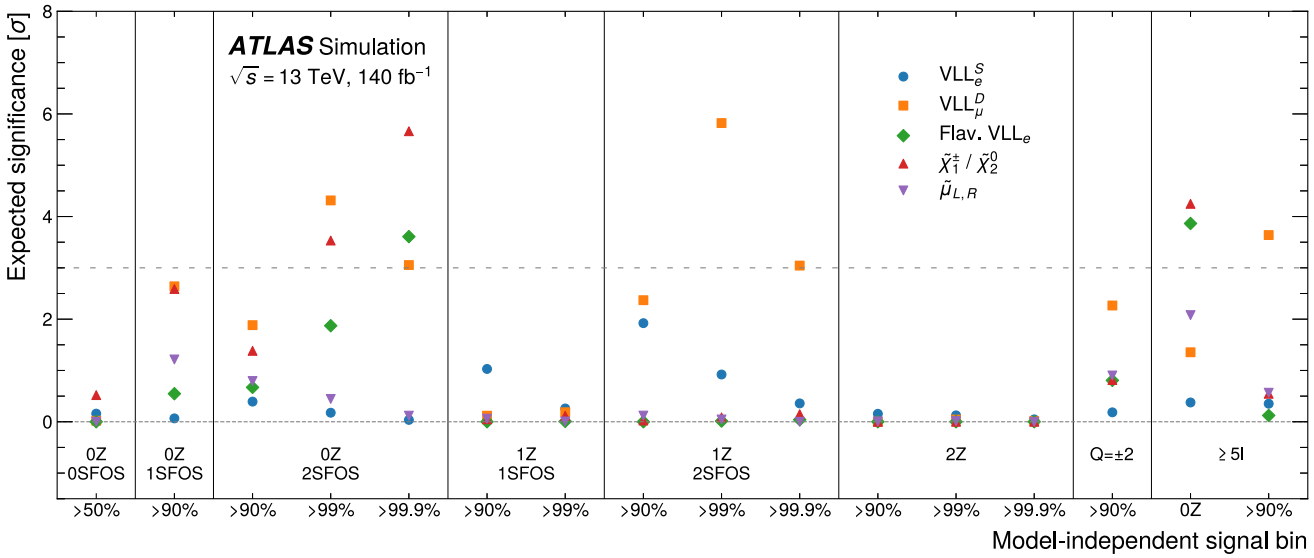


**Fig. 8** Expected significance in the model-independent regions to the benchmark signal models: VLL$_e^S$ with a mass of 200 GeV, VLL$_\mu^D$ with a mass of 600 GeV, flavourful VLL$_e$ with a mass of 1200 GeV and a scalar $S$ mass of 550 GeV, wino-like chargino with a mass of 1300 GeV and a neutralino mass of 800 GeV, and smuon with a mass of 350 GeV and a neutralino mass of 250 GeV. The various requirements on the anomaly score corresponding to the specified background rejection cuts (99.9/99/90/50%) are shown for all regions, except for the $\geq 5\ell$ 0Z SR, where no AD is applied

the dedicated ATLAS search [19] are overlaid, considering only the $4\ell$ channel. The VLL$_e^S$ is observed (expected) to be excluded at 95% CL for masses up to 290 (290) GeV while the VLL$_e^D$ is observed (expected) to be excluded at 95% CL for masses up to 925 (880) GeV. The VLL$_\mu^S$ is observed (expected) to be excluded at 95% CL for masses up to 320 (320) GeV while the VLL$_\mu^D$ is observed (expected) to be excluded at 95% CL for masses up to 850 (925) GeV. These limits are more stringent than those from the dedicated analysis considering only the $4\ell$ channel where a simple counting analysis is performed.

Figures 10e and 10f show the first ever limits on the flavourful VLL$_e$ or VLL$_\mu$ mass and the scalar $S$. The flavourful VLL$_e$ is observed (expected) to be excluded at 95% CL for masses up to 1300 (1340) GeV while the flavourful VLL$_\mu$ is observed (expected) to be excluded at 95% CL for masses up to 1280 (1375) GeV, for all allowed scalar $S$ masses except for the lowest and highest values, where the exclusion can be up to about 50 GeV weaker.

Figure 11 shows the limits on the supersymmetric models considered, wino-like chargino and neutralino, and smuon. Wino-like charginos are observed (expected) to be excluded at 95% CL for masses up to 1600 (1600) GeV. Smuon masses up to 495 (530) GeV are observed (expected) to be excluded at 95% CL. Whereas the limits from the dedicated wino-like chargino and neutralino analysis are more stringent than the current analysis, for the smuon model this result is more sensitive for $\Delta m(\tilde{\mu}_{\mathrm{L,R}}, \tilde{\chi}_1^0)$ larger than 140 GeV compared to the existing expected limits.

## 10 Conclusions

A model-independent search for BSM physics with anomaly detection techniques is presented. The search is based on a data sample of proton–proton collisions recorded at $\sqrt{s} = 13$ TeV by the ATLAS detector during Run 2 of the LHC, corresponding to an integrated luminosity of 140 fb$^{-1}$. The search is performed in final states with $\geq 4$ light leptons $(e, \mu)$. The use of anomaly detection optimises the sensitivity of the signal regions to Beyond the Standard Model physics without assuming a specific model. A model-dependent analysis is also performed to demonstrate the sensitivity of the anomaly detection technique with respect to a selection of benchmark models. The dominant backgrounds originate from $ZZ$, $t\bar{t}Z/\gamma^*$, and $VVV$ production, as well as SM processes with fake leptons, and are estimated from Monte-Carlo simulation and normalised to data in a simultaneous fit. The data are found to be consistent with the Standard Model predictions and exclusion limits are set on the visible cross section for each model-independent signal region. Additionally, exclusion limits on the mass of vector-like leptons, wino-like charginos and neutralinos, and smuons are set in the model-dependent analysis using the same anomaly detection discriminant as with the model-independent search, with a different event categorisation. The expected exclusion limits are generally competitive to the ones from dedicated searches, in some cases improving the sensitivity in corners of the available phase space.

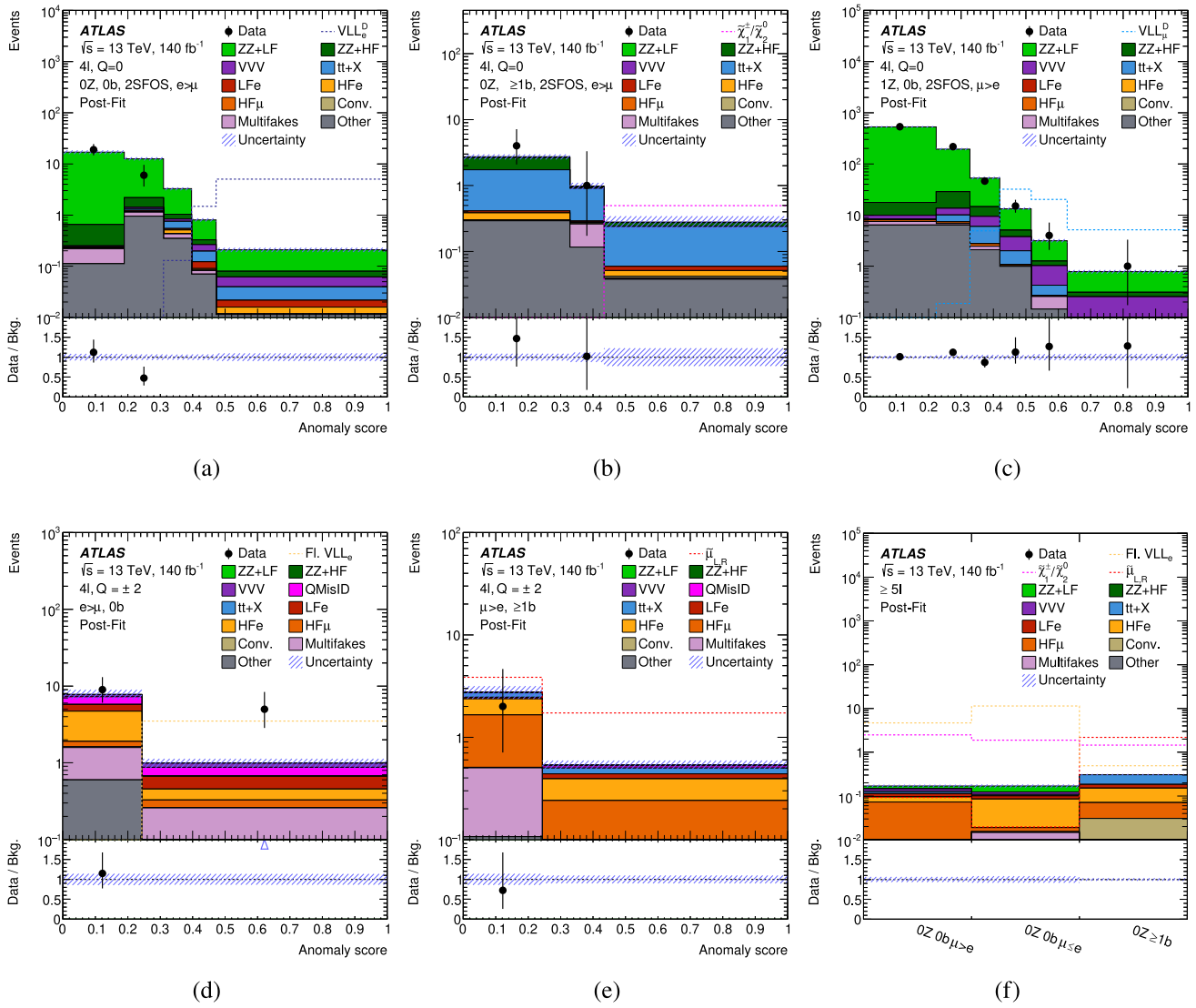


**Fig. 9** Comparison between data and the background estimate for the anomaly score distribution used in different benchmark regions, after a background-only fit to data ('post-fit'): **a** $4\ell$ $Q = 0$ 0Z 0b 2SFOS $e > \mu$, **b** $4\ell$ $Q = 0$ 0Z $\geq$1b 2SFOS $e > \mu$, **c** $4\ell$ $Q = 0$ 1Z 0b 2SFOS $\mu > e$, **d** $4\ell$ $Q = \pm 2$ 0b $e > \mu$, **e** $4\ell$ $Q = \pm 2 \geq$ 1b $\mu > e$, and **f** the three $\geq 5\ell$ regions: 0Z 0b $\mu > e$, 0Z 0b $e \geq \mu$, and 0Z $\geq$1b, defined without AD. Distributions for a $\text{VLL}_e$ and $\text{VLL}_\mu$ signal point of mass 500 GeV, one flavourful $\text{VLL}_e$ signal point for a VLL mass of 1 TeV and scalar of 550 GeV, a wino-like chargino and neutralino signal point of mass 1.3 TeV, and a smuon signal point of mass 350 GeV and neutralino mass of 250 GeV are overlaid for comparison. The lower panels show the ratio of data to the background estimate ('Bkg.'). The 'tt+X' background component includes the $t\bar{t}Z$ ($4\ell$ only) and $t\bar{t}H$ processes. The 'Other' contribution is dominated by the $VH$ process. The size of the combined statistical and systematic uncertainty in the signal-plus-background prediction is indicated by the blue hatched band. The upward-pointing blue arrow indicates a point for which the data-to-background ('Data/Bkg.') ratio exceeds the vertical range of the figure

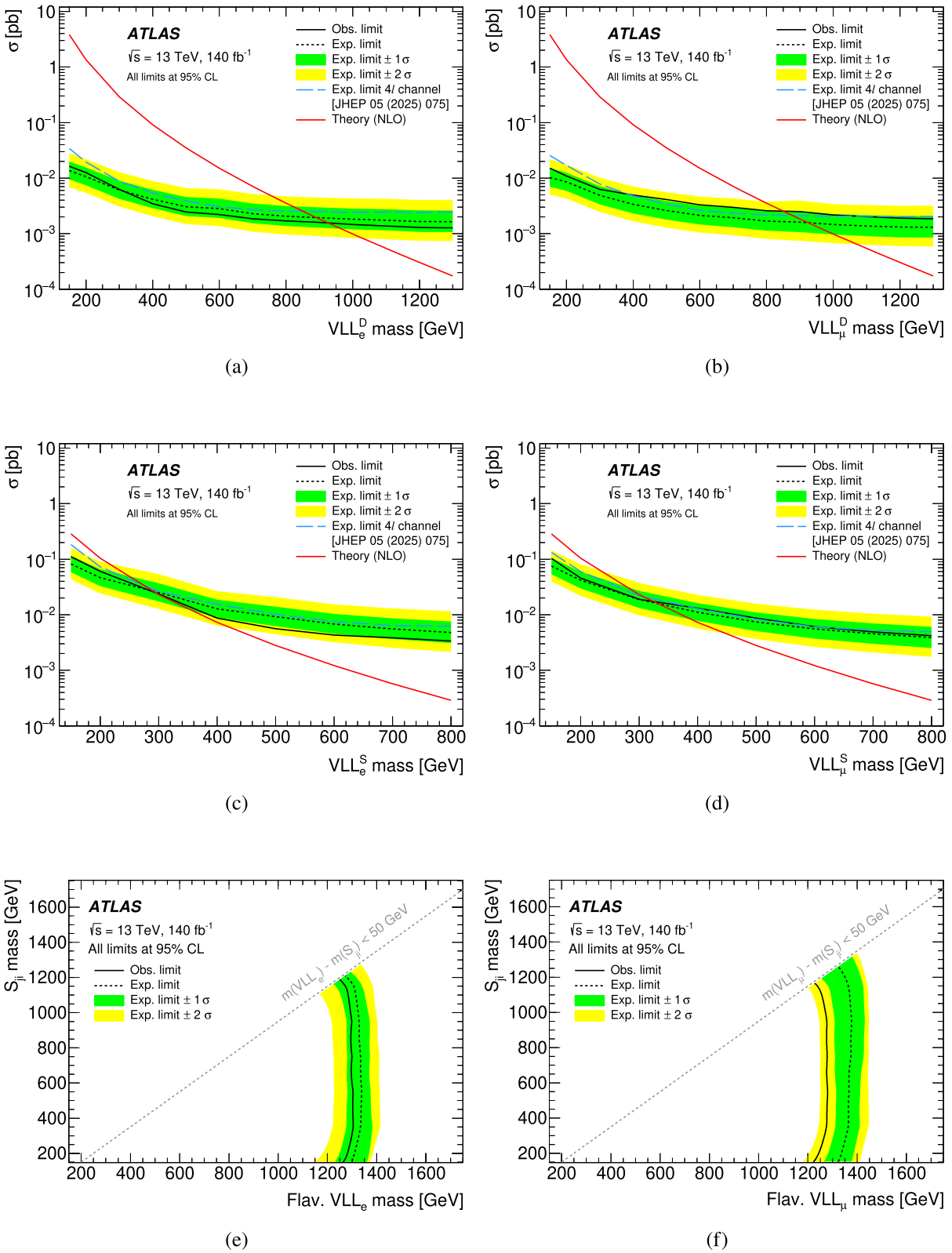


**Fig. 10** Combined observed and expected limits at 95% CL on the cross-section ($\sigma$) as a function of the VLL mass for the **a** VLL$_e^D$, **b** VLL$_\mu^D$, **c** VLL$_e^S$, **d** VLL$_\mu^S$ models, and on the plane of the $S_{ji}$ mass versus the VLL mass for the **e** flavourful VLL$_e$, and **f** flavourful VLL$_\mu$ models. The expected limits from the dedicated ATLAS search [19], considering only the $4\ell$ channel, are overlaid in dashed grey lines in **a**–**d**. The inner and outer bands around the expected limit are the $\pm1\sigma$ and $\pm2\sigma$ variations including all uncertainties, respectively

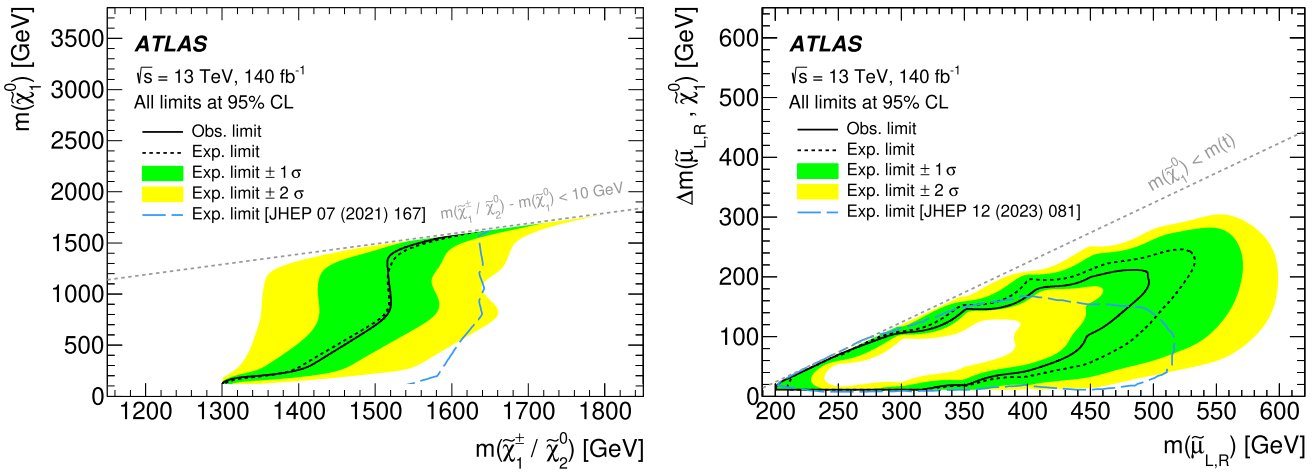


(a) (b)

**Fig. 11** Combined observed and expected limits at 95% CL for the **a** wino-like chargino and neutralino, and **b** smuon models, as a function of the masses of $\tilde{\chi}_1^{\pm}/\tilde{\chi}_2^0$ and $\tilde{\chi}_1^0$, and $\tilde{\mu}_{\mathrm{L,R}}$ and $\Delta m(\tilde{\mu}_{\mathrm{L,R}}, \tilde{\chi}_1^0)$, respectively. The expected limits from the dedicated ATLAS searches [21,22] are overlaid in dashed grey lines. The inner and outer bands around the expected limit are the $\pm 1\sigma$ and $\pm 2\sigma$ variations including all uncertainties, respectively

Exclusion limits are set on the flavourful VLL mass for the first time, excluding flavourful $\mathrm{VLL}_e$ ($\mathrm{VLL}_\mu$) masses up to 1300 (1280) GeV.

**Acknowledgements** We thank CERN for the very successful operation of the LHC and its injectors, as well as the support staff at CERN and at our institutions worldwide without whom ATLAS could not be operated efficiently. The crucial computing support from all WLCG partners is acknowledged gratefully, in particular from CERN, the ATLAS Tier-1 facilities at TRIUMF/SFU (Canada), NDGF (Denmark, Norway, Sweden), CC-IN2P3 (France), KIT/GridKA (Germany), INFN-CNAF (Italy), NL-T1 (Netherlands), PIC (Spain), RAL (UK) and BNL (USA), the Tier-2 facilities worldwide and large non-WLCG resource providers. Major contributors of computing resources are listed in Ref. [124]. We gratefully acknowledge the support of ANPCyT, Argentina; YerPhI, Armenia; ARC, Australia; BMWFW and FWF, Austria; ANAS, Azerbaijan; CNPq and FAPESP, Brazil; NSERC, NRC and CFI, Canada; CERN; ANID, Chile; CAS, MOST and NSFC, China; Minciencias, Colombia; MEYS CR, Czech Republic; DNRF and DNSRC, Denmark; IN2P3-CNRS and CEA-DRF/IRFU, France; SRNSFG, Georgia; BMFTR, HGF and MPG, Germany; GSRI, Greece; RGC and Hong Kong SAR, China; ICHEP and Academy of Sciences and Humanities, Israel; INFN, Italy; MEXT and JSPS, Japan; CNRST, Morocco; NWO, Netherlands; RCN, Norway; MNiSW, Poland; FCT, Portugal; MNE/IFA, Romania; MSTDI, Serbia; MSSR, Slovakia; ARIS and MVZI, Slovenia; DSI/NRF, South Africa; MICIU/AEI, Spain; SRC and Wallenberg Foundation, Sweden; SERI, SNSF and Cantons of Bern and Geneva, Switzerland; NSTC, Taipei; TENMAK, Türkiye; STFC/UKRI, United Kingdom; DOE and NSF, United States of America. Individual groups and members have received support from BCKDF, CANARIE, CRC and DRAC, Canada; CERN-CZ, FORTE and PRIMUS, Czech Republic; COST, ERC, ERDF, Horizon 2020, ICSC-NextGenerationEU and Marie Skłodowska-Curie Actions, European Union; Investissements d'Avenir Labex, Investissements d'Avenir Idex and ANR, France; DFG and AvH Foundation, Germany; Herakleitos, Thales and Aristeia programmes co-financed by EU-ESF and the Greek NSRF, Greece; BSF-NSF and MINERVA, Israel; NCN and NAWA, Poland; La Caixa Banking Foundation, CERCA Programme Generalitat de Catalunya and PROMETEO and GenT Programmes Generalitat Valenciana, Spain; Göran Gustafssons Stiftelse, Sweden; The Royal Society and Leverhulme Trust, United Kingdom. In addition, individual members wish to acknowledge support from CERN: European Organization for Nuclear Research (CERN DOCT); Chile: Agencia Nacional de Investigación y Desarrollo (FONDECYT 1230812, FONDECYT 1240864, Fondecyt 3240661, Fondecyt Regular 1240721); China: Chinese Ministry of Science and Technology (MOST-2023YFA1605700, MOST-2023YFA1609300), National Natural Science Foundation of China (NSFC - 12175119, NSFC 12275265); Czech Republic: Czech Science Foundation (GACR - 24-11373 S), Ministry of Education Youth and Sports (ERC-CZ-LL2327, FORTE CZ.02.01.01/00/22_008/0004632), PRIMUS Research Programme (PRIMUS/21/SCI/017); EU: H2020 European Research Council (ERC - 101002463); European Union: European Research Council (BARD No. 101116429, ERC - 948254, ERC 101089007), European Regional Development Fund (SMASH COFUND 101081355, SLO ERDF), European Union, Future Artificial Intelligence Research (FAIR-NextGenerationEU PE00000013), Italian Center for High Performance Computing, Big Data and Quantum Computing (ICSC, NextGenerationEU); France: Agence Nationale de la Recherche (ANR-21-CE31-0022, ANR-22-EDIR-0002, ANR-24-CE31-0504-01); Germany: Deutsche Forschungsgemeinschaft (DFG - 469666862, DFG - CR 312/5-2); China: Research Grants Council (GRF); Italy: Istituto Nazionale di Fisica Nucleare (ICSC, NextGenerationEU), Ministero dell'Università e della Ricerca (NextGenEU 153D23001490006 M4C2.1.1, NextGenEU I53D23000820006 M4C2.1.1, NextGenEU I53D23001490006 M4C2.1.1, SOE2024_0000023); Japan: Japan Society for the Promotion of Science (JSPS KAKENHI JP22H01227, JSPS KAKENHI JP22H04944, JSPS KAKENHI JP22KK0227, JSPS KAKENHI JP24K23939, JSPS KAKENHI JP24KK0251, JSPS KAKENHI JP25H00650, JSPS KAKENHI JP25H01291, JSPS KAKENHI JP25K01023); Norway: Research Council of Norway (RCN-314472); Poland: Ministry of Science and Higher Education (IDUB AGH, POB8, D4 no 9722), Polish National Science Centre (NCN 2021/42/E/ST2/00350, NCN OPUS 2023/51/B/ST2/02507, NCN UMO-2019/34/E/ST2/00393, UMO-2022/47/O/ST2/00148, UMO-2023/49/B/ST2/04085, UMO-2023/51/B/ST2/00920, UMO-2024/53/N/

ST2/00869); Portugal: Foundation for Science and Technology (FCT); Spain: Ministry of Science and Innovation (MCIN & NextGenEU PCI2022-135018-2, MICIN & FEDER PID2021-125273NB, RYC2019-028510-I, RYC2020-030254-I, RYC2021-031273-I, RYC2022-038164-I); Sweden: Carl Trygger Foundation (Carl Trygger Foundation CTS 22:2312), Swedish Research Council (Swedish Research Council 2023-04654, VR 2021-03651, VR 2022-03845, VR 2022-04683, VR 2023-03403, VR 2024-05451), Knut and Alice Wallenberg Foundation (KAW 2018.0458, KAW 2022.0358, KAW 2023.0366); Switzerland: Swiss National Science Foundation (SNSF - PCEFP2_194658); United Kingdom: Royal Society (NIF-R1-231091); United States of America: U.S. Department of Energy (ECA DE-AC02-76SF00515), Neubauer Family Foundation.

**Data Availability Statement** This manuscript has associated data in a data repository. [Author's comment: The public release of data supporting the findings of this article will follow the CERN Open Data Policy (CERN-OPEN-2020-013: https://cds.cern.ch/record/2745133). The values of relevant plots and tables associated with this article are stored in HEP Data https://www.hepdata.net/record/ins2964453.]

**Code Availability Statement** This manuscript has associated code/software in a data repository. [Author's comment: The ATLAS Collaboration's Athena software, including the configuration of the event generators, is open source (http://gitlab.cern.ch/atlas/athena).]


Funded by SCOAP[3].

## References

1. ATLAS Collaboration, Observation of a new particle in the search for the Standard Model Higgs boson with the ATLAS detector at the LHC. Phys. Lett. B **716**, 1 (2012). https://doi.org/10.1016/j.physletb.2012.08.020. arXiv:1207.7214 [hep-ex]
2. CMS Collaboration, Observation of a new boson at a mass of 125 GeV with the CMS experiment at the LHC. Phys. Lett. B **716**, 30 (2012). https://doi.org/10.1016/j.physletb.2012.08.021. arXiv:1207.7235 [hep-ex]
3. ATLAS Collaboration, Search for new phenomena in events with three or more charged leptons in (pp) collisions at $\sqrt{s} = 8$ TeV with the ATLAS detector. JHEP **08**, 138 (2015). https://doi.org/10.1007/JHEP08(2015)138. arXiv:1411.2921 [hep-ex]
4. ATLAS Collaboration, Search for new phenomena in three- or four-lepton events in (pp) collisions at $sqrts = 13$ TeV with the ATLAS detector. Phys. Lett. B **824**, 136832 (2022). https://doi.org/10.1016/j.physletb.2021.136832. arXiv:2107.00404 [hep-ex]
5. ATLAS Collaboration, Dijet resonance search with weak supervision using $\sqrt{s} = 13$ TeV (pp) collisions in the ATLAS detector. Phys. Rev. Lett. **125**, 131801 (2020). https://doi.org/10.1103/PhysRevLett.125.131801. arXiv:2005.02983 [hep-ex]
6. ATLAS Collaboration, Weakly supervised anomaly detection for resonant new physics in the dijet final state using proton–proton collisions at $\sqrt{s} = 13$ TeV with the ATLAS detector. Phys. Rev. D **112**, 072009 (2025). arXiv:2502.09770 [hep-ex]
7. CMS Collaboration, Model-agnostic search for dijet resonances with anomalous jet substructure in proton–proton collisions at $\sqrt{s} = 13$ TeV. Rep. Prog. Phys. **88**, 067802 (2024). https://doi.org/10.1088/1361-6633/add762. arXiv:2412.03747 [hep-ex]
8. ATLAS Collaboration, Search for new physics in final states with semivisible jets or anomalous signatures using the ATLAS detector. Phys. Rev. D **112**, 012021 (2025). https://doi.org/10.1103/44zp-mh1q. arXiv:2505.01634 [hep-ex]
9. ATLAS Collaboration, Search for new phenomena in two-body invariant mass distributions using unsupervised machine learning for anomaly detection at $\sqrt{s} = 13$ TeV with the ATLAS detector. Phys. Rev. Lett. **132**, 081801 (2024). https://doi.org/10.1103/PhysRevLett.132.081801. arXiv:2307.01612 [hep-ex]
10. ATLAS Collaboration, Anomaly detection search for new resonances decaying into a Higgs boson and a generic new particle (X) in hadronic final states using $\sqrt{s} = 13$ TeV (pp) collisions with the ATLAS detector. Phys. Rev. D **108**, 052009 (2023). https://doi.org/10.1103/PhysRevD.108.052009. arXiv:2306.03637 [hep-ex]
11. F. del Aguila, M.J. Bowick, The possibility of new fermions with $\Delta I = 0$ mass. Nucl. Phys. B **224**, 107 (1983). https://doi.org/10.1016/0550-3213(83)90316-4
12. P.M. Fishbane, R.E. Norton, M.J. Rivard, Experimental implications of heavy, isosinglet quarks and leptons. Phys. Rev. D **33**, 2632 (1986). https://doi.org/10.1103/PhysRevD.33.2632
13. P.M. Fishbane, P.Q. Hung, Lepton masses in a dynamical model of family symmetry. Z. Phys. C **38**, 649 (1988). https://doi.org/10.1007/BF01624371
14. I. Montvay, Three mirror pairs of fermion families. Phys. Lett. B **205**, 315 (1988). https://doi.org/10.1016/0370-2693(88)91671-1
15. K. Fujikawa, A vector-like extension of the standard model. Prog. Theor. Phys. **92**, 1149 (1994). https://doi.org/10.1143/PTP.92.1149. arXiv:hep-ph/9411258
16. F. del Aguila, L. Ametller, G. Kane, J. Vidal, Vector-like fermion and standard Higgs production at hadron colliders. Nucl. Phys. B **334**, 1 (1990). https://doi.org/10.1016/0550-3213(90)90655-W
17. N. Kumar, S.P. Martin, Vectorlike leptons at the large hadron collider. Phys. Rev. D **92**, 115018 (2015). https://doi.org/10.1103/PhysRevD.92.115018. arXiv:1510.03456 [hep-ph]
18. P.N. Bhattiprolu, S.P. Martin, Prospects for vectorlike leptons at future proton–proton colliders. Phys. Rev. D **100**, 015033 (2019). https://doi.org/10.1103/PhysRevD.100.015033. arXiv:1905.00498 [hep-ph]
19. ATLAS Collaboration, Search for vector-like leptons coupling to first- and second-generation Standard Model leptons in (pp) collisions at $\sqrt{s} = 13$ TeV with the ATLAS detector. JHEP **05**, 075 (2025). https://doi.org/10.1007/JHEP05(2025)075. arXiv:2411.07143 [hep-ex]
20. S. Bißmann, G. Hiller, C. Hormigos-Feliu, D.F. Litim, Multi-lepton signatures of vector-like leptons with flavor. Eur. Phys. J. C **81**, 101 (2021). https://doi.org/10.1140/epjc/s10052-021-08886-3. arXiv:2011.12964 [hep-ph]
21. ATLAS Collaboration, Search for supersymmetry in events with four or more charged leptons in 139 $\text{fb}^{-1}$ of $\sqrt{s} = 13$ TeV (pp) collisions with the ATLAS detector. JHEP **07**, 167 (2021). https://doi.org/10.1007/JHEP07(2021)167. arXiv:2103.11684 [hep-ex]
22. ATLAS Collaboration, Search for heavy Higgs bosons with flavour-violating couplings in multi-lepton plus (b)-jets final states in (pp) collisions at 13 TeV with the ATLAS detector. JHEP **12**, 081 (2023). https://doi.org/10.1007/JHEP12(2023)081. arXiv:2307.14759 [hep-ex]

23. ATLAS Collaboration, The ATLAS experiment at the CERN large hadron collider. JINST **3**, S08003 (2008). https://doi.org/10.1088/1748-0221/3/08/S08003
24. ATLAS Collaboration, ATLAS insertable B-layer: technical design report, ATLAS-TDR-19; CERN-LHCC-2010-013 (2010). https://cds.cern.ch/record/1291633. [Addendum: ATLAS-TDR-19-ADD-1; CERN-LHCC-2012-009 (2012). https://cds.cern.ch/record/1451888]
25. B. Abbott et al., Production and integration of the ATLAS insertable B-layer. JINST **13**, T05008 (2018). https://doi.org/10.1088/1748-0221/13/05/T05008. arXiv:1803.00844 [physics.ins-det]
26. G. Avoni et al., The new LUCID-2 detector for luminosity measurement and monitoring in ATLAS. JINST **13**, P07017 (2018). https://doi.org/10.1088/1748-0221/13/07/P07017
27. ATLAS Collaboration, Performance of the ATLAS trigger system in 2015. Eur. Phys. J. C **77**, 317 (2017). https://doi.org/10.1140/epjc/s10052-017-4852-3. arXiv:1611.09661 [hep-ex]
28. ATLAS Collaboration, Software and computing for Run 3 of the ATLAS experiment at the LHC. Eur. Phys. J. C **85**, 234 (2025). https://doi.org/10.1140/epjc/s10052-024-13701-w. arXiv:2404.06335 [hep-ex]
29. ATLAS Collaboration, ATLAS data quality operations and performance for 2015–2018 data-taking. JINST **15**, P04003 (2020). https://doi.org/10.1088/1748-0221/15/04/P04003 [physics.ins-det]. arXiv:1911.04632
30. ATLAS Collaboration, ATLAS Pythia 8 tunes to 7 TeV data. ATL-PHYS-PUB-2014-021 (2014). https://cds.cern.ch/record/1966419
31. J. Bellm et al., Herwig 7.0/Herwig++ 3.0 release note. Eur. Phys. J. **C 76**, 196 (2016). https://doi.org/10.1140/epjc/s10052-016-4018-8. arXiv:1512.01178 [hep-ph]
32. T. Gleisberg et al., Event generation with SHERPA 1.1. JHEP **02**, 007 (2009). https://doi.org/10.1088/1126-6708/2009/02/007. arXiv:0811.4622 [hep-ph]
33. T. Gleisberg, S. Höche, Comix, a new matrix element generator. JHEP **12**, 039 (2008). https://doi.org/10.1088/1126-6708/2008/12/039. arXiv:0808.3674 [hep-ph]
34. F. Buccioni et al., OpenLoops 2. Eur. Phys. J. C **79**, 866 (2019). https://doi.org/10.1140/epjc/s10052-019-7306-2. arXiv:1907.13071 [hep-ph]
35. F. Cascioli, P. Maierhöfer, S. Pozzorini, Scattering amplitudes with open loops. Phys. Rev. Lett. **108**, 111601 (2012). https://doi.org/10.1103/PhysRevLett.108.111601. arXiv:1111.5206 [hep-ph]
36. A. Denner, S. Dittmaier, L. Hofer, Collier: a Fortran-based complex one-loop library in extended regularizations. Comput. Phys. Commun. **212**, 220 (2017). https://doi.org/10.1016/j.cpc.2016.10.013. arXiv:1604.06792 [hep-ph]
37. S. Schumann, F. Krauss, A parton shower algorithm based on Catani–Seymour dipole factorisation. JHEP **03**, 038 (2008). https://doi.org/10.1088/1126-6708/2008/03/038. arXiv:0709.1027 [hep-ph]
38. S. Höche, F. Krauss, M. Schönherr, F. Siegert, A critical appraisal of NLO+PS matching methods. JHEP **09**, 049 (2012). https://doi.org/10.1007/JHEP09(2012)049. arXiv:1111.1220 [hep-ph]
39. S. Höche, F. Krauss, M. Schönherr, F. Siegert, QCD matrix elements + parton showers. The NLO case. JHEP **04**, 027 (2013). https://doi.org/10.1007/JHEP04(2013)027. arXiv:1207.5030 [hep-ph]
40. S. Catani, F. Krauss, B.R. Webber, R. Kuhn, QCD matrix elements + parton showers. JHEP **11**, 063 (2001). https://doi.org/10.1088/1126-6708/2001/11/063. arXiv:hep-ph/0109231
41. S. Höche, F. Krauss, S. Schumann, F. Siegert, QCD matrix elements and truncated showers. JHEP **05**, 053 (2009). https://doi.org/10.1088/1126-6708/2009/05/053. arXiv:0903.1219 [hep-ph]
42. T. Sjöstrand, S. Mrenna, P. Skands, A brief introduction to PYTHIA 8.1. Comput. Phys. Commun. **178**, 852 (2008). https://doi.org/10.1016/j.cpc.2008.01.036. arXiv:0710.3820 [hep-ph]
43. ATLAS Collaboration, The Pythia 8 A3 tune description of ATLAS minimum bias and inelastic measurements incorporating the Donnachie–Landshoff diffractive model. ATL-PHYS-PUB-2016-017 (2016). https://cds.cern.ch/record/2206965
44. ATLAS Collaboration, Emulating the impact of additional proton–proton interactions in the ATLAS simulation by presampling sets of inelastic Monte Carlo events. Comput. Softw. Big Sci. **6**, 3 (2022). https://doi.org/10.1007/s41781-021-00062-2. arXiv:2102.09495 [hep-ex]
45. P. Golonka, Z. Was, PHOTOS Monte Carlo: a precision tool for QED corrections in (Z) and (W) decays. Eur. Phys. J. C **45**, 97 (2006). https://doi.org/10.1140/epjc/s2005-02396-4. arXiv:hep-ph/0506026
46. S. Agostinelli et al., Geant4—a simulation toolkit. Nucl. Instrum. Methods A **506**, 250 (2003). https://doi.org/10.1016/S0168-9002(03)01368-8
47. ATLAS Collaboration, The ATLAS simulation infrastructure. Eur. Phys. J. C **70**, 823 (2010). https://doi.org/10.1140/epjc/s10052-010-1429-9. arXiv:1005.4568 [physics.ins-det]
48. J. Alwall et al., The automated computation of tree-level and next-to-leading order differential cross sections, and their matching to parton shower simulations. JHEP **07**, 079 (2014). https://doi.org/10.1007/JHEP07(2014)079. arXiv:1405.0301 [hep-ph]
49. NNPDF Collaboration, R.D. Ball et al., Parton distributions for the LHC run II. JHEP **04**, 040 (2015). https://doi.org/10.1007/JHEP04(2015)040. arXiv:1410.8849 [hep-ph]
50. S. Frixione, E. Laenen, P. Motylinski, B.R. Webber, Angular correlations of lepton pairs from vector boson and top quark decays in Monte Carlo simulations. JHEP **04**, 081 (2007). https://doi.org/10.1088/1126-6708/2007/04/081. arXiv:hep-ph/0702198
51. P. Artoisenet, R. Frederix, O. Mattelaer, R. Rietkerk, Automatic spin-entangled decays of heavy resonances in Monte Carlo simulations. JHEP **03**, 015 (2013). https://doi.org/10.1007/JHEP03(2013)015. arXiv:1212.3460 [hep-ph]
52. T. Sjöstrand et al., An introduction to PYTHIA 8.2. Comput. Phys. Commun. **191**, 159 (2015). https://doi.org/10.1016/j.cpc.2015.01.024. arXiv:1410.3012 [hep-ph]
53. NNPDF Collaboration, R.D. Ball et al., Parton distributions with LHC data. Nucl. Phys. B **867**, 244 (2013). https://doi.org/10.1016/j.nuclphysb.2012.10.003. arXiv:1207.1303 [hep-ph]
54. D.J. Lange, The EvtGen particle decay simulation package. Nucl. Instrum. Methods A **462**, 152 (2001). https://doi.org/10.1016/S0168-9002(01)00089-4
55. E. Bothmann et al., Event generation with Sherpa 22. SciPost Phys. **7**, 034 (2019). https://doi.org/10.21468/SciPostPhys.7.3.034. arXiv:1905.09127 [hep-ph]
56. S. Frixione, G. Ridolfi, P. Nason, A positive-weight next-to-leading-order Monte Carlo for heavy flavour hadroproduction. JHEP **09**, 126 (2007). https://doi.org/10.1088/1126-6708/2007/09/126. arXiv:0707.3088 [hep-ph]
57. P. Nason, A new method for combining NLO QCD with shower Monte Carlo algorithms. JHEP **11**, 040 (2004). https://doi.org/10.1088/1126-6708/2004/11/040. arXiv:hep-ph/0409146
58. S. Frixione, P. Nason, C. Oleari, Matching NLO QCD computations with parton shower simulations: the POWHEG method. JHEP **11**, 070 (2007). https://doi.org/10.1088/1126-6708/2007/11/070. arXiv:0709.2092 [hep-ph]
59. S. Alioli, P. Nason, C. Oleari, E. Re, A general framework for implementing NLO calculations in shower Monte Carlo programs: the POWHEG BOX. JHEP **06**, 043 (2010). https://doi.org/10.1007/JHEP06(2010)043. arXiv:1002.2581 [hep-ph]
60. E. Re, Single-top (Wt)-channel production matched with parton showers using the POWHEG method. Eur. Phys. J. C **71**,

1547 (2011). https://doi.org/10.1140/epjc/s10052-011-1547-z. arXiv:1009.2450 [hep-ph]
61. R. Frederix, E. Re, P. Torrielli, Single-top (t)-channel hadroproduction in the four-flavour scheme with POWHEG and aMC@NLO. JHEP **09**, 130 (2012). https://doi.org/10.1007/JHEP09(2012)130. arXiv:1207.5391 [hep-ph]
62. S. Alioli, P. Nason, C. Oleari, E. Re, NLO single-top production matched with shower in POWHEG: (s)- and (t)-channel contributions. JHEP **09**, 111 (2009). https://doi.org/10.1088/1126-6708/2009/09/111. arXiv:0907.4076 [hep-ph]. [Erratum: JHEP **02**, 011 (2010). https://doi.org/10.1007/JHEP02(2010)011]
63. S. Frixione, E. Laenen, P. Motylinski, C. White, B.R. Webber, Single-top hadroproduction in association with a (W) boson. JHEP **07**, 029 (2008). https://doi.org/10.1088/1126-6708/2008/07/029. arXiv:0805.3067 [hep-ph]
64. ATLAS Collaboration, Studies on top-quark Monte Carlo modelling for Top2016. ATL-PHYS-PUB-2016-020 (2016). https://cds.cern.ch/record/2216168
65. M. Beneke, P. Falgari, S. Klein, C. Schwinn, Hadronic top-quark pair production with NNLL threshold resummation. Nucl. Phys. B **855**, 695 (2012). https://doi.org/10.1016/j.nuclphysb.2011.10.021. arXiv:1109.1536 [hep-ph]
66. M. Cacciari, M. Czakon, M. Mangano, A. Mitov, P. Nason, Top-pair production at hadron colliders with next-to-next-to-leading logarithmic soft-gluon resummation. Phys. Lett. B **710**, 612 (2012). https://doi.org/10.1016/j.physletb.2012.03.013. arXiv:1111.5869 [hep-ph]
67. P. Bärnreuther, M. Czakon, A. Mitov, Percent-level-precision physics at the Tevatron: next-to-next-to-leading order QCD corrections to (q bar q to t bar t + X). Phys. Rev. Lett. **109**, 132001 (2012). https://doi.org/10.1103/PhysRevLett.109.132001. arXiv:1204.5201 [hep-ph]
68. M. Czakon, A. Mitov, NNLO corrections to top-pair production at hadron colliders: the all-fermionic scattering channels. JHEP **12**, 054 (2012). https://doi.org/10.1007/JHEP12(2012)054. arXiv:1207.0236 [hep-ph]
69. M. Czakon, A. Mitov, NNLO corrections to top pair production at hadron colliders: the quark-gluon reaction. JHEP **01**, 080 (2013). https://doi.org/10.1007/JHEP01(2013)080. arXiv:1210.6832 [hep-ph]
70. M. Czakon, P. Fiedler, A. Mitov, Total top-quark pair-production cross section at hadron colliders through $\mathcal{O}(\alpha_S^4)$. Phys. Rev. Lett. **110**, 252004 (2013). https://doi.org/10.1103/PhysRevLett.110.252004. arXiv:1303.6254 [hep-ph]
71. M. Czakon, A. Mitov, Top++: a program for the calculation of the top-pair cross-section at hadron colliders. Comput. Phys. Commun. **185**, 2930 (2014). https://doi.org/10.1016/j.cpc.2014.06.021. arXiv:1112.5675 [hep-ph]
72. S. Catani, L. Cieri, G. Ferrera, D. de Florian, M. Grazzini, Vector boson production at hadron colliders: a fully exclusive QCD calculation at next-to-next-to-leading order. Phys. Rev. Lett. **103**, 082001 (2009). https://doi.org/10.1103/PhysRevLett.103.082001. arXiv:0903.2120 [hep-ph]
73. R. Frederix, S. Frixione, Merging meets matching in MC@NLO. JHEP **12**, 061 (2012). https://doi.org/10.1007/JHEP12(2012)061. arXiv:1209.6215 [hep-ph]
74. S. Kallweit, J.M. Lindert, P. Maierhöfer, S. Pozzorini, M. Schönherr, NLO QCD+EW predictions for V + jets including off-shell vector-boson decays and multijet merging. JHEP **04**, 021 (2016). https://doi.org/10.1007/JHEP04(2016)021. arXiv:1511.08692 [hep-ph]
75. R. Frederix, D. Pagani, M. Zaro, Large NLO corrections in $t\bar{t}W^{\pm}$ and $t\bar{t}t\bar{t}$ hadroproduction from supposedly subleading EW contributions. JHEP **02**, 031 (2018). https://doi.org/10.1007/JHEP02(2018)031. arXiv:1711.02116 [hep-ph]
76. N.N.P.D.F. Collaboration, R.D. Ball et al., Parton distributions from high-precision collider data. Eur. Phys. J. **C 77**, 663 (2017). https://doi.org/10.1140/epjc/s10052-017-5199-5. arXiv:1706.00428 [hep-ph]
77. L. Lönnblad, S. Prestel, Merging multi-leg NLO matrix elements with parton showers. JHEP **03**, 166 (2013). https://doi.org/10.1007/JHEP03(2013)166. arXiv:1211.7278 [hep-ph]
78. W. Beenakker, R. Höpker, M. Spira, P. Zerwas, Squark and gluino production at hadron colliders. Nucl. Phys. B **492**, 51 (1997). https://doi.org/10.1016/S0550-3213(97)00084-9. arXiv:hep-ph/9610490
79. A. Kulesza, L. Motyka, Threshold resummation for squark–antisquark and gluino-pair production at the LHC. Phys. Rev. Lett. **102**, 111802 (2009). https://doi.org/10.1103/PhysRevLett.102.111802. arXiv:0807.2405 [hep-ph]
80. A. Kulesza, L. Motyka, Soft gluon resummation for the production of gluino–gluino and squark–antisquark pairs at the LHC. Phys. Rev. D **80**, 095004 (2009). https://doi.org/10.1103/PhysRevD.80.095004. arXiv:0905.4749 [hep-ph]
81. W. Beenakker et al., Soft-gluon resummation for squark and gluino hadroproduction. JHEP **12**, 041 (2009). https://doi.org/10.1088/1126-6708/2009/12/041. arXiv:0909.4418 [hep-ph]
82. W. Beenakker et al., Squark and gluino hadroproduction. Int. J. Mod. Phys. A **26**, 2637 (2011). https://doi.org/10.1142/S0217751X11053560. arXiv:1105.1110 [hep-ph]
83. B. Fuks, M. Klasen, D.R. Lamprea, M. Rothering, Gaugino production in proton–proton collisions at a center-of-mass energy of 8 TeV. JHEP **10**, 081 (2012). https://doi.org/10.1007/JHEP10(2012)081. arXiv:1207.2159 [hep-ph]
84. B. Fuks, M. Klasen, D.R. Lamprea, M. Rothering, Precision predictions for electroweak superpartner production at hadron colliders with resummino. Eur. Phys. J. C **73**, 2480 (2013). https://doi.org/10.1140/epjc/s10052-013-2480-0. arXiv:1304.0790 [hep-ph]
85. B. Fuks, M. Klasen, D.R. Lamprea, M. Rothering, Revisiting slepton pair production at the Large Hadron Collider. JHEP **01**, 168 (2014). https://doi.org/10.1007/JHEP01(2014)168. arXiv:1310.2621 [hep-ph]
86. ATLAS Collaboration, Vertex reconstruction performance of the ATLAS detector at $\sqrt{s} = 13$ TeV. ATL-PHYS-PUB-2015-026 (2015). https://cds.cern.ch/record/2037717
87. ATLAS Collaboration, Performance of the ATLAS muon triggers in Run 2. JINST **15**, P09015 (2020). https://doi.org/10.1088/1748-0221/15/09/p09015. arXiv:2004.13447 [physics.ins-det]
88. ATLAS Collaboration, Performance of electron and photon triggers in ATLAS during LHC Run 2. Eur. Phys. J. C **80**, 47 (2020). https://doi.org/10.1140/epjc/s10052-019-7500-2. arXiv:1909.00761 [hep-ex]
89. ATLAS Collaboration, Electron and photon performance measurements with the ATLAS detector using the 2015–2017 LHC proton–proton collision data. JINST **14**, P12006 (2019). https://doi.org/10.1088/1748-0221/14/12/P12006. arXiv:1908.00005 [hep-ex]
90. ATLAS Collaboration, Muon reconstruction and identification efficiency in ATLAS using the full Run 2 (pp) collision data set at $\sqrt{s} = 13$ TeV. Eur. Phys. J. C **81**, 578 (2021). https://doi.org/10.1140/epjc/s10052-021-09233-2. arXiv:2012.00578 [hep-ex]
91. ATLAS Collaboration, Electron reconstruction and identification in the ATLAS experiment using the 2015 and 2016 LHC proton–proton collision data at $\sqrt{s} = 13$ TeV. Eur. Phys. J. C **79**, 639 (2019). https://doi.org/10.1140/epjc/s10052-019-7140-6. arXiv:1902.04655 [physics.ins-det]

92. ATLAS Collaboration, Evidence for the associated production of the Higgs boson and a top quark pair with the ATLAS detector. Phys. Rev. D **97**, 072003 (2018). https://doi.org/10.1103/PhysRevD.97.072003. arXiv:1712.08891 [hep-ex]
93. ATLAS Collaboration, Jet reconstruction and performance using particle flow with the ATLAS detector. Eur. Phys. J. C **77**, 466 (2017). https://doi.org/10.1140/epjc/s10052-017-5031-2. arXiv:1703.10485 [hep-ex]
94. M. Cacciari, G.P. Salam, G. Soyez, The anti-(k_t) jet clustering algorithm. JHEP **04**, 063 (2008). https://doi.org/10.1088/1126-6708/2008/04/063. arXiv:0802.1189 [hep-ph]
95. M. Cacciari, G.P. Salam, G. Soyez, FastJet user manual. Eur. Phys. J. C **72**, 1896 (2012). https://doi.org/10.1140/epjc/s10052-012-1896-2. arXiv:1111.6097 [hep-ph]
96. ATLAS Collaboration, Jet energy scale and resolution measured in proton–proton collisions at $\sqrt{s} = 13$ TeV with the ATLAS detector. Eur. Phys. J. C **81**, 689 (2021). https://doi.org/10.1140/epjc/s10052-021-09402-3. arXiv:2007.02645 [hep-ex]
97. ATLAS Collaboration, Performance of pile-up mitigation techniques for jets in (pp) collisions at $\sqrt{s} = 8$ TeV using the ATLAS detector. Eur. Phys. J. C **76**, 581 (2016). https://doi.org/10.1140/epjc/s10052-016-4395-z. arXiv:1510.03823 [hep-ex]
98. ATLAS Collaboration, Selection of jets produced in 13 TeV proton–proton collisions with the ATLAS detector. ATLAS-CONF-2015-029 (2015). https://cds.cern.ch/record/2037702
99. ATLAS Collaboration, ATLAS flavour-tagging algorithms for the LHC Run 2 (pp) collision dataset. Eur. Phys. J. C **83**, 681 (2023). https://doi.org/10.1140/epjc/s10052-023-11699-1. arXiv:2211.16345 [physics.data-an]
100. ATLAS Collaboration, ATLAS (b)-jet identification performance and efficiency measurement with (t bar t) events in (pp) collisions at $\sqrt{s} = 13$ TeV. Eur. Phys. J. C **79**, 970 (2019). https://doi.org/10.1140/epjc/s10052-019-7450-8. arXiv:1907.05120 [hep-ex]
101. ATLAS Collaboration, Measurement of the (c)-jet mistagging efficiency in (t bar t) events using (pp) collision data at $\sqrt{s} = 13$ TeV collected with the ATLAS detector. Eur. Phys. J. C **82**, 95 (2022). https://doi.org/10.1140/epjc/s10052-021-09843-w. arXiv:2109.10627 [hep-ex]
102. ATLAS Collaboration, Calibration of the light-flavour jet mistagging efficiency of the (b)-tagging algorithms with (Z)+jets events using 139 fb$^{-1}$ of ATLAS proton–proton collision data at $\sqrt{s} = 13$ TeV. Eur. Phys. J. C **83**, 728 (2023). https://doi.org/10.1140/epjc/s10052-023-11736-z. arXiv:2301.06319 [hep-ex]
103. ATLAS Collaboration, The performance of missing transverse momentum reconstruction and its significance with the ATLAS detector using 140, $fb^{-1}) of \sqrt{s} = 13, TeV$ (pp) collisions, Eur. Phys. J. C 85 (2025) 606, https://doi.org/10.1140/epjc/s10052-025-14062-8 arxiv:2402.05858 [hep-ex]
104. D. J. Rezende and S. Mohamed, Variational Inference with Normalizing Flows, (2016), arXiv: arxiv:1505.05770 [stat.ML]
105. L. Dinh, J. Sohl-Dickstein and S. Bengio, Density estimation using Real NVP, (2016), arXiv: arxiv:1605.08803 [cs.LG]
106. A. Paszke et al., PyTorch: An Imperative Style, High-Performance Deep Learning Library, (2019), arXiv: arxiv:1912.01703 [cs.LG]
107. V. Stimper et al., normflows: A PyTorch Package for Normalizing Flows, Open Source Softw. 8, 5361. (2023) https://doi.org/10.21105/joss.05361
108. D.P. Kingma, J. Ba, *Adam: A Method for Stochastic Optimization* (2017). arXiv: arxiv:1412.6980 [cs.LG]
109. G.J. Székely, M.L. Rizzo, Energy statistics: A class of statistics based on distances. J. Stat. Plan. Infer. **143**, 1249 (2013). https://doi.org/10.1016/j.jspi.2013.03.018
110. M. Czakon et al., Top-pair production at the LHC through NNLO QCD and NLO EW. JHEP **10**, 186 (2017). https://doi.org/10.1007/jhep10(2017)186. arXiv:1705.04105 [hep-ph]
111. ATLAS Collaboration, Luminosity determination in (pp) collisions at $\sqrt{s} = 13, TeV$ using the ATLAS detector at the LHC, Eur. Phys. J. C 83 (2023) 982, https://doi.org/10.1140/epjc/s10052-023-11747-w arxiv:2212.09379 [hep-ex]
112. ATLAS Collaboration, Muon reconstruction performance of the ATLAS detector in proton–proton collision data at $\sqrt{s} = 13, TeV$, Eur. Phys. J. C 76 (2016) 292, https://doi.org/10.1140/epjc/s10052-016-4120-y arxiv:1603.05598 [hep-ex]
113. ATLAS Collaboration, Studies of the muon momentum calibration and performance of the ATLAS detector with (pp) collisions at $\sqrt{s} = 13, TeV$, Eur. Phys. J. C 83 (2023) 686, https://doi.org/10.1140/epjc/s10052-023-11584-x arxiv:2212.07338 [hep-ex]
114. F. Febres Cordero, M. Kraus and L. Reina, Top-quark pair production in association with a $W^{\pm}$ gauge boson in the POWHEG-BOX, Phys. Rev. D 103 (2021) 094014, https://doi.org/10.1103/PhysRevD.103.094014 arxiv:2101.11808 [hep-ph]
115. ATLAS Collaboration, Studies on the improvement of the matching uncertainty definition in top-quark processes simulated with Powheg+Pythia8, ATL-PHYS-PUB-2023-029, 2023, https://cds.cern.ch/record/2872787
116. D. de Florian et al., Handbook of LHC Higgs Cross Sections: 4. Deciphering the Nature of the Higgs Sector, https://doi.org/10.23731/CYRM-2017-002(2017), arxiv:1610.07922 [hep-ph]
117. ATLAS Collaboration, Observation of the associated production of a top quark and a (Z) boson in (pp) collisions at $\sqrt{s} = 13, TeV$ with the ATLAS detector, JHEP 07 (2020) 124, https://doi.org/10.1007/JHEP07(2020)124 arxiv:2002.07546 [hep-ex]
118. ROOT Collaboration, HistFactory: A tool for creating statistical models for use with RooFit and RooStats, CERN-OPEN-2012-016 (2012). https://doi.org/10.17181/CERN-OPEN-2012-016
119. J.S. Conway, *Incorporating Nuisance Parameters in Likelihoods for Multisource Spectra*, arXiv:1103.0354 [physics.data-an] (2011)
120. W. Verkerke, D. Kirkby, *The RooFit toolkit for data modeling*, arxiv:physics/0306116 [physics.data-an] (2003)
121. T. Junk, Confidence level computation for combining searches with small statistics. Nucl. Instrum. Meth. A **434**, 435 (1999). https://doi.org/10.1016/S0168-9002(99)00498-2. arxiv:hep-ex/9902006
122. A.L. Read, Presentation of search results: the (CL_s) technique. J. Phys. G **28**, 2693 (2002). https://doi.org/10.1088/0954-3899/28/10/313
123. G. Cowan, K. Cranmer, E. Gross, O. Vitells, Asymptotic formulae for likelihood-based tests of new physics, Eur. Phys. J. C 71, 1554, (2011) https://doi.org/10.1140/epjc/s10052-011-1554-0 arxiv:1007.1727 [physics.data-an], Erratum: https://doi.org/10.1140/epjc/s10052-013-2501-z Eur. Phys. J. C 73, 2501 (2013)
124. ATLAS Collaboration, ATLAS Computing Acknowledgements, ATL-SOFT-PUB-2025-001, (2025), https://cds.cern.ch/record/2922210

**ATLAS Collaboration**[★]

G. Aad[104], E. Aakvaag[17], B. Abbott[123], S. Abdelhameed[119a], K. Abeling[55], N. J. Abicht[49], S. H. Abidi[30], M. Aboelela[45], A. Aboulhorma[36e], H. Abramowicz[157], Y. Abulaiti[120], B. S. Acharya[69a,69b,m], A. Ackermann[63a], C. Adam Bourdarios[4], L. Adamczyk[87a], S. V. Addepalli[149], M. J. Addison[103], J. Adelman[118], A. Adiguzel[22c], T. Adye[137], A. A. Affolder[139], Y. Afik[40], M. N. Agaras[13], A. Aggarwal[102], C. Agheorghiesei[28c], F. Ahmadov[39,ad], S. Ahuja[97], S. Ahuja[169], X. Ai[143b], G. Aielli[76a,76b], A. Aikot[169], M. Ait Tamlihat[36e], B. Aitbenchikh[36a], M. Akbiyik[102], T. P. A. Åkesson[100], A. V. Akimov[151], D. Akiyama[174], N. N. Akolkar[25], S. Aktas[172], G. L. Alberghi[24b], J. Albert[171], U. Alberti[20], P. Albicocco[53], G. L. Albouy[60], S. Alderweireldt[52], Z. L. Alegria[124], M. Aleksa[37], I. N. Aleksandrov[39], C. Alexa[28b], T. Alexopoulos[10], F. Alfonsi[24b], M. Algren[56], M. Alhroob[173], B. Ali[135], H. M. J. Ali[93,w], S. Ali[32], S. W. Alibocus[94], M. Aliev[34c], G. Alimonti[71a], W. Alkakhi[55], C. Allaire[66], B. M. M. Allbrooke[152], D. R. Allen[124], J. S. Allen[103], J. F. Allen[52], P. P. Allport[21], A. Aloisio[72a,72b], F. Alonso[92], C. Alpigiani[142], Z. M. K. Alsolami[93], A. Alvarez Fernandez[102], M. Alves Cardoso[56], M. G. Alviggi[72a,72b], M. Aly[103], Y. Amaral Coutinho[83b], A. Ambler[106], C. Amelung[37], M. Amerl[103], C. G. Ames[111], T. Amezza[130], D. Amidei[108], B. Amini[54], K. Amirie[161], A. Amirkhanov[39], S. P. Amor Dos Santos[133a], K. R. Amos[169], D. Amperiadou[158], S. An[84], C. Anastopoulos[145], T. Andeen[11], J. K. Anders[94], A. C. Anderson[59], A. Andreazza[71a,71b], S. Angelidakis[9], A. Angerami[42], A. V. Anisenkov[39], A. Annovi[74a], C. Antel[37], E. Antipov[151], M. Antonelli[53], F. Anulli[75a], M. Aoki[84], T. Aoki[159], M. A. Aparo[152], L. Aperio Bella[48], M. Apicella[31], C. Appelt[157], A. Apyan[27], M. Arampatzi[10], S. J. Arbiol Val[88], C. Arcangeletti[53], A. T. H. Arce[51], J.-F. Arguin[110], S. Argyropoulos[158], J.-H. Arling[48], O. Arnaez[4], H. Arnold[151], G. Artoni[75a,75b], H. Asada[113], K. Asai[121], S. Asatryan[179], N. A. Asbah[37], R. A. Ashby Pickering[173], A. M. Aslam[97], K. Assamagan[30], R. Astalos[29a], K. S. V. Astrand[100], S. Atashi[165], R. J. Atkin[34a], H. Atmani[36f], P. A. Atmasiddha[131], K. Augsten[135], A. D. Auriol[41], V. A. Austrup[103], A. S. Avad[96], G. Avolio[37], K. Axiotis[56], A. Azzam[13], D. Babal[29b], H. Bachacou[138], K. Bachas[158,q], A. Bachiu[35], E. Bachmann[50], M. J. Backes[63a], A. Badea[40], T. M. Baer[108], P. Bagnaia[75a,75b], M. Bahmani[19], D. Bahner[54], K. Bai[126], J. T. Baines[137], L. Baines[96], O. K. Baker[178], E. Bakos[16], D. Bakshi Gupta[8], L. E. Balabram Filho[83b], V. Balakrishnan[123], R. Balasubramanian[4], E. M. Baldin[38], P. Balek[87a], E. Ballabene[24a,24b], F. Balli[138], L. M. Baltes[63a], W. K. Balunas[33], J. Balz[102], I. Bamwidhi[119b], E. Banas[88], M. Bandieramonte[132], A. Bandyopadhyay[25], S. Bansal[25], L. Barak[157], M. Barakat[48], E. L. Barberio[107], D. Barberis[18b], M. Barbero[104], M. Z. Barel[117], T. Barillari[112], M.-S. Barisits[37], T. Barklow[149], P. Baron[136], D. A. Baron Moreno[103], A. Baroncelli[62], A. J. Barr[129], J. D. Barr[98], F. Barreiro[101], J. Barreiro Guimarães da Costa[14], M. G. Barros Teixeira[133a], S. Barsov[38], F. Bartels[63a], R. Bartoldus[149], A. E. Barton[93], P. Bartos[29a], M. Baselga[49], S. Bashiri[88], A. Bassalat[66,b], M. J. Basso[162a], S. Bataju[45], R. Bate[170], R. L. Bates[59], S. Batlamous[101], M. Battaglia[139], D. Battulga[19], M. Bauce[75a,75b], M. Bauer[79], P. Bauer[25], L. T. Bayer[48], L. T. Bazzano Hurrell[31], J. B. Beacham[112], T. Beau[130], J. Y. Beaucamp[92], P. H. Beauchemin[164], P. Bechtle[25], H. P. Beck[20,p], K. Becker[173], A. J. Beddall[82], V. A. Bednyakov[39], C. P. Bee[151], L. J. Beemster[16], M. Begalli[83d], M. Begel[30], J. K. Behr[48], J. F. Beirer[37], F. Beisiegel[25], M. Belfkir[119b], G. Bella[157], L. Bellagamba[24b], A. Bellerive[35], C. D. Bellgraph[68], P. Bellos[21], K. Beloborodov[38], I. Benaoumeur[21], D. Benchekroun[36a], F. Bendebba[36a], Y. Benhammou[157], K. C. Benkendorfer[61], L. Beresford[48], M. Beretta[53], E. Bergeaas Kuutmann[167], N. Berger[4], B. Bergmann[135], J. Beringer[18a], G. Bernardi[5], C. Bernius[149], F. U. Bernlochner[25], A. Berrocal Guardia[13], T. Berry[97], P. Berta[136], A. Berthold[50], A. Berti[133a], R. Bertrand[104], S. Bethke[112], A. Betti[75a,75b], A. J. Bevan[96], L. Bezio[56], N. K. Bhalla[54], S. Bharthuar[112], S. Bhatta[151], P. Bhattarai[149], Z. M. Bhatti[120], K. D. Bhide[54], V. S. Bhopatkar[124], R. M. Bianchi[132], G. Bianco[24a,24b], O. Biebel[111], M. Biglietti[77a], C. S. Billingsley[45], Y. Bimgdi[36f], M. Bindi[55], A. Bingham[177], A. Bingul[22b], C. Bini[75a,75b], G. A. Bird[33], M. Birman[175], M. Biros[136], S. Biryukov[152], T. Bisanz[49], E. Bisceglie[24a,24b], J. P. Biswal[137], D. Biswas[147], I. Bloch[48], A. Blue[59], U. Blumenschein[96], V. S. Bobrovnikov[39], L. Boccardo[57a,57b], M. Boehler[54], B. Boehm[172], D. Bogavac[13], A. G. Bogdanchikov[38], L. S. Boggia[130], V. Boisvert[97], P. Bokan[37], T. Bold[87a], M. Bomben[5], M. Bona[96], M. Boonekamp[138], A. G. Borbély[59], I. S. Bordulev[38], G. Borissov[93], D. Bortoletto[129], D. Boscherini[24b], M. Bosman[13], K. Bouaouda[36a], N. Bouchhar[169], L. Boudet[4], J. Boudreau[132], E. V. Bouhova-Thacker[93], D. Boumediene[41], R. Bouquet[57a,57b], A. Boveia[122], J. Boyd[37], D. Boye[30], I. R. Boyko[39], L. Bozianu[56], J. Bracinik[21], N. Brahimi[4], G. Brandt[177], O. Brandt[33], B. Brau[105],

J. E. Brau[126], R. Brener[175], L. Brenner[117], R. Brenner[167], S. Bressler[175], G. Brianti[78a,78b], D. Britton[59], D. Britzger[112], I. Brock[25], R. Brock[109], G. Brooijmans[42], A. J. Brooks[68], E. M. Brooks[162b], E. Brost[30], L. M. Brown[162a,171], L. E. Bruce[61], T. L. Bruckler[129], P. A. Bruckman de Renstrom[88], B. Brüers[48], A. Bruni[24b], G. Bruni[24b], D. Brunner[47a,47b], M. Bruschi[24b], N. Bruscino[75a,75b], T. Buanes[17], Q. Buat[142], D. Buchin[112], A. G. Buckley[59], O. Bulekov[82], B. A. Bullard[149], S. Burdin[94], C. D. Burgard[49], A. M. Burger[91], B. Burghgrave[8], O. Burlayenko[54], J. Burleson[168], J. C. Burzynski[148], E. L. Busch[42], V. Büscher[102], P. J. Bussey[59], O. But[25], J. M. Butler[26], C. M. Buttar[59], J. M. Butterworth[98], W. Buttinger[137], C. J. Buxo Vazquez[109], A. R. Buzykaev[39], S. Cabrera Urbán[169], L. Cadamuro[66], H. Cai[37], Y. Cai[24a,24b,114c], Y. Cai[114a], V. M. M. Cairo[37], O. Cakir[3a], N. Calace[37], P. Calafiura[18a], G. Calderini[130], P. Calfayan[35], L. Calic[100], G. Callea[59], L. P. Caloba[83b], D. Calvet[41], S. Calvet[41], R. Camacho Toro[130], S. Camarda[37], D. Camarero Munoz[27], P. Camarri[76a,76b], C. Camincher[171], M. Campanelli[98], A. Camplani[43], V. Canale[72a,72b], A. C. Canbay[3a], E. Canonero[97], J. Cantero[169], Y. Cao[168], F. Capocasa[27], M. Capua[44a,44b], A. Carbone[71a,71b], R. Cardarelli[76a], J. C. J. Cardenas[8], M. P. Cardiff[27], G. Carducci[44a,44b], T. Carli[37], G. Carlino[72a], J. I. Carlotto[13], B. T. Carlson[132,r], E. M. Carlson[171], J. Carmignani[94], L. Carminati[71a,71b], A. Carnelli[4], M. Carnesale[37], S. Caron[116], E. Carquin[140g], I. B. Carr[107], S. Carrá[73a,73b], G. Carratta[24a,24b], C. Carrion Martinez[169], A. M. Carroll[126], M. P. Casado[13,h], P. Casolaro[72a,72b], M. Caspar[48], W. R. Castiglioni[40], F. L. Castillo[4], L. Castillo Garcia[13], V. Castillo Gimenez[169], N. F. Castro[133a,133e], A. Catinaccio[37], J. R. Catmore[128], T. Cavaliere[4], V. Cavaliere[30], L. J. Caviedes Betancourt[23b], E. Celebi[82], S. Cella[37], V. Cepaitis[56], K. Cerny[125], A. S. Cerqueira[83a], A. Cerri[74a,74b,am], L. Cerrito[76a,76b], F. Cerutti[18a], B. Cervato[71a,71b], A. Cervelli[24b], G. Cesarini[53], S. A. Cetin[82], P. M. Chabrillat[130], R. Chakkappai[66], S. Chakraborty[173], A. Chambers[61], J. Chan[18a], W. Y. Chan[159], J. D. Chapman[33], E. Chapon[138], B. Chargeishvili[155b], D. G. Charlton[21], C. Chauhan[136], Y. Che[114a], S. Chekanov[6], G. A. Chelkov[39,a], B. Chen[157], B. Chen[171], H. Chen[114a], H. Chen[30], J. Chen[144a], J. Chen[148], M. Chen[129], S. Chen[89], S. J. Chen[114a], X. Chen[144a], X. Chen[15,ah], Z. Chen[62], C. L. Cheng[176], H. C. Cheng[64a], S. Cheong[149], A. Cheplakov[39], E. Cherepanova[117], R. Cherkaoui El Moursli[36e], E. Cheu[7], K. Cheung[65], L. Chevalier[138], V. Chiarella[53], G. Chiarelli[74a], G. Chiodini[70a], A. S. Chisholm[21], A. Chitan[28b], M. Chitishvili[169], M. V. Chizhov[39,s], K. Choi[11], Y. Chou[142], E. Y. S. Chow[116], K. L. Chu[175], M. C. Chu[64a], X. Chu[14,114c], Z. Chubinidze[53], J. Chudoba[134], J. J. Chwastowski[88], D. Cieri[112], K. M. Ciesla[87a], V. Cindro[95], A. Ciocio[18a], F. Cirotto[72a,72b], Z. H. Citron[175], M. Citterio[71a], D. A. Ciubotaru[28b], A. Clark[56], P. J. Clark[52], N. Clarke Hall[98], C. Clarry[161], S. E. Clawson[48], C. Clement[47a,47b], L. Clissa[24a,24b], Y. Coadou[104], M. Cobal[69a,69c], A. Coccaro[57b], R. F. Coelho Barrue[133a], R. Coelho Lopes De Sa[105], S. Coelli[71a], M. M. Cohen[131], L. S. Colangeli[161], B. Cole[42], P. Collado Soto[101], J. Collot[60], R. Coluccia[70a,70b], P. Conde Muiño[133a,133g], M. P. Connell[34c], S. H. Connell[34c], E. I. Conroy[129], M. Contreras Cossio[11], F. Conventi[72a,aj], A. M. Cooper-Sarkar[129], L. Corazzina[75a,75b], F. A. Corchia[24a,24b], A. Cordeiro Oudot Choi[142], L. D. Corpe[41], M. Corradi[75a,75b], F. Corriveau[106,ab], A. Cortes-Gonzalez[159], M. J. Costa[169], F. Costanza[4], D. Costanzo[145], J. Couthures[4], G. Cowan[97], K. Cranmer[176], L. Cremer[49], D. Cremonini[24a,24b], S. Crépé-Renaudin[60], F. Crescioli[130], T. Cresta[73a,73b], M. Cristinziani[147], M. Cristoforetti[78a,78b], E. Critelli[98], V. Croft[117], G. Crosetti[44a,44b], A. Cueto[101], H. Cui[98], Z. Cui[7], B. M. Cunnett[152], W. R. Cunningham[59], F. Curcio[169], J. R. Curran[52], M. J. Da Cunha Sargedas De Sousa[57a,57b], J. V. Da Fonseca Pinto[83b], C. Da Via[103], W. Dabrowski[87a], T. Dado[37], S. Dahbi[154], T. Dai[108], D. Dal Santo[20], C. Dallapiccola[105], M. Dam[43], G. D'amen[30], V. D'Amico[111], J. R. Dandoy[35], M. D'Andrea[57a,57b], D. Dannheim[37], G. D'anniballe[74a,74b], M. Danninger[148], V. Dao[151], G. Darbo[57b], S. J. Das[30], F. Dattola[48], S. D'Auria[71a,71b], A. D'Avanzo[72a,72b], T. Davidek[136], J. Davidson[173], I. Dawson[96], K. De[8], C. De Almeida Rossi[161], R. De Asmundis[72a], N. De Biase[48], S. De Castro[24a,24b], N. De Groot[116], P. de Jong[117], H. De la Torre[118], A. De Maria[114a], A. De Salvo[75a], U. De Sanctis[76a,76b], F. De Santis[70a,70b], A. De Santo[152], J. B. De Vivie De Regie[60], J. Debevc[95], D. V. Dedovich[39], J. Degens[94], A. M. Deiana[45], J. Del Peso[101], L. Delagrange[130], F. Deliot[138], C. M. Delitzsch[49], M. Della Pietra[72a,72b], D. Della Volpe[56], A. Dell'Acqua[37], L. Dell'Asta[71a,71b], M. Delmastro[4], C. C. Delogu[57a,57b], P. A. Delsart[60], S. Demers[178], M. Demichev[39], S. P. Denisov[38], H. Denizli[22a,l], L. D'Eramo[41], D. Derendarz[88], F. Derue[130], P. Dervan[94,*], A. M. Desai[1], K. Desch[25], F. A. Di Bello[57a,57b], A. Di Ciaccio[76a,76b], L. Di Ciaccio[4], A. Di Domenico[75a,75b], C. Di Donato[72a,72b], A. Di Girolamo[37], G. Di Gregorio[62], A. Di Luca[78a,78b], B. Di Micco[77a,77b], R. Di Nardo[77a,77b], K. F. Di Petrillo[40], M. Diamantopoulou[35], F. A. Dias[117], M. A. Diaz[140a,140b], A. R. Didenko[39], M. Didenko[169], S. D. Diefenbacher[18a], E. B. Diehl[108],

S. Díez Cornell[48], C. Diez Pardos[147], C. Dimitriadi[150], A. Dimitrievska[21], A. Dimri[151], Y. Ding[62], J. Dingfelder[25], T. Dingley[129], I.-M. Dinu[28b], S. J. Dittmeier[63b], F. Dittus[37], M. Divisek[136], B. Dixit[94], F. Djama[104], T. Djobava[155b], C. Doglioni[100,103], A. Dohnalova[29a], Z. Dolezal[136], K. Domijan[87a], K. M. Dona[40], M. Donadelli[83d], B. Dong[109], J. Donini[41], A. D'Onofrio[72a,72b], M. D'Onofrio[94], J. Dopke[137], A. Doria[72a], N. Dos Santos Fernandes[133a], I. A. Dos Santos Luz[83e], P. Dougan[103], M. T. Dova[92], A. T. Doyle[59], M. P. Drescher[55], E. Dreyer[175], I. Drivas-koulouris[10], M. Drnevich[120], D. Du[62], T. A. du Pree[117], Z. Duan[114a], M. Dubau[4], F. Dubinin[39], M. Dubovsky[29a], E. Duchovni[175], G. Duckeck[111], P. K. Duckett[98], O. A. Ducu[28b], D. Duda[52], A. Dudarev[37], M. M. Dudek[88], E. R. Duden[27], M. D'uffizi[103], L. Duflot[66], M. Dührssen[37], I. Duminica[28g], A. E. Dumitriu[28b], M. Dunford[63a], K. Dunne[47a,47b], A. Duperrin[104], H. Duran Yildiz[3a], A. Durglishvili[155b], G. I. Dyckes[18a], M. Dyndal[87a], B. S. Dziedzic[37], Z. O. Earnshaw[152], G. H. Eberwein[129], B. Eckerova[29a], S. Eggebrecht[55], E. Egidio Purcino De Souza[83e], G. Eigen[17], K. Einsweiler[18a], T. Ekelof[167], P. A. Ekman[100], S. El Farkh[36b], Y. El Ghazali[62], H. El Jarrari[34j], A. El Moussaouy[36a], D. Elitez[37], M. Ellert[167], F. Ellinghaus[177], T. A. Elliot[97], N. Ellis[37], J. Elmsheuser[30], M. Elsawy[119a], M. Elsing[37], D. Emeliyanov[137], Y. Enari[84], S. Epari[110], D. Ernani Martins Neto[88], F. Ernst[37], M. Escalier[66], C. Escobar[169], E. Etzion[157], G. Evans[133a,133b], H. Evans[68], L. S. Evans[48], A. Ezhilov[38], S. Ezzarqtouni[36a], F. Fabbri[24a,24b], L. Fabbri[24a,24b], G. Facini[98], V. Fadeyev[139], R. M. Fakhrutdinov[38], D. Fakoudis[102], S. Falciano[75a], L. F. Falda Ulhoa Coelho[133a], F. Fallavollita[112], G. Falsetti[44a,44b], J. Faltova[136], C. Fan[168], K. Y. Fan[64b], Y. Fan[14], Y. Fang[14,114c], M. Fanti[71a,71b], M. Faraj[69a,69b], Z. Farazpay[99], A. Farbin[8], A. Farilla[77a], K. Farman[154], T. Farooque[109], J. N. Farr[178], M. S. Farrington[61], S. M. Farrington[52,137], F. Fassi[36e], D. Fassouliotis[9], L. Fayard[66], P. Federic[136], P. Federicova[134], O. L. Fedin[38,a], M. Feickert[176], L. Feligioni[104], D. E. Fellers[18a], C. Feng[143a], Y. Feng[14], Z. Feng[117], M. J. Fenton[165], L. Ferencz[48], B. Fernandez Barbadillo[93], P. Fernandez Martinez[67], M. J. V. Fernoux[104], J. Ferrando[93], A. Ferrari[167], P. Ferrari[116,117], R. Ferrari[73a], D. Ferrere[56], C. Ferretti[108], M. P. Fewell[1], D. Fiacco[75a,75b], F. Fiedler[102], P. Fiedler[135], S. Filimonov[39], M. S. Filip[28b,t], A. Filipčič[95], E. K. Filmer[162a], F. Filthaut[116], M. C. N. Fiolhais[133a,133c,c], L. Fiorini[169], W. C. Fisher[109], T. Fitschen[103], P. M. Fitzhugh[138], I. Fleck[147], P. Fleischmann[108], T. Flick[177], M. Flores[34d,ag], L. R. Flores Castillo[64a], L. Flores Sanz De Acedo[37], F. M. Follega[78a,78b], N. Fomin[33], J. H. Foo[161], A. Formica[138], A. C. Forti[103], E. Fortin[37], A. W. Fortman[18a], L. Foster[18a], L. Fountas[9,i], D. Fournier[66], H. Fox[93], P. Francavilla[74a,74b], S. Francescato[61], S. Franchellucci[56], M. Franchini[24a,24b], S. Franchino[63a], D. Francis[37], L. Franco[116], L. Franconi[48], M. Franklin[61], G. Frattari[27], Y. Y. Frid[157], J. Friend[59], N. Fritzsche[37], A. Froch[56], D. Froidevaux[37], J. A. Frost[137], Y. Fu[109], S. Fuenzalida Garrido[140g], M. Fujimoto[151], K. Y. Fung[64a], E. Furtado De Simas Filho[83e], M. Furukawa[159], M. Fuste Costa[48], J. Fuster[169], A. Gaa[55], A. Gabrielli[24a,24b], A. Gabrielli[161], P. Gadow[37], G. Gagliardi[57a,57b], L. G. Gagnon[18a], S. Gaid[85b], S. Galantzan[157], J. Gallagher[1], E. J. Gallas[129], A. L. Gallen[167], B. J. Gallop[137], K. K. Gan[122], S. Ganguly[159], Y. Gao[52], A. Garabaglu[142], F. M. Garay Walls[140a,140b], C. García[169], A. Garcia Alonso[117], A. G. Garcia Caffaro[178], J. E. García Navarro[169], M. A. Garcia Ruiz[23b], M. Garcia-Sciveres[18a], G. L. Gardner[131], R. W. Gardner[40], N. Garelli[164], R. B. Garg[149], J. M. Gargan[33], C. A. Garner[161], C. M. Garvey[34a], V. K. Gassmann[164], G. Gaudio[73a], V. Gautam[13], P. Gauzzi[75a,75b], J. Gavranovic[95], I. L. Gavrilenko[133a], A. Gavrilyuk[38], C. Gay[170], G. Gaycken[126], E. N. Gazis[10], A. Gekow[122], C. Gemme[57b], M. H. Genest[60], A. D. Gentry[115], S. George[97], T. Geralis[46], A. A. Gerwin[123], P. Gessinger-Befurt[37], M. E. Geyik[177], M. Ghani[173], K. Ghorbanian[96], A. Ghosal[147], A. Ghosh[165], A. Ghosh[7], B. Giacobbe[24b], S. Giagu[75a,75b], T. Giani[117], A. Giannini[62], S. M. Gibson[97], M. Gignac[139], D. T. Gil[87b], A. K. Gilbert[87a], B. J. Gilbert[42], D. Gillberg[35], G. Gilles[117], D. M. Gingrich[2,ai], M. P. Giordani[69a,69c], P. F. Giraud[138], G. Giugliarelli[69a,69c], D. Giugni[71a], F. Giuli[76a,76b], I. Gkialas[9,i], L. K. Gladilin[38], C. Glasman[101], M. Glazewska[20], R. M. Gleason[165], G. Glemža[48], M. Glisic[126], I. Gnesi[44b], Y. Go[30], M. Goblirsch-Kolb[37], B. Gocke[49], D. Godin[110], B. Gokturk[22a], S. Goldfarb[107], T. Golling[56], M. G. D. Gololo[34c], A. Golub[142], D. Golubkov[38], J. P. Gombas[109], A. Gomes[133a,133b], G. Gomes Da Silva[147], A. J. Gomez Delegido[37], R. Gonçalo[133a], L. Gonella[21], A. Gongadze[155c], F. Gonnella[21], J. L. Gonski[149], R. Y. González Andana[52], S. González de la Hoz[169], M. V. Gonzalez Rodrigues[48], R. Gonzalez Suarez[167], S. Gonzalez-Sevilla[56], L. Goossens[37], B. Gorini[37], E. Gorini[70a,70b], A. Gorišek[95], T. C. Gosart[131], A. T. Goshaw[51], M. I. Gostkin[39], S. Goswami[124], C. A. Gottardo[37], S. A. Gotz[111], M. Gouighri[36b], A. G. Goussiou[142], N. Govender[34c], R. P. Grabarczyk[129], I. Grabowska-Bold[87a], K. Graham[35], E. Gramstad[128], S. Grancagnolo[70a,70b], C. M. Grant[1], P. M. Gravila[28f], F. G. Gravili[70a,70b], H. M. Gray[18a], M. Greco[112], M. J. Green[1], C. Grefe[25], A. S. Grefsrud[17], I. M. Gregor[48],

K. T. Greif[165], P. Grenier[149], S. G. Grewe[112], A. A. Grillo[139], K. Grimm[32], S. Grinstein[13,x], J.-F. Grivaz[66], E. Gross[175], J. Grosse-Knetter[55], L. Guan[108], G. Guerrieri[37], R. Guevara[128], R. Gugel[102], J. A. M. Guhit[108], A. Guida[19], E. Guilloton[173], S. Guindon[37], F. Guo[14,114c], J. Guo[144a], L. Guo[48], L. Guo[114b,v], Y. Guo[108], Y. Guo[42], A. Gupta[49], R. Gupta[132], S. Gupta[27], S. Gurbuz[25], S. S. Gurdasani[48], G. Gustavino[75a,75b], P. Gutierrez[123], L. F. Gutierrez Zagazeta[131], M. Gutsche[50], C. Gutschow[98], C. Gwenlan[129], C. B. Gwilliam[94], E. S. Haaland[128], A. Haas[120], M. Habedank[59], C. Haber[18a], H. K. Hadavand[8], A. Haddad[41], A. Hadef[50], A. I. Hagan[93], J. J. Hahn[147], E. H. Haines[98], M. Haleem[172], J. Haley[124], G. D. Hallewell[104], J. A. Hallford[48], K. Hamano[171], H. Hamdaoui[167], M. Hamer[25], S. E. D. Hammoud[66], E. J. Hampshire[97], J. Han[143a], L. Han[114a], L. Han[62], S. Han[14], K. Hanagaki[84], M. Hance[139], D. A. Hangal[42], H. Hanif[148], M. D. Hank[131], J. B. Hansen[43], P. H. Hansen[43], T. Harenberg[177], S. Harkusha[179], M. L. Harris[105], Y. T. Harris[25], J. Harrison[13], N. M. Harrison[122], P. F. Harrison[173], M. L. E. Hart[98], N. M. Hartman[112], N. M. Hartmann[111], R. Z. Hasan[97,137], Y. Hasegawa[146], F. Haslbeck[129], S. Hassan[17], R. Hauser[109], M. Haviernik[136], C. M. Hawkes[21], R. J. Hawkings[37], Y. Hayashi[159], D. Hayden[109], C. Hayes[108], R. L. Hayes[117], C. P. Hays[129], J. M. Hays[96], H. S. Hayward[94], M. He[14,114c], Y. He[48], Y. He[98], N. B. Heatley[96], V. Hedberg[100], J. Heilman[35], S. Heim[48], T. Heim[18a], J. J. Heinrich[126], L. Heinrich[112], J. Hejbal[134], M. Helbig[50], A. Held[176], S. Hellesund[17], C. M. Helling[170], S. Hellman[47a,47b], A. M. Henriques Correia[37], H. Herde[100], Y. Hernández Jiménez[151], L. M. Herrmann[25], T. Herrmann[50], G. Herten[54], R. Hertenberger[111], L. Hervas[37], M. E. Hesping[102], N. P. Hessey[162a], J. Hessler[112], M. Hidaoui[36b], N. Hidic[136], E. Hill[161], T. S. Hillersoy[17], S. J. Hillier[21], J. R. Hinds[109], F. Hinterkeuser[25], M. Hirose[127], S. Hirose[163], D. Hirschbuehl[177], T. G. Hitchings[103], B. Hiti[95], J. Hobbs[151], R. Hobincu[28e], N. Hod[175], A. M. Hodges[168], M. C. Hodgkinson[145], B. H. Hodkinson[129], A. Hoecker[37], D. D. Hofer[108], J. Hofer[169], J. Hofner[102], M. Holzbock[37], L. B. A. H. Hommels[33], V. Homsak[129], B. P. Honan[103], J. J. Hong[68], T. M. Hong[132], B. H. Hooberman[168], W. H. Hopkins[6], M. C. Hoppesch[168], Y. Horii[113], M. E. Horstmann[112], S. Hou[154], M. R. Housenga[168], J. Howarth[59], J. Hoya[6], M. Hrabovsky[125], T. Hryn'ova[4], P. J. Hsu[65], S.-C. Hsu[142], T. Hsu[66], M. Hu[18a], Q. Hu[62], S. Huang[33], X. Huang[14,114c], Y. Huang[136], Y. Huang[114b], Y. Huang[14], Z. Huang[66], Z. Hubacek[135], F. Huegging[25], T. B. Huffman[129], M. Hufnagel Maranha De Faria[83a], C. A. Hugli[48], M. Huhtinen[37], S. K. Huiberts[128], R. Hulsken[106], C. E. Hultquist[18a], D. L. Humphreys[105], N. Huseynov[12], J. Huston[109], J. Huth[61], L. Huth[48], R. Hyneman[7], G. Iacobucci[56], G. Iakovidis[30], L. Iconomidou-Fayard[66], J. P. Iddon[37], P. Iengo[72a,72b], Y. Iiyama[159], T. Iizawa[159], Y. Ikegami[84], D. Iliadis[158], N. Ilic[161], H. Imam[36a], G. Inacio Goncalves[83d], S. A. Infante Cabanas[140c], T. Ingebretsen Carlson[47a,47b], J. M. Inglis[96], G. Introzzi[73a,73b], M. Iodice[77a], V. Ippolito[75a,75b], R. K. Irwin[94], M. Ishino[159], W. Islam[176], C. Issever[19], S. Istin[22a,ao], K. Itabashi[127], H. Ito[174], R. Iuppa[78a,78b], A. Ivina[175], V. Izzo[72a], P. Jacka[135], P. Jackson[1], P. Jain[48], K. Jakobs[54], T. Jakoubek[175], J. Jamieson[59], W. Jang[159], S. Jankovych[136], M. Javurkova[105], P. Jawahar[103], L. Jeanty[126], J. Jejelava[155a,ae], P. Jenni[54,f], C. E. Jessiman[35], C. Jia[143a], H. Jia[170], J. Jia[151], X. Jia[112,114c], Z. Jia[114a], C. Jiang[52], Q. Jiang[64b], S. Jiggins[48], M. Jimenez Ortega[169], J. Jimenez Pena[13], S. Jin[114a], A. Jinaru[28b], O. Jinnouchi[141], P. Johansson[145], K. A. Johns[7], J. W. Johnson[139], F. A. Jolly[48], D. M. Jones[152], E. Jones[48], K. S. Jones[8], P. Jones[33], R. W. L. Jones[93], T. J. Jones[94], H. L. Joos[55], R. Joshi[122], J. Jovicevic[16], X. Ju[18a], J. J. Junggeburth[37], T. Junkermann[63a], A. Juste Rozas[13,x], M. K. Juzek[88], S. Kabana[140f], A. Kaczmarska[88], S. A. Kadir[149], M. Kado[112], H. Kagan[122], M. Kagan[149], A. Kahn[131], C. Kahra[102], T. Kaji[159], E. Kajomovitz[156], N. Kakati[175], N. Kakoty[13], I. Kalaitzidou[54], S. Kandel[8], N. Kanellos[10], N. J. Kang[139], D. Kar[34j], E. Karentzos[25], K. Karki[8], O. Karkout[117], S. N. Karpov[39], Z. M. Karpova[39], V. Kartvelishvili[93,155b], A. N. Karyukhin[38], E. Kasimi[158], J. Katzy[48], S. Kaur[35], K. Kawade[146], M. P. Kawale[123], C. Kawamoto[89], T. Kawamoto[62], E. F. Kay[37], S. Kazakos[109], V. F. Kazanin[38], J. M. Keaveney[34a], R. Keeler[171], G. V. Kehris[61], J. S. Keller[35], J. M. Kelly[171], J. J. Kempster[152], O. Kepka[134], J. Kerr[162b], B. P. Kerridge[137], B. P. Kerševan[95], L. Keszeghova[29a], R. A. Khan[132], A. Khanov[124], A. G. Kharlamov[38], T. Kharlamova[38], E. E. Khoda[142], M. Kholodenko[133a], T. J. Khoo[19], G. Khoriauli[172], Y. Khoulaki[36a], Y. A. R. Khwaira[130], B. Kibirige[34j], D. Kim[6], D. W. Kim[18b], Y. K. Kim[40], N. Kimura[98], M. K. Kingston[55], A. Kirchhoff[55], C. Kirfel[25], F. Kirfel[25], J. Kirk[137], A. E. Kiryunin[112], S. Kita[163], O. Kivernyk[25], M. Klassen[164], C. Klein[35], L. Klein[172], M. H. Klein[45], S. B. Klein[56], U. Klein[94], A. Klimentov[30], T. Klioutchnikova[37], P. Kluit[117], S. Kluth[112], E. Kneringer[79], T. M. Knight[161], A. Knue[49], M. Kobel[50], D. Kobylianskii[175], S. F. Koch[129], M. Kocian[149], P. Kodyš[136], D. M. Koeck[126], T. Koffas[35], O. Kolay[50], I. Koletsou[4], T. Komarek[88], K. Köneke[55], A. X. Y. Kong[1], T. Kono[121],

N. Konstantinidis[98], P. Kontaxakis[56], B. Konya[100], R. Kopeliansky[42], S. Koperny[87a], R. Koppenhofer[54], K. Korcyl[88], K. Kordas[158,d], A. Korn[98], S. Korn[55], I. Korolkov[13], N. Korotkova[38], B. Kortman[117], O. Kortner[112], S. Kortner[112], W. H. Kostecka[118], M. Kostov[29a], V. V. Kostyukhin[147], A. Kotsokechagia[37], A. Kotwal[51], A. Koulouris[37], A. Kourkoumeli-Charalampidi[73a,73b], C. Kourkoumelis[9], E. Kourlitis[112], O. Kovanda[126], R. Kowalewski[171], W. Kozanecki[126], A. S. Kozhin[38], V. A. Kramarenko[38], G. Kramberger[95], P. Kramer[25], M. W. Krasny[130], A. Krasznahorkay[105], A. C. Kraus[118], J. W. Kraus[177], J. A. Kremer[48], N. B. Krengel[147], T. Kresse[50], L. Kretschmann[177], J. Kretzschmar[94], P. Krieger[161], K. Krizka[21], K. Kroeninger[49], H. Kroha[112], J. Kroll[134], J. Kroll[131], K. S. Krowpman[109], U. Kruchonak[39], H. Krüger[25], N. Krumnack[81], M. C. Kruse[51], O. Kuchinskaia[39], S. Kuday[3a], S. Kuehn[37], R. Kuesters[54], T. Kuhl[48], V. Kukhtin[39], Y. Kulchitsky[39], S. Kuleshov[140b,140d], J. Kull[1], E. V. Kumar[111], M. Kumar[34j], N. Kumari[48], P. Kumari[162b], A. Kupco[134], A. Kupich[38], O. Kuprash[54], H. Kurashige[86], L. L. Kurchaninov[162a], O. Kurdysh[4], A. Kurova[38], M. Kuze[141], A. K. Kvam[105], J. Kvita[125], N. G. Kyriacou[142], M. Laassiri[30], C. Lacasta[169], F. Lacava[75a,75b], H. Lacker[19], D. Lacour[130], N. N. Lad[98], E. Ladygin[39], A. Lafarge[41], B. Laforge[130], T. Lagouri[178], F. Z. Lahbabi[36a], S. Lai[37,55], W. S. Lai[98], I. K. Lakomiec[55], J. E. Lambert[171], S. Lammers[68], W. Lampl[7], C. Lampoudis[158,d], G. Lamprinoudis[172], A. N. Lancaster[118], E. Lançon[30], U. Landgraf[54], M. P. J. Landon[96], V. S. Lang[54], A. J. Lankford[165], F. Lanni[37], K. Lantzsch[25], A. Lanza[73a], M. Lanzac Berrocal[169], J. F. Laporte[138], T. Lari[71a], D. Larsen[17], L. Larson[11], F. Lasagni Manghi[24b], M. Lassnig[37], S. D. Lawlor[145], R. Lazaridou[165], M. Lazzaroni[71a,71b], E. T. T. Le[165], H. D. M. Le[109], E. M. Le Boulicaut[178], L. T. Le Pottier[18a], B. Leban[24a,24b], F. Ledroit-Guillon[60], T. F. Lee[162b], L. L. Leeuw[34c], M. Lefebvre[171], C. Leggett[18a], G. Lehmann Miotto[37], M. Leigh[56], W. A. Leight[105], W. Leinonen[116], A. Leisos[158,u], M. A. L. Leite[83c], C. E. Leitgeb[19], R. Leitner[136], K. J. C. Leney[45], T. Lenz[25], S. Leone[74a], C. Leonidopoulos[52], A. Leopold[150], J. H. Lepage Bourbonnais[35], R. Les[109], C. G. Lester[33], M. Levchenko[38], J. Levêque[4], L. J. Levinson[175], G. Levrini[24a,24b], M. P. Lewicki[88], C. Lewis[142], D. J. Lewis[4], L. Lewitt[145], A. Li[30], B. Li[143a], C. Li[108], C.-Q. Li[112], H. Li[143a], H. Li[103], H. Li[15], H. Li[62], H. Li[143a], J. Li[144a], K. Li[14], L. Li[144a], R. Li[178], S. Li[14,114c], S. Li[144a,144b], T. Li[5], X. Li[106], Y. Li[14], Z. Li[159], Z. Li[14,114c], Z. Li[62], S. Liang[14,114c], Z. Liang[14], M. Liberatore[138], B. Liberti[76a], G. B. Libotte[83d], K. Lie[64c], J. Lieber Marin[83e], H. Lien[68], H. Lin[108], S. F. Lin[151], L. Linden[111], R. E. Lindley[7], J. H.Y. Lindon[37], J. Ling[61], E. Lipeles[131], A. Lipniacka[17], A. Lister[170], J. D. Little[68], B. Liu[14], B. X. Liu[114b], D. Liu[144b], D. Liu[139], E. H. L. Liu[21], J. K. K. Liu[120], K. Liu[144b], K. Liu[144a,144b], M. Liu[62], M. Y. Liu[62], P. Liu[14], Q. Liu[149], S. Liu[151], X. Liu[62], X. Liu[143a], Y. Liu[114b,114c], Y. Liu[168], Y. L. Liu[143a], Y. W. Liu[62], Z. Liu[66,k], S. L. Lloyd[96], E. M. Lobodzinska[48], P. Loch[7], E. Lodhi[161], K. Lohwasser[145], E. Loiacono[48], J. D. Lomas[21], J. D. Long[42], I. Longarini[165], R. Longo[168], A. Lopez Solis[13], N. A. Lopez-canelas[7], N. Lorenzo Martinez[4], A. M. Lory[111], M. Losada[119a], G. Löschcke Centeno[4], X. Lou[47a,47b], X. Lou[14,114c], A. Lounis[66], P. A. Love[93], M. Lu[66], S. Lu[131], Y. J. Lu[154], H. J. Lubatti[142], C. Luci[75a,75b], F. L. Lucio Alves[114a], F. Luehring[68], B. S. Lunday[131], O. Lundberg[150], J. Lunde[37], N. A. Luongo[6], M. S. Lutz[37], A. B. Lux[26], D. Lynn[30], R. Lysak[134], V. Lysenko[135], E. Lytken[100], V. Lyubushkin[39], T. Lyubushkina[39], M. M. Lyukova[151], H. Ma[30], K. Ma[62], L. L. Ma[143a], W. Ma[62], Y. Ma[124], J. C. MacDonald[102], P. C. Machado De Abreu Farias[83e], D. Macina[37], R. Madar[41], T. Madula[98], J. Maeda[86], T. Maeno[30], P. T. Mafa[34c,j], H. Maguire[145], M. Maheshwari[33], V. Maiboroda[66], A. Maio[133a,133b,133d], K. Maj[87a], O. Majersky[48], S. Majewski[126], R. Makhmanazarov[38], N. Makovec[66], V. Maksimovic[16], B. Malaescu[130], J. Malamant[128], Pa. Malecki[88], V. P. Maleev[38], F. Malek[60,o], M. Mali[95], D. Malito[97], U. Mallik[80,*], A. Maloizel[5], S. Maltezos[10], A. Malvezzi Lopes[83d], S. Malyukov[39], J. Mamuzic[95], G. Mancini[53], M. N. Mancini[27], G. Manco[73a,73b], J. P. Mandalia[96], S. S. Mandarry[152], I. Mandić[95], L. Manhaes de Andrade Filho[83a], I. M. Maniatis[175], J. Manjarres Ramos[91], D. C. Mankad[175], A. Mann[111], T. Manoussos[37], M. N. Mantinan[40], S. Manzoni[37], L. Mao[144a], X. Mapekula[34c], A. Marantis[158], R. R. Marcelo Gregorio[96], G. Marchiori[5], C. Marcon[71a], E. Maricic[16], M. Marinescu[48], S. Marium[48], M. Marjanovic[123], A. Markhoos[54], M. Markovitch[66], M. K. Maroun[105], M. C. Marr[148], G. T. Marsden[103], E. J. Marshall[93], Z. Marshall[18a], S. Marti-Garcia[169], J. Martin[98], T. A. Martin[137], V. J. Martin[52], B. Martin dit Latour[17], L. Martinelli[75a,75b], M. Martinez[13,x], P. Martinez Agullo[169], V. I. Martinez Outschoorn[105], P. Martinez Suarez[37], S. Martin-Haugh[137], G. Martinovicova[136], V. S. Martoiu[28b], A. C. Martyniuk[98], A. Marzin[37], D. Mascione[78a,78b], L. Masetti[102], J. Masik[103], A. L. Maslennikov[39], S. L. Mason[42], P. Massarotti[72a,72b], P. Mastrandrea[74a,74b], A. Mastroberardino[44a,44b], T. Masubuchi[127], T. T. Mathew[126], J. Matousek[136], D. M. Mattern[49], K. Mauer[48], J. Maurer[28b], T. Maurin[59], A. J. Maury[66], B. Maček[95], C. Mavungu Tsava[104], D. A. Maximov[38], A. E. May[103], E. Mayer[41],

R. Mazini[34j], I. Maznas[118], S. M. Mazza[139], E. Mazzeo[37], J. P. Mc Gowan[171], S. P. Mc Kee[108], C. A. Mc Lean[6], C. C. McCracken[170], E. F. McDonald[107], A. E. McDougall[117], L. F. Mcelhinney[93], J. A. Mcfayden[152], R. P. McGovern[131], R. P. Mckenzie[34j], T. C. Mclachlan[48], D. J. Mclaughlin[98], S. J. McMahon[137], C. M. Mcpartland[94], R. A. McPherson[171,ab], S. Mehlhase[111], A. Mehta[94], D. Melini[169], B. R. Mellado Garcia[34j], A. H. Melo[55], F. Meloni[48], A. M. Mendes Jacques Da Costa[103], L. Meng[93], S. Menke[112], M. Mentink[37], E. Meoni[44a,44b], G. Mercado[118], S. Merianos[158], C. Merlassino[69a,69c], C. Meroni[71a,71b], J. Metcalfe[6], A. S. Mete[6], E. Meuser[102], C. Meyer[68], J.-P. Meyer[138], Y. Miao[114a], R. P. Middleton[137], M. Mihovilovic[66], L. Mijović[52], G. Mikenberg[175], M. Mikestikova[134], M. Mikuž[95], H. Mildner[102], A. Milic[37], D. W. Miller[40], E. H. Miller[149], A. Milov[175], D. A. Milstead[47a,47b], T. Min[114a], A. A. Minaenko[38], I. A. Minashvili[155b], A. I. Mincer[120], B. Mindur[87a], M. Mineev[39], Y. Mino[89], L. M. Mir[13], M. Miralles Lopez[59], M. Mironova[18a], M. Missio[41], A. Mitra[173], V. A. Mitsou[169], Y. Mitsumori[113], O. Miu[161], P. S. Miyagawa[96], T. Mkrtchyan[37], M. Mlinarevic[98], T. Mlinarevic[98], M. Mlynarikova[136], L. Mlynarska[87a], C. Mo[144a], S. Mobius[20], M. H. Mohamed Farook[115], S. Mohapatra[42], M. F. Mohd Soberi[52], S. Mohiuddin[124], G. Mokgatitswane[34j], L. Moleri[175], U. Molinatti[129], L. G. Mollier[20], B. Mondal[134], S. Mondal[135], K. Mönig[48], E. Monnier[104], L. Monsonis Romero[169], J. Montejo Berlingen[13], A. Montella[47a,47b], M. Montella[122], F. Montereali[77a,77b], F. Monticelli[92], S. Monzani[69a,69c], A. Morancho Tarda[43], N. Morange[66], A. L. Moreira De Carvalho[48], M. Moreno Llácer[169], C. Moreno Martinez[56], J. M. Moreno Perez[23b], P. Morettini[57b], S. Morgenstern[37], M. Morii[61], M. Morinaga[159], M. Moritsu[90], F. Morodei[75a,75b], P. Moschovakos[37], B. Moser[54], M. Mosidze[155b], T. Moskalets[45], P. Moskvitina[116], J. Moss[32], P. Moszkowicz[87a], T. Motta Quirino[83d], A. Moussa[36d], Y. Moyal[175], H. Moyano Gomez[13], E. J. W. Moyse[105], T. G. Mroz[88], S. Muanza[104], M. Mucha[25], J. Mueller[132], R. Müller[37], G. A. Mullier[167], A. J. Mullin[33], J. J. Mullin[51], A. C. Mullins[45], A. E. Mulski[61], D. P. Mungo[161], D. Munoz Perez[169], F. J. Munoz Sanchez[103], W. J. Murray[137,173], M. Muškinja[95], C. Mwewa[48], A. G. Myagkov[38,a], A. J. Myers[8], G. Myers[108], M. Myska[135], B. P. Nachman[149], K. Nagai[129], K. Nagano[84], R. Nagasaka[159], J. L. Nagle[30,al], E. Nagy[104], A. M. Nairz[37], Y. Nakahama[84], K. Nakamura[84], K. Nakkalil[5], A. Nandi[63b], H. Nanjo[127], E. A. Narayanan[45], Y. Narukawa[159], I. Naryshkin[38], L. Nasella[71a,71b], S. Nasri[119b], C. Nass[25], G. Navarro[23a], A. Nayaz[19], P. Y. Nechaeva[38], S. Nechaeva[24a,24b], F. Nechansky[134], L. Nedic[129], T. J. Neep[21], A. Negri[73a,73b], M. Negrini[24b], C. Nellist[117], C. Nelson[106], K. Nelson[108], S. Nemecek[134], M. Nessi[37,g], M. S. Neubauer[168], J. Newell[94], P. R. Newman[21], Y. W. Y. Ng[168], B. Ngair[119a], H. D. N. Nguyen[110], J. D. Nichols[123], R. B. Nickerson[129], R. Nicolaidou[138], J. Nielsen[139], M. Niemeyer[55], J. Niermann[37], N. Nikiforou[37], V. Nikolaenko[38,a], I. Nikolic-Audit[130], P. Nilsson[30], I. Ninca[48], G. Ninio[157], A. Nisati[75a], R. Nisius[112], N. Nitika[175], E. K. Nkadimeng[34b], T. Nobe[159], D. Noll[149], T. Nommensen[153], M. B. Norfolk[145], B. J. Norman[35], L. C. Nosler[18a], M. Noury[36a], J. Novak[95], T. Novak[95], R. Novotny[135], L. Nozka[125], K. Ntekas[165], D. Ntounis[149], N. M. J. Nunes De Moura Junior[83b], J. Ocariz[130], I. Ochoa[133a], A. Odella Rodriguez[13], S. Oerdek[48,y], J. T. Offermann[40], A. Ogrodnik[88], A. Oh[103], C. C. Ohm[150], H. Oide[84], M. L. Ojeda[37], Y. Okumura[159], L. F. Oleiro Seabra[133a], I. Oleksiyuk[56], G. Oliveira Correa[13], D. Oliveira Damazio[30], J. L. Oliver[1], R. Omar[68], Ö. O. Öncel[54], A. P. O'Neill[20], A. Onofre[133a,133e,e], P. U. E. Onyisi[11], M. J. Oreglia[40], D. Orestano[77a,77b], R. Orlandini[77a,77b], R. S. Orr[161], L. M. Osojnak[42], Y. Osumi[113], G. Otero y Garzon[31], H. Otono[90], M. Ouchrif[36d], F. Ould-Saada[128], T. Ovsiannikova[142], M. Owen[59], R. E. Owen[137], V. E. Ozcan[22a], F. Ozturk[88], N. Ozturk[8], S. Ozturk[82], H. A. Pacey[129], K. Pachal[162a], A. Pacheco Pages[13], C. Padilla Aranda[13], G. Padovano[75a,75b], S. Pagan Griso[18a], J. Pampel[25], J. Pan[178], D. K. Panchal[11], C. E. Pandini[60], J. G. Panduro Vazquez[137], H. D. Pandya[1], H. Pang[138], P. Pani[48], G. Panizzo[69a,69c], L. Panwar[130], L. Paolozzi[56], S. Parajuli[168], A. Paramonov[6], C. Paraskevopoulos[53], D. Paredes Hernandez[64b], S. R. Paredes Saenz[52], A. Pareti[73a,73b], K. R. Park[42], T. H. Park[112], F. Parodi[57a,57b], J. A. Parsons[42], U. Parzefall[54], B. Pascual Dias[41], L. Pascual Dominguez[101], E. Pasqualucci[75a], S. Passaggio[57b], F. Pastore[97], P. Patel[88], U. M. Patel[51], J. R. Pater[103], T. Pauly[37], F. Pauwels[136], C. I. Pazos[164], M. Pedersen[128], R. Pedro[133a], S. V. Peleganchuk[38], O. Penc[134], S. Peng[15], G. D. Penn[178], K. E. Penski[111], M. Penzin[38], B. S. Peralva[83d], A. P. Pereira Peixoto[142], L. Pereira Sanchez[149], D. V. Perepelitsa[30,al], G. Perera[105], E. Perez Codina[37], M. Perganti[10], H. Pernegger[37], S. Perrella[75a,75b], K. Peters[48], R. F. Y. Peters[103], B. A. Petersen[37], T. C. Petersen[43], E. Petit[104], V. Petousis[135], A. R. Petri[71a,71b], C. Petridou[158,d], T. Petru[136], M. Pettee[18a], A. Petukhov[82], K. Petukhova[37], R. Pezoa[140g], L. Pezzotti[24a,24b], G. Pezzullo[178], L. Pfaffenbichler[37], A. J. Pfleger[79], T. M. Pham[176], T. Pham[107], P. W. Phillips[137], G. Piacquadio[151],

E. Pianori[18a], F. Piazza[126], R. Piegaia[31], D. Pietreanu[28b], A. D. Pilkington[103], M. Pinamonti[69a,69c], J. L. Pinfold[2], G. Pinheiro Matos[42], B. C. Pinheiro Pereira[133a], J. Pinol Bel[13], A. E. Pinto Pinoargote[130], L. Pintucci[69a,69c], K. M. Piper[152], A. Pirttikoski[56], D. A. Pizzi[35], L. Pizzimento[64b], A. Plebani[33], M.-A. Pleier[30], V. Pleskot[136], E. Plotnikova[39], G. Poddar[96], R. Poettgen[100], L. Poggioli[130], S. Polacek[136], G. Polesello[73a], A. Poley[148], A. Polini[24b], C. S. Pollard[173], Z. B. Pollock[122], E. Pompa Pacchi[123], N. I. Pond[98], D. Ponomarenko[68], L. Pontecorvo[37], S. Popa[28a], G. A. Popeneciu[28d], A. Poreba[37], D. M. Portillo Quintero[162a], S. Pospisil[135], M. A. Postill[145], P. Postolache[28c], K. Potamianos[173], P. A. Potepa[87a], I. N. Potrap[39], C. J. Potter[33], H. Potti[153], J. Poveda[169], M. E. Pozo Astigarraga[37], R. Pozzi[37], A. Prades Ibanez[76a,76b], S. R. Pradhan[145], J. Pretel[171], D. Price[103], M. Primavera[70a], L. Primomo[69a,69c], M. A. Principe Martin[101], R. Privara[125], T. Procter[87b], M. L. Proffitt[142], N. Proklova[131], K. Prokofiev[64c], G. Proto[112], J. Proudfoot[6], M. Przybycien[87a], W. W. Przygoda[87b], A. Psallidas[46], J. E. Puddefoot[145], D. Pudzha[53], H. I. Purnell[1], D. Pyatiizbyantseva[116], J. Qian[108], R. Qian[109], D. Qichen[129], Y. Qin[13], T. Qiu[52], A. Quadt[55], M. Queitsch-Maitland[103], G. Quetant[56], R. P. Quinn[170], G. Rabanal Bolanos[61], D. Rafanoharana[112], F. Raffaeli[76a,76b], F. Ragusa[71a,71b], J. L. Rainbolt[40], S. Rajagopalan[30], E. Ramakoti[39], L. Rambelli[57a,57b], I. A. Ramirez-Berend[35], K. Ran[108,114c], D. S. Rankin[131], N. P. Rapheeha[34j], H. Rasheed[28b], A. Rastogi[18a], S. Rave[102], S. Ravera[57a,57b], B. Ravina[37], I. Ravinovich[175], M. Raymond[37], A. L. Read[128], N. P. Readioff[145], D. M. Rebuzzi[73a,73b], A. S. Reed[59], K. Reeves[27], D. Reikher[37], A. Rej[49], C. Rembser[37], H. Ren[62], M. Renda[28b], F. Renner[48], A. G. Rennie[59], M. Repik[56], A. L. Rescia[57a,57b], S. Resconi[71a], M. Ressegotti[57a,57b], S. Rettie[117], W. F. Rettie[35], M. M. Revering[33], E. Reynolds[18a], O. L. Rezanova[39], P. Reznicek[136], H. Riani[36d], N. Ribaric[51], B. Ricci[69a,69c], E. Ricci[78a,78b], R. Richter[112], S. Richter[47a,47b], E. Richter-Was[87b], M. Ridel[130], S. Ridouani[36d], P. Rieck[120], P. Riedler[37], E. M. Riefel[47a,47b], J. O. Rieger[117], M. Rijssenbeek[151], M. Rimoldi[37], L. Rinaldi[24a,24b], P. Rincke[55,167], G. Ripellino[167], I. Riu[13], J. C. Rivera Vergara[171], F. Rizatdinova[124], E. Rizvi[96], B. R. Roberts[18a], S. S. Roberts[139], D. Robinson[33], A. Robson[59], A. Rocchi[76a,76b], C. Roda[74a,74b], F. A. Rodriguez[118], S. Rodriguez Bosca[37], Y. Rodriguez Garcia[23a], A. M. Rodríguez Vera[118], S. Roe[37], J. T. Roemer[37], O. Røhne[128], R. A. Rojas[37], C. P. A. Roland[130], A. Romaniouk[79], E. Romano[73a,73b], M. Romano[24b], A. C. Romero Hernandez[168], N. Rompotis[94], L. Roos[130], S. Rosati[75a], B. J. Rosser[40], E. Rossi[129], E. Rossi[72a,72b], L. P. Rossi[61], L. Rossini[54], R. Rosten[122], M. Rotaru[28b], D. Rousseau[66], D. Rousso[48], S. Roy-Garand[161], A. Rozanov[104], Z. M. A. Rozario[59], Y. Rozen[156], A. Rubio Jimenez[169], V. H. Ruelas Rivera[19], T. A. Ruggeri[1], A. Ruggiero[129], A. Ruiz-Martinez[169], A. Rummler[37], G. B. Rupnik Boero[37], Z. Rurikova[54], N. A. Rusakovich[39], S. Ruscelli[49], H. L. Russell[171], G. Russo[75a,75b], J. P. Rutherfoord[7], S. Rutherford Colmenares[33], M. Rybar[136], P. Rybczynski[87a], A. Ryzhov[45], J. A. Sabater Iglesias[56], H. F.-W. Sadrozinski[139], F. Safai Tehrani[75a], S. Saha[1], M. Sahinsoy[82], B. Sahoo[175], A. Saibel[169], B. T. Saifuddin[123], M. Saimpert[138], G. T. Saito[83c], M. Saito[159], T. Saito[159], A. Sala[71a,71b], A. Salnikov[149], J. Salt[169], A. Salvador Salas[157], F. Salvatore[152], A. Salzburger[37], D. Sammel[54], E. Sampson[93], D. Sampsonidis[158,d], D. Sampsonidou[126], M. A. A. Samy[59], J. Sánchez[169], V. Sanchez Sebastian[169], H. Sandaker[128], C. O. Sander[48], J. A. Sandesara[176], M. Sandhoff[177], C. Sandoval[23b], L. Sanfilippo[63a], D. P. C. Sankey[137], T. Sano[89], A. Sansoni[53], M. Santana Queiroz[18b], L. Santi[37], C. Santoni[41], H. Santos[133a,133b], A. Santra[175], E. Sanzani[24a,24b], K. A. Saoucha[85b], J. G. Saraiva[133a,133d], J. Sardain[7], O. Sasaki[84], K. Sato[163], C. Sauer[37], E. Sauvan[4], P. Savard[161,ai], R. Sawada[159], C. Sawyer[137], L. Sawyer[99], A. M. Sayed[27], C. Sbarra[24b], A. Sbrizzi[24a,24b], T. Scanlon[98], J. Schaarschmidt[142], U. Schäfer[102], A. C. Schaffer[45,66], D. Schaile[111], R. D. Schamberger[151], C. Scharf[19], M. M. Schefer[20], V. A. Schegelsky[38], D. Scheirich[136], M. Schernau[140f], C. Scheulen[56], C. Schiavi[57a,57b], M. Schioppa[44a,44b], B. Schlag[149], S. Schlenker[37], J. Schmeing[177], E. Schmidt[112], M. A. Schmidt[177], K. Schmieden[25], C. Schmitt[102], N. Schmitt[102], S. Schmitt[48], N. A. Schneider[111], L. Schoeffel[138], A. Schoening[63b], P. G. Scholer[35], E. Schopf[147], M. Schott[25], S. Schramm[56], T. Schroer[56], H.-C. Schultz-Coulon[63a], M. Schumacher[54], B. A. Schumm[139], Ph. Schune[138], H. R. Schwartz[7], A. Schwartzman[149], T. A. Schwarz[108], Ph. Schwemling[138], R. Schwienhorst[109], F. G. Sciacca[20], A. Sciandra[30], G. Sciolla[27], F. Scuri[74a], C. D. Sebastiani[37], K. Sedlaczek[118], S. C. Seidel[115], A. Seiden[139], B. D. Seidlitz[42], C. Seitz[48], J. M. Seixas[83b], G. Sekhniaidze[72a], L. Selem[60], N. Semprini-Cesari[24a,24b], A. Semushin[179], D. Sengupta[56], V. Senthilkumar[169], L. Serin[66], M. Sessa[72a,72b], H. Severini[123], F. Sforza[57a,57b], A. Sfyrla[56], Q. Sha[14], H. Shaddix[118], A. H. Shah[33], R. Shaheen[150], J. D. Shahinian[131], M. Shamim[37], L. Y. Shan[14], M. Shapiro[18a], A. Sharma[37], A. S. Sharma[170], P. Sharma[30], P. B. Shatalov[38], K. Shaw[152], S. M. Shaw[103],

Q. Shen[14], D. J. Sheppard[148], P. Sherwood[98], L. Shi[98], X. Shi[14], S. Shimizu[84], I. P. J. Shipsey[129,*], S. Shirabe[90], M. Shiyakova[39,z], M. J. Shochet[40], D. R. Shope[128], B. Shrestha[123], S. Shrestha[122,an], I. Shreyber[39], M. J. Shroff[171], P. Sicho[134], A. M. Sickles[168], E. Sideras Haddad[34j,166], A. C. Sidley[117], A. Sidoti[24b], F. Siegert[50], Dj. Sijacki[16], F. Sili[62], J. M. Silva[52], I. Silva Ferreira[83b], M. V. Silva Oliveira[30], S. B. Silverstein[47a], S. Simion[66], R. Simoniello[37], E. L. Simpson[103], H. Simpson[152], L. R. Simpson[6], S. Simsek[82], S. Sindhu[55], P. Sinervo[161], S. N. Singh[27], S. Singh[30], S. Sinha[48], S. Sinha[103], M. Sioli[24a,24b], K. Sioulas[9], I. Siral[37], E. Sitnikova[48], J. Sjölin[47a,47b], A. Skaf[55], E. Skorda[21], P. Skubic[123], M. Slawinska[88], I. Slazyk[17], I. Sliusar[128], V. Smakhtin[175], B. H. Smart[137], S. Yu. Smirnov[140b], Y. Smirnov[82], L. N. Smirnova[38,a], O. Smirnova[100], A. C. Smith[42], D. R. Smith[165], J. L. Smith[103], M. B. Smith[35], R. Smith[149], H. Smitmanns[102], M. Smizanska[93], K. Smolek[135], P. Smolyanskiy[135], A. A. Snesarev[39], H. L. Snoek[117], S. Snyder[30], R. Sobie[171,ab], A. Soffer[157], C. A. Solans Sanchez[37], E. Yu. Soldatov[39], U. Soldevila[169], A. A. Solodkov[34j], S. Solomon[27], A. Soloshenko[39], K. Solovieva[54], O. V. Solovyanov[41], P. Sommer[50], A. Sonay[13], A. Sopczak[135], A. L. Sopio[52], F. Sopkova[29b], J. D. Sorenson[115], I. R. Sotarriva Alvarez[141], V. Sothilingam[63a], O. J. Soto Sandoval[140b,140c], S. Sottocornola[68], R. Soualah[85a], Z. Soumaimi[36e], D. South[48], N. Soybelman[175], S. Spagnolo[70a,70b], M. Spalla[112], D. Sperlich[54], B. Spisso[72a,72b], D. P. Spiteri[59], L. Splendori[104], M. Spousta[136], E. J. Staats[35], R. Stamen[63a], E. Stanecka[88], W. Stanek-Maslouska[48], M. V. Stange[50], B. Stanislaus[18a], M. M. Stanitzki[48], E. A. Starchenko[38], G. H. Stark[139], J. Stark[91], P. Staroba[134], P. Starovoitov[85b], R. Staszewski[88], C. Stauch[111], G. Stavropoulos[46], A. Steffl[37], A. Stein[102], P. Steinberg[30], B. Stelzer[148,162a], H. J. Stelzer[132], O. Stelzer[162a], H. Stenzel[58], T. J. Stevenson[152], G. A. Stewart[37], J. R. Stewart[124], G. Stoicea[28b], M. Stolarski[133a], S. Stonjek[112], A. Straessner[50], J. Strandberg[150], S. Strandberg[47a,47b], M. Stratmann[177], M. Strauss[123], T. Strebler[104], P. Strizenec[29b], R. Ströhmer[172], D. M. Strom[126], R. Stroynowski[45], A. Strubig[47a,47b], S. A. Stucci[30], B. Stugu[17], J. Stupak[123], N. A. Styles[48], D. Su[149], S. Su[62], X. Su[62], D. Suchy[29a], A. D. Sudhakar Ponnu[55], K. Sugizaki[131], V. V. Sulin[38], D. M. S. Sultan[129], L. Sultanaliyeva[25], S. Sultansoy[3b], S. Sun[176], W. Sun[14], N. Sur[100], M. R. Sutton[152], M. Svatos[134], P. N. Swallow[33], M. Swiatlowski[162a], A. Swoboda[37], I. Sykora[29a], M. Sykora[136], T. Sykora[136], D. Ta[102], K. Tackmann[48,y], A. Taffard[165], R. Tafirout[162a], Y. Takubo[84], M. Talby[104], A. A. Talyshev[38], K. C. Tam[64b], N. M. Tamir[157], A. Tanaka[159], J. Tanaka[159], R. Tanaka[66], M. Tanasini[151], Z. Tao[170], S. Tapia Araya[140g], S. Tapprogge[102], A. Tarek Abouelfadl Mohamed[37], S. Tarem[156], K. Tariq[14], G. Tarna[37], G. F. Tartarelli[71a], M. J. Tartarin[91], P. Tas[136], M. Tasevsky[134], E. Tassi[44a,44b], A. C. Tate[168], Y. Tayalati[36e,aa], G. N. Taylor[107], W. Taylor[162b], R. J. Taylor Vara[169], A. S. Tegetmeier[91], P. Teixeira-Dias[97], J. J. Teoh[161], K. Terashi[159], J. Terron[101], S. Terzo[13], M. Testa[53], R. J. Teuscher[161,ab], A. Thaler[79], O. Theiner[56], T. Theveneaux-Pelzer[104], D. W. Thomas[97], J. P. Thomas[21], E. A. Thompson[18a], P. D. Thompson[21], E. Thomson[131], R. E. Thornberry[45], C. Tian[62], Y. Tian[56], V. Tikhomirov[82], Yu. A. Tikhonov[39], S. Timoshenko[38], D. Timoshyn[136], E. X. L. Ting[1], P. Tipton[178], A. Tishelman-Charny[30], K. Todome[141], S. Todorova-Nova[136], L. Toffolin[69a,69c], M. Togawa[84], J. Tojo[90], S. Tokár[29a], O. Toldaiev[68], G. Tolkachev[104], M. Tomoto[84], L. Tompkins[149,n], E. Torrence[126], H. Torres[91], D. I. Torres Arza[140g], E. Torró Pastor[169], M. Toscani[31], C. Tosciri[40], M. Tost[11], D. R. Tovey[145], T. Trefzger[172], P. M. Tricarico[13], A. Tricoli[30], I. M. Trigger[162a], S. Trincaz-Duvoid[130], D. A. Trischuk[171], A. Tropina[39], D. Truncali[76a,76b], L. Truong[34c], M. Trzebinski[88], A. Trzupek[88], F. Tsai[151], M. Tsai[108], A. Tsiamis[158], P. V. Tsiareshka[39], S. Tsigaridas[162a], A. Tsirigotis[158,u], V. Tsiskaridze[155a], E. G. Tskhadadze[155a], Y. Tsujikawa[89], I. I. Tsukerman[38], V. Tsulaia[18a], S. Tsuno[84], K. Tsuri[121], D. Tsybychev[151], Y. Tu[64b], A. Tudorache[28b], V. Tudorache[28b], S. B. Tuncay[129], S. Turchikhin[57a,57b], I. Turk Cakir[3a], R. Turra[71a], T. Turtuvshin[39,ac], P. M. Tuts[42], S. Tzamarias[158,d], Y. Uematsu[84], F. Ukegawa[163], P. A. Ulloa Poblete[140b,140c], E. N. Umaka[30], G. Unal[37], A. Undrus[30], G. Unel[165], J. Urban[29b], P. Urrejola[140e], G. Usai[8], R. Ushioda[160], M. Usman[110], F. Ustuner[52], Z. Uysal[82], V. Vacek[135], B. Vachon[106], T. Vafeiadis[37], A. Vaitkus[98], C. Valderanis[111], E. Valdes Santurio[47a,47b], M. Valente[37], S. Valentinetti[24a,24b], A. Valero[169], E. Valiente Moreno[169], A. Vallier[91], J. A. Valls Ferrer[169], D. R. Van Arneman[117], A. Van Der Graaf[49], H. Z. Van Der Schyf[34j], P. Van Gemmeren[6], M. Van Rijnbach[37], S. Van Stroud[98], I. Van Vulpen[117], P. Vana[136], M. Vanadia[76a,76b], U. M. Vande Voorde[150], W. Vandelli[37], E. R. Vandewall[149], D. Vannicola[157], L. Vannoli[53], R. Vari[75a], M. Varma[178], E. W. Varnes[7], C. Varni[118], D. Varouchas[66], L. Varriale[169], K. E. Varvell[153], M. E. Vasile[28b], L. Vaslin[84], M. D. Vassilev[149], A. Vasyukov[39], L. M. Vaughan[124], R. Vavricka[136], T. Vazquez Schroeder[13], J. Veatch[32], V. Vecchio[103], M. J. Veen[105], I. Veliscek[30], I. Velkovska[95], L. M. Veloce[161], F. Veloso[133a,133c], A. G. Veltman[52], S. Veneziano[75a], A. Ventura[70a,70b], A. Verbytskyi[112],

M. Verducci[74a,74b], C. Vergis[96], M. Verissimo De Araujo[83b], W. Verkerke[117], J. C. Vermeulen[117], C. Vernieri[149], M. Vessella[165], M. C. Vetterli[148,ai], A. Vgenopoulos[102], N. Viaux Maira[140g,af], T. Vickey[145], O. E. Vickey Boeriu[145], G. H. A. Viehhauser[129], L. Vigani[63b], M. Vigl[112], M. Villa[24a,24b], M. Villaplana Perez[169], E. M. Villhauer[40], E. Vilucchi[53], M. Vincent[169], M. G. Vincter[35], A. Visibile[117], A. Visive[117], C. Vittori[37], I. Vivarelli[24a,24b], M. I. Vivas Albornoz[48], E. Voevodina[112], F. Vogel[111], J. C. Voigt[50], P. Vokac[135], Yu. Volkotrub[87b], L. Vomberg[25], E. Von Toerne[25], B. Vormwald[37], K. Vorobev[51], M. Vos[169], K. Voss[147], M. Vozak[37], L. Vozdecky[123], N. Vranjes[16], M. Vranjes Milosavljevic[16], M. Vreeswijk[117], N. K. Vu[144a,144b], R. Vuillermet[37], O. Vujinovic[102], I. Vukotic[40], I. K. Vyas[35], J. F. Wack[33], S. Wada[163], C. Wagner[149], J. M. Wagner[18a], W. Wagner[177], S. Wahdan[177], H. Wahlberg[92], C. H. Waits[123], J. Walder[137], R. Walker[111], K. Walkingshaw Pass[59], W. Walkowiak[147], A. Wall[131], E. J. Wallin[100], T. Wamorkar[18a], K. Wandall-Christensen[169], A. Wang[62], A. Z. Wang[139], C. Wang[102], C. Wang[11], H. Wang[18a], J. Wang[64c], P. Wang[103], P. Wang[98], R. Wang[61], R. Wang[6], S. M. Wang[154], S. Wang[14], T. Wang[116], T. Wang[62], W. T. Wang[129], W. Wang[14], X. Wang[168], X. Wang[144a], X. Wang[48], Y. Wang[151], Y. Wang[62], Z. Wang[108], Z. Wang[144b], Z. Wang[108], C. Wanotayaroj[84], A. Warburton[106], A. L. Warnerbring[147], S. Waterhouse[97], A. T. Watson[21], H. Watson[52], M. F. Watson[21], E. Watton[37], G. Watts[142], B. M. Waugh[98], J. M. Webb[54], C. Weber[30], H. A. Weber[19], M. S. Weber[20], S. M. Weber[63a], C. Wei[62], Y. Wei[54], A. R. Weidberg[129], E. J. Weik[120], J. Weingarten[49], C. Weiser[54], C. J. Wells[48], T. Wenaus[30], T. Wengler[37], N. S. Wenke[112], N. Wermes[25], M. Wessels[63a], A. M. Wharton[93], A. S. White[61], A. White[8], M. J. White[1], D. Whiteson[165], L. Wickremasinghe[127], W. Wiedenmann[176], M. Wielers[137], R. Wierda[150], C. Wiglesworth[43], H. G. Wilkens[37], J. J. H. Wilkinson[33], D. M. Williams[42], H. H. Williams[131], S. Williams[33], S. Willocq[105], B. J. Wilson[103], D. J. Wilson[103], P. J. Windischhofer[40], F. I. Winkel[31], F. Winklmeier[126], B. T. Winter[54], M. Wittgen[149], M. Wobisch[99], T. Wojtkowski[60], Z. Wolffs[117], J. Wollrath[37], M. W. Wolter[88], H. Wolters[133a,133c], M. C. Wong[139], E. L. Woodward[42], S. D. Worm[48], B. K. Wosiek[88], K. W. Woźniak[88], S. Wozniewski[55], K. Wraight[59], C. Wu[161], C. Wu[21], J. Wu[159], M. Wu[114b], M. Wu[116], S. L. Wu[176], S. Wu[14,ak], X. Wu[62], Y. Q. Wu[161], Y. Wu[62], Z. Wu[4], Z. Wu[114a], J. Wuerzinger[112], T. R. Wyatt[103], B. M. Wynne[52], S. Xella[43], L. Xia[114a], M. Xie[62], A. Xiong[126], D. Xu[14], H. Xu[62], L. Xu[62], R. Xu[131], T. Xu[108], W. Xu[114a], Y. Xu[142], Z. Xu[52], R. Xue[132], B. Yabsley[153], S. Yacoob[34a], Y. Yamaguchi[84], E. Yamashita[159], H. Yamauchi[163], T. Yamazaki[18a], Y. Yamazaki[86], S. Yan[59], Z. Yan[105], H. J. Yang[144a,144b], H. T. Yang[62], S. Yang[62], T. Yang[64c], X. Yang[37], X. Yang[14], Y. Yang[159], Y. Yang[62], W.-M. Yao[18a], C. L. Yardley[152], J. Ye[14], S. Ye[30], X. Ye[62], Y. Yeh[98], I. Yeletskikh[39], B. Yeo[18b], M. R. Yexley[98], T. P. Yildirim[129], K. Yorita[174], C. J. S. Young[37], C. Young[149], N. D. Young[126], Y. Yu[62], J. Yuan[14,114c], M. Yuan[108], R. Yuan[144b], L. Yue[98], M. Zaazoua[62], B. Zabinski[88], I. Zahir[36a], A. Zaio[57a,57b], Z. K. Zak[88], T. Zakareishvili[169], S. Zambito[56], J. A. Zamora Saa[140d], J. Zang[159], R. Zanzottera[71a,71b], O. Zaplatilek[135], C. Zeitnitz[177], H. Zeng[14], D. T. Zenger Jr.[27], O. Zenin[38], T. Ženiš[29a], S. Zenz[96], D. Zerwas[66], M. Zhai[14,114c], D. F. Zhang[145], G. Zhang[14,ak], J. Zhang[143a], J. Zhang[6], L. Zhang[62], L. Zhang[114a], P. Zhang[14,114c], R. Zhang[114a], S. Zhang[91], T. Zhang[159], Y. Zhang[142], Y. Zhang[98], Y. Zhang[62], Y. Zhang[114a], Z. Zhang[18a], Z. Zhang[143a], Z. Zhang[66], H. Zhao[142], T. Zhao[143a], Y. Zhao[35], Z. Zhao[62], Z. Zhao[62], A. Zhemchugov[39], J. Zheng[114a], K. Zheng[168], X. Zheng[62], Z. Zheng[149], D. Zhong[168], B. Zhou[108], H. Zhou[7], N. Zhou[144a], Y. Zhou[15], Y. Zhou[114a], Y. Zhou[7], J. Zhu[108], X. Zhu[144b], Y. Zhu[144a], Y. Zhu[62], X. Zhuang[14], K. Zhukov[68], N. I. Zimine[39], J. Zinsser[63b], M. Ziolkowski[147], L. Živković[16], A. Zoccoli[24a,24b], K. Zoch[61], A. Zografos[37], T. G. Zorbas[145], O. Zormpa[46], L. Zwalinski[37]

[1] Department of Physics, University of Adelaide, Adelaide, Australia
[2] Department of Physics, University of Alberta, Edmonton, AB, Canada
[3] [(a)]Department of Physics, Ankara University, Ankara, Turkey; [(b)]Division of Physics, TOBB University of Economics and Technology, Ankara, Turkey
[4] LAPP, Université Savoie Mont Blanc, CNRS/IN2P3, Annecy, France
[5] APC, Université Paris Cité, CNRS/IN2P3, Paris, France
[6] High Energy Physics Division, Argonne National Laboratory, Argonne, IL, USA
[7] Department of Physics, University of Arizona, Tucson, AZ, USA
[8] Department of Physics, University of Texas at Arlington, Arlington, TX, USA
[9] Physics Department, National and Kapodistrian University of Athens, Athens, Greece
[10] Physics Department, National Technical University of Athens, Zografou, Greece

[11] Department of Physics, University of Texas at Austin, Austin, TX, USA
[12] Institute of Physics, Azerbaijan Academy of Sciences, Baku, Azerbaijan
[13] Institut de Física d'Altes Energies (IFAE), Barcelona Institute of Science and Technology, Barcelona, Spain
[14] Institute of High Energy Physics, Chinese Academy of Sciences, Beijing, China
[15] Physics Department, Tsinghua University, Beijing, China
[16] Institute of Physics, University of Belgrade, Belgrade, Serbia
[17] Department for Physics and Technology, University of Bergen, Bergen, Norway
[18] [(a)]Physics Division, Lawrence Berkeley National Laboratory, Berkeley, CA, USA; [(b)]University of California, Berkeley, CA, USA
[19] Institut für Physik, Humboldt Universität zu Berlin, Berlin, Germany
[20] Albert Einstein Center for Fundamental Physics and Laboratory for High Energy Physics, University of Bern, Bern, Switzerland
[21] School of Physics and Astronomy, University of Birmingham, Birmingham, UK
[22] [(a)]Department of Physics, Bogazici University, Istanbul, Turkey; [(b)]Department of Physics Engineering, Gaziantep University, Gaziantep, Turkey; [(c)]Department of Physics, Istanbul University, Istanbul, Turkey
[23] [(a)]Facultad de Ciencias y Centro de Investigaciónes, Universidad Antonio Nariño, Bogotá, Colombia; [(b)]Departamento de Física, Universidad Nacional de Colombia, Bogotá, Colombia
[24] [(a)]Dipartimento di Fisica e Astronomia A. Righi, Università di Bologna, Bologna, Italy; [(b)]INFN Sezione di Bologna, Bologna, Italy
[25] Physikalisches Institut, Universität Bonn, Bonn, Germany
[26] Department of Physics, Boston University, Boston, MA, USA
[27] Department of Physics, Brandeis University, Waltham, MA, USA
[28] [(a)]Transilvania University of Brasov, Brasov, Romania; [(b)]Horia Hulubei National Institute of Physics and Nuclear Engineering, Bucharest, Romania; [(c)]Department of Physics, Alexandru Ioan Cuza University of Iasi, Iasi, Romania ; [(d)]Physics Department, National Institute for Research and Development of Isotopic and Molecular Technologies, Cluj-Napoca, Romania; [(e)]National University of Science and Technology Politechnica, Bucharest, Romania; [(f)]West University in Timisoara, Timisoara, Romania; [(g)]Faculty of Physics, University of Bucharest, Bucharest, Romania
[29] [(a)]Faculty of Mathematics, Physics and Informatics, Comenius University, Bratislava, Slovak Republic; [(b)]Department of Subnuclear Physics, Institute of Experimental Physics of the Slovak Academy of Sciences, Kosice, Slovak Republic
[30] Physics Department, Brookhaven National Laboratory, Upton, NY, USA
[31] Departamento de Física, y CONICET, Facultad de Ciencias Exactas y Naturales, Instituto de Física de Buenos Aires (IFIBA), Universidad de Buenos Aires, Buenos Aires, Argentina
[32] California State University, Long Beach, CA, USA
[33] Cavendish Laboratory, University of Cambridge, Cambridge, UK
[34] [(a)]Department of Physics, University of Cape Town, Cape Town, South Africa; [(b)]iThemba Labs, Western Cape, South Africa; [(c)]Department of Mechanical Engineering Science, University of Johannesburg, Johannesburg, South Africa ; [(d)]National Institute of Physics, University of the Philippines Diliman (Philippines), Quezon City, Philippines ; [(e)]Department of Physics, Stellenbosch University, Matieland, Stellenbosch, South Africa; [(f)]School of Agriculture and Science, Mathematics, University of KwaZulu-Natal, Westville, South Africa; [(g)]Department of Physics, University of South Africa, Pretoria, South Africa; [(h)]Department of Mechanical and Aeronautical Engineering, University of Pretoria, Pretoria, South Africa; [(i)]University of Zululand, KwaDlangezwa, Empangeni, South Africa; [(j)]School of Physics, University of the Witwatersrand, Johannesburg, South Africa
[35] Department of Physics, Carleton University, Ottawa, ON, Canada
[36] [(a)]Faculté des Sciences Ain Chock, Université Hassan II de Casablanca, Casablanca, Morocco; [(b)]Faculté des Sciences, Université Ibn-Tofail, Kenitra, Morocco; [(c)]Faculté des Sciences Semlalia, Université Cadi Ayyad, LPHEA-Marrakech, Marrakech, Morocco; [(d)]LPMR, Faculté des Sciences, Université Mohamed Premier, Oujda, Morocco; [(e)]Faculté des sciences, Université Mohammed V, Rabat, Morocco; [(f)]Institute of Applied Physics, Mohammed VI Polytechnic University, Ben Guerir, Morocco
[37] CERN, Geneva, Switzerland
[38] Affiliated with an Institute Formerly Covered by a Cooperation Agreement with CERN, Geneva, Switzerland
[39] Affiliated with an International Laboratory Covered by a Cooperation agreement with CERN, Geneva, Switzerland
[40] Enrico Fermi Institute, University of Chicago, Chicago, IL, USA
[41] LPC, Université Clermont Auvergne, CNRS/IN2P3, Clermont-Ferrand, France

[42] Nevis Laboratory, Columbia University, Irvington, NY, USA
[43] Niels Bohr Institute, University of Copenhagen, Copenhagen, Denmark
[44] [(a)]Dipartimento di Fisica, Università della Calabria, Rende, Italy; [(b)]INFN Gruppo Collegato di Cosenza, Laboratori Nazionali di Frascati, Frascati, Italy
[45] Physics Department, Southern Methodist University, Dallas, TX, USA
[46] National Centre for Scientific Research "Demokritos", Agia Paraskevi, Greece
[47] [(a)]Department of Physics, Stockholm University, Stockholm, Sweden; [(b)]Oskar Klein Centre, Stockholm, Sweden
[48] Deutsches Elektronen-Synchrotron DESY, Hamburg and Zeuthen, Germany
[49] Fakultät Physik , Technische Universität Dortmund, Dortmund, Germany
[50] Institut für Kern-und Teilchenphysik, Technische Universität Dresden, Dresden, Germany
[51] Department of Physics, Duke University, Durham, NC, USA
[52] SUPA-School of Physics and Astronomy, University of Edinburgh, Edinburgh, UK
[53] INFN e Laboratori Nazionali di Frascati, Frascati, Italy
[54] Physikalisches Institut, Albert-Ludwigs-Universität Freiburg, Freiburg, Germany
[55] II. Physikalisches Institut, Georg-August-Universität Göttingen, Göttingen, Germany
[56] Département de Physique Nucléaire et Corpusculaire, Université de Genève, Geneva, Switzerland
[57] [(a)]Dipartimento di Fisica, Università di Genova, Genoa, Italy; [(b)]INFN Sezione di Genova, Genoa, Italy
[58] II. Physikalisches Institut, Justus-Liebig-Universität Giessen, Giessen, Germany
[59] SUPA-School of Physics and Astronomy, University of Glasgow, Glasgow, UK
[60] LPSC, Université Grenoble Alpes, CNRS/IN2P3, Grenoble INP, Grenoble, France
[61] Laboratory for Particle Physics and Cosmology, Harvard University, Cambridge, MA, USA
[62] Department of Modern Physics and State Key Laboratory of Particle Detection and Electronics, University of Science and Technology of China, Hefei, China
[63] [(a)]Kirchhoff-Institut für Physik, Ruprecht-Karls-Universität Heidelberg, Heidelberg, Germany; [(b)]Physikalisches Institut, Ruprecht-Karls-Universität Heidelberg, Heidelberg, Germany
[64] [(a)]Department of Physics, Chinese University of Hong Kong, Shatin, N.T., Hong Kong, China; [(b)]Department of Physics, University of Hong Kong, Hong Kong, China; [(c)]Department of Physics and Institute for Advanced Study, Hong Kong University of Science and Technology, Clear Water Bay, Kowloon, Hong Kong, China
[65] Department of Physics, National Tsing Hua University, Hsinchu, Taiwan
[66] IJCLab, Université Paris-Saclay, CNRS/IN2P3, 91405 Orsay, France
[67] Centro Nacional de Microelectrónica (IMB-CNM-CSIC), Barcelona, Spain
[68] Department of Physics, Indiana University, Bloomington, IN, USA
[69] [(a)]INFN Gruppo Collegato di Udine, Sezione di Trieste, Udine, Italy; [(b)]ICTP, Trieste, Italy; [(c)]Dipartimento Politecnico di Ingegneria e Architettura, Università di Udine, Udine, Italy
[70] [(a)]INFN Sezione di Lecce, Lecce, Italy; [(b)]Dipartimento di Matematica e Fisica, Università del Salento, Lecce, Italy
[71] [(a)]INFN Sezione di Milano, Milan, Italy; [(b)]Dipartimento di Fisica, Università di Milano, Milan, Italy
[72] [(a)]INFN Sezione di Napoli, Naples, Italy; [(b)]Dipartimento di Fisica, Università di Napoli, Naples, Italy
[73] [(a)]INFN Sezione di Pavia, Pavia, Italy; [(b)]Dipartimento di Fisica, Università di Pavia, Pavia, Italy
[74] [(a)]INFN Sezione di Pisa, Pisa, Italy; [(b)]Dipartimento di Fisica E. Fermi, Università di Pisa, Pisa, Italy
[75] [(a)]INFN Sezione di Roma, Rome, Italy; [(b)]Dipartimento di Fisica, Sapienza Università di Roma, Rome, Italy
[76] [(a)]INFN Sezione di Roma Tor Vergata, Rome, Italy; [(b)]Dipartimento di Fisica, Università di Roma Tor Vergata, Rome, Italy
[77] [(a)]INFN Sezione di Roma Tre, Rome, Italy; [(b)]Dipartimento di Matematica e Fisica, Università Roma Tre, Rome, Italy
[78] [(a)]INFN-TIFPA, Trento, Italy; [(b)]Università degli Studi di Trento, Trento, Italy
[79] Department of Astro and Particle Physics, Universität Innsbruck, Innsbruck, Austria
[80] University of Iowa, Iowa City, IA, USA
[81] Department of Physics and Astronomy, Iowa State University, Ames, IA, USA
[82] Istinye University, Sariyer, Istanbul, Turkey
[83] [(a)]Departamento de Engenharia Elétrica, Universidade Federal de Juiz de Fora (UFJF), Juiz de Fora, Brazil; [(b)]Universidade Federal do Rio De Janeiro COPPE/EE/IF, Rio de Janeiro, Brazil; [(c)]Instituto de Física, Universidade de São Paulo, São Paulo, Brazil; [(d)]Rio de Janeiro State University, Rio de Janeiro, Brazil; [(e)]Federal University of Bahia, Bahia, Brazil
[84] KEK, High Energy Accelerator Research Organization, Tsukuba, Japan

[85] [(a)]Khalifa University of Science and Technology, Abu Dhabi, United Arab Emirates; [(b)]University of Sharjah, Sharjah, United Arab Emirates
[86] Graduate School of Science, Kobe University, Kobe, Japan
[87] [(a)]Faculty of Physics and Applied Computer Science, AGH University of Krakow, Kraków, Poland; [(b)]Marian Smoluchowski Institute of Physics, Jagiellonian University, Kraków, Poland
[88] Institute of Nuclear Physics Polish Academy of Sciences, Kraków, Poland
[89] Faculty of Science, Kyoto University, Kyoto, Japan
[90] Research Center for Advanced Particle Physics and Department of Physics, Kyushu University, Fukuoka, Japan
[91] L2IT, Université de Toulouse, CNRS/IN2P3, UPS, Toulouse, France
[92] Instituto de Física La Plata, Universidad Nacional de La Plata and CONICET, La Plata, Argentina
[93] Physics Department, Lancaster University, Lancaster, UK
[94] Oliver Lodge Laboratory, University of Liverpool, Liverpool, UK
[95] Department of Experimental Particle Physics, Jožef Stefan Institute and Department of Physics, University of Ljubljana, Ljubljana, Slovenia
[96] Department of Physics and Astronomy, Queen Mary University of London, London, UK
[97] Department of Physics, Royal Holloway University of London, Egham, UK
[98] Department of Physics and Astronomy, University College London, London, UK
[99] Louisiana Tech University, Ruston, LA, USA
[100] Fysiska institutionen, Lunds universitet, Lund, Sweden
[101] Departamento de Física Teorica C-15 and CIAFF, Universidad Autónoma de Madrid, Madrid, Spain
[102] Institut für Physik, Universität Mainz, Mainz, Germany
[103] School of Physics and Astronomy, University of Manchester, Manchester, UK
[104] CPPM, Aix-Marseille Université, CNRS/IN2P3, Marseille, France
[105] Department of Physics, University of Massachusetts, Amherst, MA, USA
[106] Department of Physics, McGill University, Montreal, QC, Canada
[107] School of Physics, University of Melbourne, Victoria, Australia
[108] Department of Physics, University of Michigan, Ann Arbor, MI, USA
[109] Department of Physics and Astronomy, Michigan State University, East Lansing, MI, USA
[110] Group of Particle Physics, University of Montreal, Montreal, QC, Canada
[111] Fakultät für Physik, Ludwig-Maximilians-Universität München, Munich, Germany
[112] Max-Planck-Institut für Physik (Werner-Heisenberg-Institut), Munich, Germany
[113] Graduate School of Science and Kobayashi-Maskawa Institute, Nagoya University, Nagoya, Japan
[114] [(a)]Department of Physics, Nanjing University, Nanjing, China; [(b)]School of Science, Shenzhen Campus of Sun Yat-sen University, Shenzhen, China; [(c)]University of Chinese Academy of Science (UCAS), Beijing, China
[115] Department of Physics and Astronomy, University of New Mexico, Albuquerque, NM, USA
[116] Institute for Mathematics, Astrophysics and Particle Physics, Radboud University/Nikhef, Nijmegen, The Netherlands
[117] Nikhef National Institute for Subatomic Physics and University of Amsterdam, Amsterdam, The Netherlands
[118] Department of Physics, Northern Illinois University, DeKalb, IL, USA
[119] [(a)]New York University Abu Dhabi, Abu Dhabi, United Arab Emirates; [(b)]United Arab Emirates University, Al Ain, United Arab Emirates
[120] Department of Physics, New York University, New York, NY, USA
[121] Ochanomizu University, Otsuka, Bunkyo-ku, Tokyo, Japan
[122] Ohio State University, Columbus, OH, USA
[123] Homer L. Dodge Department of Physics and Astronomy, University of Oklahoma, Norman, OK, USA
[124] Department of Physics, Oklahoma State University, Stillwater, OK, USA
[125] Joint Laboratory of Optics, Palacký University, Olomouc, Czech Republic
[126] Institute for Fundamental Science, University of Oregon, Eugene, OR, USA
[127] Graduate School of Science, University of Osaka, Osaka, Japan
[128] Department of Physics, University of Oslo, Oslo, Norway
[129] Department of Physics, Oxford University, Oxford, UK
[130] LPNHE, Sorbonne Université, Université Paris Cité, CNRS/IN2P3, Paris, France
[131] Department of Physics, University of Pennsylvania, Philadelphia, PA, USA
[132] Department of Physics and Astronomy, University of Pittsburgh, Pittsburgh, PA, USA

[133] [(a)]Laboratório de Instrumentação e Física Experimental de Partículas-LIP, Lisbon, Portugal; [(b)]Departamento de Física, Faculdade de Ciências, Universidade de Lisboa, Lisbon, Portugal; [(c)]Departamento de Física, Universidade de Coimbra, Coimbra, Portugal; [(d)]Centro de Física Nuclear da Universidade de Lisboa, Lisbon, Portugal; [(e)]Departamento de Física, Escola de Ciências, Universidade do Minho, Braga, Portugal; [(f)]Departamento de Física Teórica y del Cosmos, Universidad de Granada, Granada, Spain; [(g)]Departamento de Física, Instituto Superior Técnico, Universidade de Lisboa, Lisbon, Portugal
[134] Institute of Physics of the Czech Academy of Sciences, Prague, Czech Republic
[135] Czech Technical University in Prague, Prague, Czech Republic
[136] Faculty of Mathematics and Physics, Charles University, Prague, Czech Republic
[137] Particle Physics Department, Rutherford Appleton Laboratory, Didcot, UK
[138] IRFU, CEA, Université Paris-Saclay, Gif-sur-Yvette, France
[139] Santa Cruz Institute for Particle Physics, University of California Santa Cruz, Santa Cruz, CA, USA
[140] [(a)]Departamento de Física, Pontificia Universidad Católica de Chile, Santiago, Chile; [(b)]Millennium Institute for Subatomic Physics at High Energy Frontier (SAPHIR), Santiago, Chile; [(c)]Instituto de Investigación Multidisciplinario en Ciencia y Tecnología, y Departamento de Física, Universidad de La Serena, La Serena, Chile; [(d)]Department of Physics, Universidad Andres Bello, Santiago, Chile; [(e)]Universidad San Sebastian, Recoleta, Chile; [(f)]Instituto de Alta Investigación, Universidad de Tarapacá, Arica, Chile; [(g)]Departamento de Física, Universidad Técnica Federico Santa María, Valparaiso, Chile
[141] Department of Physics, Institute of Science, Tokyo, Japan
[142] Department of Physics, University of Washington, Seattle, WA, USA
[143] [(a)]Institute of Frontier and Interdisciplinary Science and Key Laboratory of Particle Physics and Particle Irradiation (MOE), Shandong University, Qingdao, China; [(b)]School of Physics, Zhengzhou University, Zhengzhou, China
[144] [(a)]State Key Laboratory of Dark Matter Physics, School of Physics and Astronomy, Key Laboratory for Particle Astrophysics and Cosmology (MOE), SKLPPC, Shanghai Jiao Tong University, Shanghai, China; [(b)]State Key Laboratory of Dark Matter Physics, Tsung-Dao Lee Institute, Shanghai Jiao Tong University, Shanghai, China
[145] Department of Physics and Astronomy, University of Sheffield, Sheffield, UK
[146] Department of Physics, Shinshu University, Nagano, Japan
[147] Department Physik, Universität Siegen, Siegen, Germany
[148] Department of Physics, Simon Fraser University, Burnaby, BC, Canada
[149] SLAC National Accelerator Laboratory, Stanford, CA, USA
[150] Department of Physics, Royal Institute of Technology, Stockholm, Sweden
[151] Departments of Physics and Astronomy, Stony Brook University, Stony Brook, NY, USA
[152] Department of Physics and Astronomy, University of Sussex, Brighton, UK
[153] School of Physics, University of Sydney, Sydney, Australia
[154] Institute of Physics, Academia Sinica, Taipei, Taiwan
[155] [(a)]E. Andronikashvili Institute of Physics, Iv. Javakhishvili Tbilisi State University, Tbilisi, Georgia; [(b)]High Energy Physics Institute, Tbilisi State University, Tbilisi, Georgia; [(c)]University of Georgia, Tbilisi, Georgia
[156] Department of Physics, Technion, Israel Institute of Technology, Haifa, Israel
[157] Raymond and Beverly Sackler School of Physics and Astronomy, Tel Aviv University, Tel Aviv, Israel
[158] Department of Physics, Aristotle University of Thessaloniki, Thessaloníki, Greece
[159] International Center for Elementary Particle Physics and Department of Physics, University of Tokyo, Tokyo, Japan
[160] Graduate School of Science and Technology, Tokyo Metropolitan University, Tokyo, Japan
[161] Department of Physics, University of Toronto, Toronto, ON, Canada
[162] [(a)]TRIUMF, Vancouver, BC, Canada; [(b)]Department of Physics and Astronomy, York University, Toronto, ON, Canada
[163] Division of Physics and Tomonaga Center for the History of the Universe, Faculty of Pure and Applied Sciences, University of Tsukuba, Tsukuba, Japan
[164] Department of Physics and Astronomy, Tufts University, Medford, MA, USA
[165] Department of Physics and Astronomy, University of California Irvine, Irvine, CA, USA
[166] University of West Attica, Athens, Greece
[167] Department of Physics and Astronomy, University of Uppsala, Uppsala, Sweden
[168] Department of Physics, University of Illinois, Urbana, IL, USA
[169] Instituto de Física Corpuscular (IFIC), Centro Mixto Universidad de Valencia-CSIC, Valencia, Spain
[170] Department of Physics, University of British Columbia, Vancouver, BC, Canada

[171] Department of Physics and Astronomy, University of Victoria, Victoria, BC, Canada
[172] Fakultät für Physik und Astronomie, Julius-Maximilians-Universität Würzburg, Würzburg, Germany
[173] Department of Physics, University of Warwick, Coventry, UK
[174] Waseda University, Tokyo, Japan
[175] Department of Particle Physics and Astrophysics, Weizmann Institute of Science, Rehovot, Israel
[176] Department of Physics, University of Wisconsin, Madison, WI, USA
[177] Fakultät für Mathematik und Naturwissenschaften, Fachgruppe Physik, Bergische Universität Wuppertal, Wuppertal, Germany
[178] Department of Physics, Yale University, New Haven, CT, USA
[179] Yerevan Physics Institute, Yerevan, Armenia

[a] Also at Affiliated with an Institute Formerly Covered by a Cooperation Agreement with CERN, Geneva, Switzerland
[b] Also at An-Najah National University, Nablus, Palestine
[c] Also at Borough of Manhattan Community College, City University of New York, New York, NY, USA
[d] Also at Center for Interdisciplinary Research and Innovation (CIRI-AUTH), Thessaloníki, Greece
[e] Also at Centre of Physics of the Universities of Minho and Porto (CF-UM-UP), Braga, Portugal
[f] Also at CERN, Geneva, Switzerland
[g] Also at Département de Physique Nucléaire et Corpusculaire, Université de Genève, Geneva, Switzerland
[h] Also at Departament de Fisica de la Universitat Autonoma de Barcelona, Barcelona, Spain
[i] Also at Department of Financial and Management Engineering, University of the Aegean, Chios, Greece
[j] Also at Department of Mathematical Sciences, University of South Africa, Johannesburg, South Africa
[k] Also at Department of Modern Physics and State Key Laboratory of Particle Detection and Electronics, University of Science and Technology of China, Hefei, China
[l] Also at Department of Physics, Bolu Abant Izzet Baysal University, Bolu, Turkey
[m] Also at Department of Physics, King's College London, London, UK
[n] Also at Department of Physics, Stanford University, Stanford, CA, USA
[o] Also at Department of Physics, Stellenbosch University, Stellenbosch, South Africa
[p] Also at Department of Physics, University of Fribourg, Fribourg, Switzerland
[q] Also at Department of Physics, University of Thessaly, Vólos, Greece
[r] Also at Department of Physics, Westmont College, Santa Barbara, USA
[s] Also at Faculty of Physics, Sofia University, 'St. Kliment Ohridski', Sofia, Bulgaria
[t] Also at Faculty of Physics, University of Bucharest, Bucharest, Romania
[u] Also at Hellenic Open University, Patras, Greece
[v] Also at Henan University, Kaifeng, China
[w] Also at Imam Mohammad Ibn Saud Islamic University, Riyadh, Saudi Arabia
[x] Also at Institucio Catalana de Recerca i Estudis Avancats, ICREA, Barcelona, Spain
[y] Also at Institut für Experimentalphysik, Universität Hamburg, Hamburg, Germany
[z] Also at Institute for Nuclear Research and Nuclear Energy (INRNE) of the Bulgarian Academy of Sciences, Sofia, Bulgaria
[aa] Also at Institute of Applied Physics, Mohammed VI Polytechnic University, Ben Guerir, Morocco
[ab] Also at Institute of Particle Physics (IPP), Victoria, Canada
[ac] Also at Institute of Physics and Technology, Mongolian Academy of Sciences, Ulaanbaatar, Mongolia
[ad] Also at Institute of Physics, Azerbaijan Academy of Sciences, Baku, Azerbaijan
[ae] Also at Institute of Theoretical Physics, Ilia State University, Tbilisi, Georgia
[af] Also at Millennium Institute for Subatomic Physics at High Energy Frontier (SAPHIR), Santiago, Chile
[ag] Also at National Institute of Physics, University of the Philippines Diliman (Philippines), Quezon City, Philippines
[ah] Also at The Collaborative Innovation Center of Quantum Matter (CICQM), Beijing, China
[ai] Also at TRIUMF, Vancouver, BC, Canada
[aj] Also at Università di Napoli Parthenope, Naples, Italy
[ak] Also at University of Chinese Academy of Sciences (UCAS), Beijing, China
[al] Also at Department of Physics, University of Colorado Boulder, Colorado, USA
[am] Also at University of Sienna, Sienna, Italy
[an] Also at Washington College, Chestertown, MD, USA

[ao] Also at Physics Department, Yeditepe University, Istanbul, Turkey
* Deceased